Published for SISSA by Springer

Received: *June 15, 2026*
Accepted: *September 30, 2026*
Published: *October 28, 2026*

Search for dark photons from Higgs boson decays in the gluon-gluon fusion channel in proton-proton collisions at $\sqrt{s} = 13.6$ TeV with the ATLAS detector



The ATLAS collaboration

Full author list at the end of the paper

E-mail: atlas.publications@cern.ch

Abstract: This paper presents a search for semi-visible Higgs boson decays in final states with a photon (γ) and missing transverse momentum $p_{\mathrm{T}}^{\mathrm{miss}}$. The analysis is optimised for the gluon-gluon fusion production channel and exploits a novel trigger deployed in 2023, with reduced thresholds down to 50 GeV on the photon transverse momentum (p_{T}^{γ}) and 70 GeV on the $p_{\mathrm{T}}^{\mathrm{miss}}$, in combination with a selection on the transverse mass of the $p_{\mathrm{T}}^{\mathrm{miss}}$-$\gamma$ system (m_{T}) above 80 GeV. The results are interpreted in terms of Higgs boson decays into a γ and a dark photon γ_{d} ($H \to \gamma\gamma_d$). The analysis is performed using 135 fb^{-1} of Run 3 data collected by ATLAS in 2023 and 2024. A boosted decision tree is used to identify events with misreconstructed primary vertices, which can affect the $p_{\mathrm{T}}^{\mathrm{miss}}$ calculation. Data-driven methods are employed to estimate the backgrounds from jets and electrons misidentified as photons, while the backgrounds with genuine photons are taken from Monte Carlo simulations, normalised to data in control regions with muons. A binned maximum-likelihood fit to the m_{T} distribution is performed to evaluate the compatibility of the observed data with the Standard Model expectation. No significant excess is observed over the Standard Model prediction, and an observed (expected) upper limit on the branching ratio of $H \to \gamma\gamma_d$ of 1.4% (1.2%) is obtained at 95% confidence level. Combining this result with previous Run 2 searches improves the observed (expected) upper limit to 0.9% (0.9%).

Keywords: Hadron-Hadron Scattering

ArXiv ePrint: 2606.14362

Open Access, © The Authors.
Article funded by SCOAP^3.

https://doi.org/10.1007/JHEP10(2026)270

JHEP10(2026)270

Contents

1 Introduction **1**

2 ATLAS detector **3**

3 Data and simulation **4**

4 Analysis trigger **6**

5 Event reconstruction **8**

6 Signature and backgrounds **9**

7 Event selection **11**
7.1 Baseline selection 11
7.2 Signal region 13

8 Analysis strategy and background modelling **14**
8.1 Estimation of $e \rightsquigarrow \gamma$ 16
8.2 Estimation of $j \rightsquigarrow \gamma$ 18

9 Systematic uncertainties **21**
9.1 Experimental uncertainties 21
9.2 Uncertainties in data-driven methods 23
9.3 Theoretical uncertainties 23

10 Statistical treatment and results **23**

11 Conclusion **27**

The ATLAS collaboration **35**

1 Introduction

Exotic decays of the Higgs boson are well motivated by a variety of models beyond the Standard Model (BSM) [1], including supersymmetry, dark sector or extended Higgs sectors, and provide a unique opportunity to probe new physics.

This paper presents a new strategy to search for exotic Higgs boson decays into a final state with a photon (γ) and missing transverse momentum ($p_{\mathrm{T}}^{\mathrm{miss}}$), probing a region of phase space with low kinematic thresholds that was previously unexplored by ATLAS. This semi-visible decay of the Higgs boson provides an interesting production channel for the dark photon (γ_{d}), which arises as the gauge boson of an additional $U(1)_D$ gauge group in dark sector models. Strong motivations for searches for this particle arise from its potential role as a "portal" to the dark sector, as well as from its possible contribution to addressing small-scale structure formation problems [2, 3] and enabling viable asymmetric DM scenarios [4]. In

JHEP10(2026)270

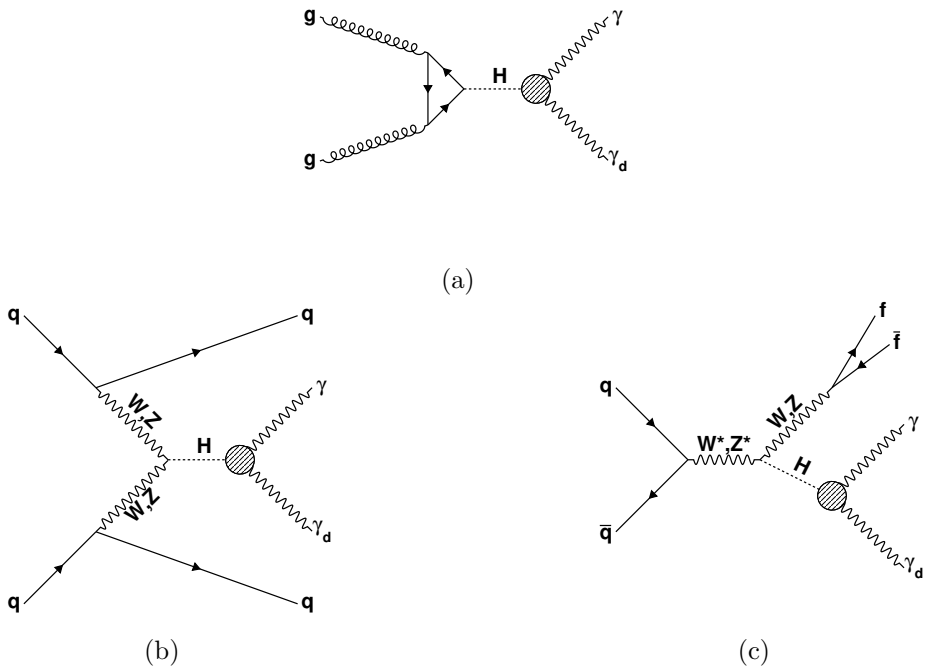


Figure 1. Feynman diagrams illustrating Higgs boson production via (a) the gluon-gluon fusion, (b) vector-boson fusion and (c) Higgsstrahlung processes, all followed by the decay into a photon and a dark photon ($H \to \gamma\gamma_\mathrm{d}$). The hatched circle in the $H\gamma\gamma_\mathrm{d}$ vertex represents the interaction through messenger fields.

addition, this signature can arise in several BSM models, such as those with very low-scale supersymmetry breaking where the Higgs boson can decay into a gravitino ($\tilde{G}$) and a bino ($\tilde{B}$) that subsequently decays via $\tilde{B} \to \gamma\tilde{G}$ [5], in the Peccei-Quinn limit of next-to-minimal-supersymmetric models (NMSSM) [6], or in the decay of the Higgs boson into a pair of right-handed neutrinos (N) subsequently decaying via $N \to \nu\bar{\nu}\nu$ and $N \to \gamma\nu$ [7].

While γ_d searches typically target the massive γ_d [8–10], which can couple directly to the Standard Model (SM) via kinetic mixing with the ordinary photon [11], this paper focuses on a massless γ_d scenario. In this case, the kinetic mixing between the γ_d and the photon can be tuned away through a rotation of the gauge fields, and the γ_d can interact with ordinary matter only through operators of dimension higher than four [11]. The Higgs boson can decay through a loop interaction involving additional scalar or pseudo-scalar BSM messenger fields, which couple both to the SM and the dark sector [12, 13], represented as an effective vertex in figure 1. Due to the non-decoupling properties of the Higgs boson, a branching ratio of $H \to \gamma\gamma_\mathrm{d}$ ($\mathcal{B}_{\gamma\gamma_\mathrm{d}}$) up to $\sim 0.4\%$ may be allowed [14, 15], depending on the parameters of the model and taking into account constraints from searches for invisible Higgs boson decays and measurements of the branching ratio of $H \to \gamma\gamma$.

Searches for the semi-visible decay $H \to \gamma\gamma_\mathrm{d}$ have been conducted at the LHC by the ATLAS and CMS collaborations, in the vector boson fusion (VBF) Higgs boson production channel and in associated production with a Z boson (ZH) [16–19]. The combination of

JHEP10(2026)270

ATLAS results in the ZH and VBF channels [20] provides the best limit so far, excluding a $\mathcal{B}_{\gamma\gamma_d} > 1.3\%$ (1.5% expected) at 95% confidence level (CL) with 139 fb^{-1} of data collected during the LHC Run 2 at $\sqrt{s} = 13$ TeV. The CMS results provide independent constraints, with an observed (expected) 95% CL upper limit of $\mathcal{B}_{\gamma\gamma_d} > 2.9\%$ (2.1%), obtained from the combination of the VBF and the ZH channel [19]. These production modes take advantage of a richer final state in addition to the $\gamma + p_T^{miss}$ signature from the $H \to \gamma\gamma_d$ decay, with additional jets or leptons that provide powerful handles for triggering, background rejection and identification of the hard-scatter primary vertex. In contrast, the gluon-gluon fusion mode (ggF), leading to the $\gamma + p_T^{miss}$ final state, is the dominant production mode, with a cross-section about an order of magnitude larger than that of the VBF channel. This final state has been explored by CMS [21] and ATLAS in the context of other exotic models [22] or by focusing on the decay into $\gamma\gamma_d$ of BSM Higgs bosons with masses higher than 400 GeV [23]. However, the $H \to \gamma\gamma_d$ decay of a Higgs boson with a mass of 125 GeV has not been specifically targeted, as the low thresholds on the photon transverse momentum (p_T^γ) and p_T^{miss} required for this signature constitute a challenge for the trigger. Developments in the ATLAS trigger system between Run 2 and Run 3 led to the implementation of a composite trigger that combines selections on p_T^{miss}, p_T^γ, and the transverse mass between the γ and the p_T^{miss}, $m_T = \sqrt{2p_T^\gamma p_T^{miss}(1-\cos(\Delta\phi))}$,[1] where $\Delta\phi$ is the azimuthal separation between the photon and the p_T^{miss}. This new trigger allows to increase the acceptance of ggF events by approximately a factor of two, while keeping the trigger rate under control. By exploiting this new trigger, the analysis presented in this paper is optimised for the $H \to \gamma\gamma_d$ decay in the ggF production channel for the first time in ATLAS, while also retaining sensitivity to the VBF, ZH and WH channels.

2 ATLAS detector

The ATLAS detector [24, 25] at the LHC consists of an inner tracking detector system (ID) surrounded by a thin superconducting solenoid, electromagnetic and hadronic calorimeters (ECAL and HCAL), and a muon spectrometer (MS) incorporating three large superconducting air-core toroidal magnets, with an almost complete solid angle coverage around the collision point.

The ID system is immersed in a 2 T axial magnetic field and provides charged-particle tracking in the range of $|\eta| < 2.5$. The high-granularity silicon pixel detector covers the interaction region and typically provides four measurements per track, the first hit generally being in the insertable B-layer installed before Run 2 [26, 27]. It is followed by the silicon microstrip tracker, which usually provides eight measurements per track. The outermost part of the ID is the transition radiation tracker (TRT), which enables radially extended track reconstruction up to $|\eta| = 2.0$. The TRT also provides electron identification information

[1] ATLAS uses a right-handed coordinate system with its origin at the nominal interaction point (IP) in the centre of the detector and the z-axis along the beam pipe. The x-axis points from the IP to the centre of the LHC ring, and the y-axis points upwards. Polar coordinates (r, ϕ) are used in the transverse plane, ϕ being the azimuthal angle around the z-axis. The pseudorapidity is defined in terms of the polar angle θ as $\eta = -\ln\tan(\theta/2)$ and is equal to the rapidity $y = \frac{1}{2}\ln\left(\frac{E+p_z}{E-p_z}\right)$ in the relativistic limit. Angular distance is measured in units of $\Delta R \equiv \sqrt{(\Delta y)^2 + (\Delta\phi)^2}$.

JHEP10(2026)270

based on the fraction of hits (typically 30 in total) above a higher energy-deposit threshold corresponding to transition radiation.

The calorimeter system covers the pseudorapidity range $|\eta| < 4.9$. The ECAL [28, 29] is a lead/liquid-argon (LAr) sampling calorimeter covering the region $|\eta| < 3.2$, divided into a barrel and two endcaps, and longitudinally segmented into three layers: the strips, the middle and the back layer. The 3-dimensional high-granularity in the fiducial acceptances $|\eta| < 1.37$ and $1.52 < |\eta| < 2.37$ allows observation of the shape of the electromagnetic showers. Before the ECAL, a thin LAr presampler covering $|\eta| < 1.8$ detects energy losses of showers starting in the material upstream. The HCAL consists of a steel/scintillator-tile calorimeter, segmented into three barrel structures within $|\eta| < 1.7$, and two copper/LAr hadron endcap calorimeters. The solid angle coverage is completed with forward copper/LAr and tungsten/LAr calorimeter modules optimised for electromagnetic and hadronic energy measurements respectively.

The MS comprises separate trigger and high-precision tracking chambers measuring the deflection of muons in a magnetic field generated by the superconducting air-core toroidal magnets. The field integral of the toroids ranges between 2.0 and 6.0 T m across most of the detector. Three layers of precision chambers, each consisting of layers of monitored drift tubes, cover the region $|\eta| < 2.7$, except in the innermost layer of the endcap region, where layers of small-strip thin-gap chambers and Micromegas chambers provide precision tracking in the region $1.3 < |\eta| < 2.7$. The muon trigger system covers the range $|\eta| < 2.4$ with resistive-plate chambers in the barrel, thin-gap chambers in the endcap regions, and the small-strip thin-gap chambers and Micromegas chambers in the innermost layer of the endcap.

Interesting events are selected by the first-level (L1) trigger system implemented in custom hardware, followed by selections made by software-implemented algorithms in the high-level trigger (HLT) [30]. The first-level trigger selects events at a rate below 100 kHz from the 40 MHz bunch crossings; the high-level trigger further reduces that rate, in order to record events to disk at about 3 kHz. An extensive software suite [31] is used in data simulation, in the reconstruction and analysis of real and simulated data, in detector operations, and in the trigger and data acquisition systems of the experiment.

3 Data and simulation

This analysis uses proton-proton (pp) collision data at a centre-of-mass energy of 13.6 TeV, collected in 2023 and 2024 by the ATLAS detector. Only data recorded during stable beam conditions and with all sub-detectors operational are considered [32], corresponding to a total integrated luminosity of 135 fb^{-1}, with an uncertainty of 1.9% [33]. Events were selected by using a dedicated trigger ('analysis trigger') deployed in 2023, optimised for the $\gamma + p_{\mathrm{T}}^{\mathrm{miss}}$ final state and described in section 4. In addition, samples with e^+e^-, γe and $\gamma\mu$ final states, used for the modelling of the background from electrons misidentified as photons (section 8.1) and for the efficiency studies of the analysis trigger (section 4), were selected using dielectron, single-electron, and single-muon triggers, respectively.

Monte Carlo (MC) simulations are used to model the signal and background processes described in section 6. In particular, the backgrounds containing genuine photons ($Z\gamma$, $W\gamma$, and processes with a direct photon, γ(dir)+jets) are estimated using MC simulations. The

JHEP10(2026)270

remaining backgrounds are estimated with data-driven methods, with W+jets and Z+jets MC samples used as input for the data-driven estimation of the background arising from jets misidentified as photons (section 8.2). All the samples, including processes with photons from fragmentation, γ(frag)+jets, and multijets samples, are used in the training of the algorithm that identifies wrongly reconstructed hard scattering vertices (section 7.1). Simulations of events from top-quark production are not used, as the analysis applies a veto on jets emanating from b-quarks (section 7.1).

The simulation of the geometry and response of the ATLAS detector [34] was performed using GEANT4 [35], and all simulated events were processed through the same reconstruction chain as collision data. The effect of multiple interactions in the same and neighbouring bunch crossings, pile-up (PU), was modelled by overlaying [36] the simulated hard-scattering event with inelastic pp events generated using EPOS 2.0.1.4 [37] and PYTHIA 8.308 [38]. The EPOS events were generated with the EPOS LHC set of tuned parameters (tune) [39] and the PYTHIA events with the A3 tune [40] and the NNPDF2.3LO [41] set of parton distribution functions (PDF). PYTHIA PU events include either a high p_{T} jet, a prompt photon, or a lepton from a b-hadron decay, while events generated using EPOS were filtered to simulate all remaining PU events in the overlay sample. The individual simulations were first reweighted to ensure a smooth jet p_{T} distribution. The combination was then reweighted to match the distribution of the actual number of interactions per bunch crossing measured in data.

The signal samples include multiple Higgs boson production channels. The dominant process and main target of this analysis is the ggF channel, but non-negligible contributions arise from the VBF, WH and ZH channels. One MC sample for each production mode was generated, with WH production divided into W^+H and W^-H. The matrix elements were estimated using POWHEG v2 [42, 43] at next-to-leading order (NLO), with the PDF4LHC21 set of PDFs [44]. For the ggF channel, next-to-next-to-leading order (NNLO) precision was achieved through a reweighting of the events computed in bins of the p_{T} and rapidity of the generated Higgs boson, to match NNLOPS predictions [45]. The samples were generated with the SM Higgs boson mass set to 125 GeV. All the signal samples were normalised to state-of-the-art cross-section predictions for the centre-of-mass energy of 13 TeV [46], extrapolated to 13.6 TeV [47]. The decay into photons and dark photons, as well as the hadronisation and showering, was simulated using PYTHIA 8.245 with the CTEQ6L1 PDF set and the AZNLO tune [48]. The 'Hidden Valley' scenario [49] was used for modelling the $H \to \gamma\gamma_{\mathrm{d}}$ decay.

The $V\gamma$ and V+jets processes were simulated using the SHERPA 2.2.14 generator [50], with up to one jet (two jets) at NLO and up to three additional jets at leading order (LO) for $Z\gamma$ and $W\gamma$ (Z+jets and W+jets). The matrix elements were matched and merged with the SHERPA parton shower [51], using the MEPS@NLO prescription [52, 53] and the NNPDF3.0 NNLO PDF set [54] with the dedicated SHERPA tune. The γ(dir)+jets, γ(frag)+jets and multijets samples were generated at LO using PYTHIA 8.186 [55, 56] with the NNPDF2.3 LO PDF set and the A14 tune [57] for the parton shower. Table 1 summarises the configurations used for the signal and background MC simulations of the analysis.

JHEP10(2026)270

Process	Generator	ME order	PDF	Parton Shower	Tune
$H \to \gamma\gamma_d$	Powheg v2	NLO	PDF4LHC21	Pythia 8.245	AZNLO
$Z\gamma, W\gamma$	Sherpa v2.2.14	0,1j@NLO + 2,3,4j@LO	NNPDF3.0 NNLO	Sherpa	Sherpa
Z+jets, W+jets	Sherpa v2.2.14	0,1,2j@NLO + 3,4,5j@LO	NNPDF3.0 NNLO	Sherpa	Sherpa
γ(dir)+jets	Pythia 8.186	LO	NNPDF2.3 LO	Pythia 8.308	A14
γ(frag)+jets	Pythia 8.186	LO	NNPDF2.3 LO	Pythia 8.308	A14
multijets	Pythia 8.186	LO	NNPDF2.3 LO	Pythia 8.308	A14

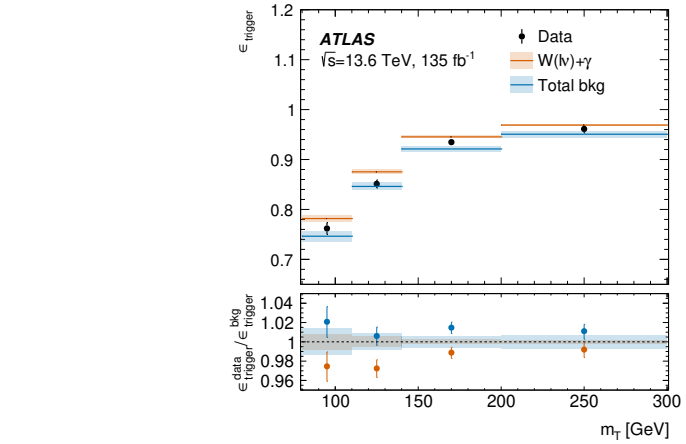
Table 1. Configurations used for event generation and parton shower of signal (ggF, VBF, ZH and WH) and background MC samples. The matrix element (ME) order, leading-order (LO) or next-to-leading order (NLO), refers to the order in the strong coupling constant of the perturbative calculation in the MC event generation. PDF refers to the parton density libraries used with the generator. The tune refers to the underlying-event tune of the parton shower model.

4 Analysis trigger

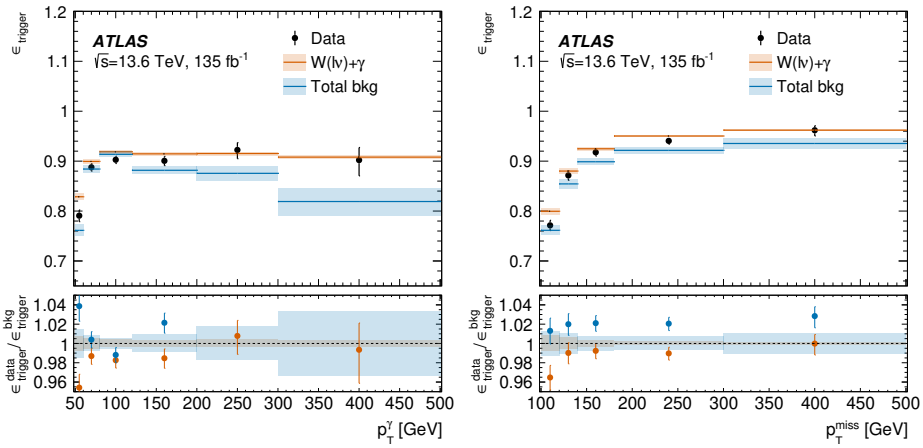
The 'analysis trigger' combines selections on the photon p_{T}, the $p_{\mathrm{T}}^{\mathrm{miss}}$ and the m_{T}. It selects 10% of the total generated signal events in the ggF channel, with a factor of two increase relative to previous single-photon or inclusive $p_{\mathrm{T}}^{\mathrm{miss}}$ triggers. A similar trigger efficiency is observed also in the VBF and VH channels. At L1, the trigger selected electrons or photons with p_{T} above 26 GeV. The HLT further required a 50 GeV photon fulfilling tight identification criteria [30]. To compute the $p_{\mathrm{T}}^{\mathrm{miss}}$ at HLT level, a two-stage sequence of algorithms was employed, starting with the 'cell' $p_{\mathrm{T}}^{\mathrm{miss}}$ computed using only the calorimeter cells as input [58]. This fast step was followed by a more sophisticated $p_{\mathrm{T}}^{\mathrm{miss}}$ algorithm using particle flow [59] constituents, combining tracks and calorimeter clusters, with a dedicated PU subtraction algorithm ('pfopufit') [30]. A minimum threshold of 40 GeV was applied for the first 'cell' $p_{\mathrm{T}}^{\mathrm{miss}}$ requirement, while the second 'pfopufit' step had a threshold of 70 GeV. To further reduce the rate, the trigger required a minimum m_{T} (computed using 'pfopufit' $p_{\mathrm{T}}^{\mathrm{miss}}$) of 80 GeV. Since muons are invisible to the 'cell' $p_{\mathrm{T}}^{\mathrm{miss}}$ algorithm [60], particle flow constituents consistent with muons were removed also in the 'pfopufit' algorithm, to preserve the same behaviour. Therefore both the 'cell' and the 'pfopufit' algorithms were insensitive to the presence of muons, which were treated as invisible in the computation of $p_{\mathrm{T}}^{\mathrm{miss}}$. This feature allowed samples to be selected with reconstructed muons in the final state and to treat them as invisible to mimic $p_{\mathrm{T}}^{\mathrm{miss}}$, without introducing a bias induced by the analysis trigger. In particular, events with muons are used to constrain the $W\gamma$ and $Z\gamma$ backgrounds in control regions with one or two muons as described in section 8.

Events with one muon are also used to assess the accuracy of the simulation of the analysis trigger in $\gamma\mu$ final states, selected by a muon trigger used as a baseline trigger. The muon was treated as invisible in the computation of $p_{\mathrm{T}}^{\mathrm{miss}}$ and m_{T} in the full (offline) reconstruction. Figure 2 shows the trigger efficiency as a function of offline p_{T}^{γ}, $p_{\mathrm{T}}^{\mathrm{miss}}$ and m_{T}. The efficiency in data is compared to that of the dominant background contribution from $W\gamma$ events (75%), and that of the total background, which includes contributions from $Z\gamma$ events (2%) and from events with a jet misidentified as a photon (23%). The latter may exhibit a different trigger efficiency due to an expected different trigger response to misidentified jets. The trigger

JHEP10(2026)270



(a)



(b) (c)

Figure 2. Analysis trigger efficiency as a function of (a) m_{T} (b) p_{T}^{γ} and (c) $p_{\mathrm{T}}^{\mathrm{miss}}$ for data, simulation of the dominant background $W\gamma$ and total background. Events were selected using single-muon triggers and requiring one muon treated as invisible in the evaluation of $p_{\mathrm{T}}^{\mathrm{miss}}$ and m_{T}. In addition, a subset of the selections used in the analysis is applied: $p_{\mathrm{T}}^{\mathrm{miss}} > 100$ GeV, $m_{\mathrm{T}} > 80$ GeV, one photon with $p_{\mathrm{T}}^{\gamma} > 50$ GeV and a requirement of $|\Delta\phi(\vec{p}_{\mathrm{T}}^{\,\mathrm{miss}}, \vec{p}_{\mathrm{T}}^{\,\mathrm{miss},\gamma})| > 1.25$ on the azimuthal separation between the $\vec{p}_{\mathrm{T}}^{\,\mathrm{miss}}$ and its photon term $\vec{p}_{\mathrm{T}}^{\,\mathrm{miss},\gamma}$, equivalent to $-\vec{p}_{\mathrm{T}}^{\,\gamma}$. The bottom panels show the ratios of the efficiency in data to those in the $W\gamma$ MC simulation and in the total background expectation. The shaded bands and the error bars represent the statistical uncertainties associated with the MC simulation and the data, respectively.

efficiency measured in data is observed to lie in between the one predicted by the simulations for $W\gamma$ background and for the total background. Up and down uncertainties in the trigger efficiency are therefore assigned as the differences between the efficiency measured in data and the one predicted for the total background and for the $W\gamma$ simulation, respectively. This procedure also accounts for the uncertainty in the modelling of the background from jets misidentified as photons. The m_{T} variable is correlated with both the p_{T}^{γ} and the $p_{\mathrm{T}}^{\mathrm{miss}}$. While the trigger efficiency curve rapidly reaches a plateau as a function of p_{T}^{γ}, a slower turn-on is observed as a function of $p_{\mathrm{T}}^{\mathrm{miss}}$. For this reason, uncertainties at the 2%–3% level are applied

JHEP10(2026)270

in bins of $p_{\mathrm{T}}^{\mathrm{miss}}$. Since the trigger efficiency for signal events is found to be consistent with that observed in the $W\gamma$ simulation, the same uncertainty is assigned to the signal sample.

5 Event reconstruction

For each event, vertex candidates are required to have at least two associated tracks with $p_{\mathrm{T}} > 500$ MeV. Among the reconstructed vertices, the hard-scattering (HS) primary vertex (PV) is selected as the one with the highest sum of squared transverse momenta of contributing tracks [61].

For each reconstructed physics object, looser selection criteria are first applied to define *baseline* objects, which are used for event vetos, $p_{\mathrm{T}}^{\mathrm{miss}}$ reconstruction, and overlap removal. More stringent criteria are then required, to define *selected* objects.

Electrons are reconstructed by matching energy clusters in the ECAL to tracks in the ID [62, 63]. *Baseline* electrons are required to satisfy $p_{\mathrm{T}} > 10$ GeV and $|\eta| < 2.47$, be outside the transition region between the ECAL barrel and endcaps ($1.37 < |\eta| < 1.52$), and be consistent with originating from the PV through requirements on the longitudinal and transverse impact parameters, $|z_0 \sin(\theta)| < 0.5$ mm and $|d_0/\sigma(d_0)| < 5$ where $\sigma(d_0)$ is the uncertainty in d_0. All baseline electron candidates are required to satisfy `Loose` likelihood-based identification criteria [64], based on calorimeter, tracking and combined variables that provide separation between electrons and jets. *Selected* electrons are further required to satisfy `Tight` identification and `Tight` isolation requirements [64].

Muons are reconstructed by matching ID tracks to MS tracks or track segments, by associating ID tracks with calorimeter energy deposits compatible with a minimum-ionizing particle, or by identifying MS tracks satisfying the `Loose` requirement and compatible with the interaction point [65, 66]. *Baseline* muon candidates must satisfy $p_{\mathrm{T}} > 10$ GeV and $|\eta| < 2.7$ and `Medium` identification criteria. Similar selections on the impact parameter as for electrons are applied, but with $|d_0/\sigma(d_0)| < 3$. *Selected* muons are further required to satisfy `Loose` isolation selections [66].

Photon candidates are reconstructed from clustered energy deposits in the ECAL [62, 63]. For photons that undergo conversions in the material upstream the ECAL, tracks in the ID are also used. *Baseline* photons are required to satisfy $p_{\mathrm{T}}^{\gamma} > 25$ GeV, $|\eta| < 2.37$ and be outside the transition region between the ECAL barrel and endcaps ($1.37 < |\eta| < 1.52$). Photon candidates must satisfy a `Tight` identification criterion, based on several requirements on the 'shower shape' variables [67], which can be grouped into three categories: energy leakage in the HCAL, width in the middle layer of the ECAL, and shape in the strips. *Selected* photon candidates are additionally required to be isolated. A dimensionless isolation variable is introduced:

$$\Upsilon = \frac{E_{\mathrm{T}}^{\mathrm{cone}} - 2.45 \text{ GeV}}{p_{\mathrm{T}}^{\gamma}}, \tag{5.1}$$

where $E_{\mathrm{T}}^{\mathrm{cone}}$ is the transverse energy measured by the calorimeters in a cone of size $\Delta R = 0.4$ around the photon candidate. Isolated photons are required to satisfy the `TightCaloOnly` working point, $\Upsilon < 0.022$, a typical requirement to select prompt, isolated photons in ATLAS [68]. Non-isolated photons are used in the evaluation of the background induced

JHEP10(2026)270

by jets misidentified as photons (see sections 6 and 8.2). In this context, a `Loose` photon selection is required, with relaxed requirements on the HCAL and ECAL middle layer, and no requirements on strips. Removing `Tight` photons from the `Loose` sample provides a `Loose`$'$ sample enriched in this background. Further photon selections `Loose`$''$ are introduced as subsets of the `Loose`$'$ sample, by applying the same selections as for `Tight` to the HCAL and middle layer shower shapes, but at most one requirement on one of the strips shower shapes.

Particle flow (PFlow) jets are reconstructed using the anti-k_t algorithm [69], as implemented in FastJet [70], with a radius parameter $R = 0.4$. The algorithm takes PFlow objects as inputs, combining measurements from the ID and the calorimeters [59]. *Selected* jets are required to satisfy $p_{\mathrm{T}} > 20$ GeV. In addition, central jets ($|\eta| < 2.5$) are classified as originating from the HS interaction using a neural-network-based jet-vertex-tagger (NN-JVT) (an evolution of the JVT described in ref. [71]), while a forward jet vertex tagging (fJVT) algorithm [72] is applied to forward jets ($|\eta| > 2.5$). Jets containing b-hadrons (b-jets) are identified using a graph neural network tagger with 85% b-tagging efficiency [73]. To suppress the background originating from detector noise, hardware issues, beam-induced background or cosmic-ray muons, events containing jets failing to satisfy `Loose` jet-quality criteria are rejected [74].

Hadronically decaying τ-leptons (τ_{had}) are seeded by anti-k_t jets with $R = 0.4$ and identified using a recurrent neural network algorithm that uses tracks and calorimeter energy clusters associated with τ_{had} candidates, as well as high-level discriminating variables [75]. *Baseline* τ_{had} are required to satisfy a `Medium` identification working point and have $p_{\mathrm{T}} > 20$ GeV and $|\eta| < 2.5$.

The $\vec{p}_{\mathrm{T}}^{\,\mathrm{miss}}$, with magnitude $p_{\mathrm{T}}^{\mathrm{miss}} = |\vec{p}_{\mathrm{T}}^{\,\mathrm{miss}}|$, is defined as the negative vector sum of the transverse momenta of the *baseline* reconstructed objects ('hard term'), and of the 'soft term' estimated from charged PFlow objects associated with the primary vertex and not matched to any of the reconstructed hard objects [76]. In the $\vec{p}_{\mathrm{T}}^{\,\mathrm{miss}}$ calculation, a NN-JVT selection is applied to the jets for PU subtraction. An alternative $\vec{p}_{\mathrm{T}}^{\,\mathrm{miss}}$ with no PU subtraction, referred to as $\vec{p}_{\mathrm{T,noJVT}}^{\,\mathrm{miss}}$, is also exploited to help tag events with a misidentified PV, as explained in section 7. In addition, a key quantity to identify events with fake $p_{\mathrm{T}}^{\mathrm{miss}}$ is the $p_{\mathrm{T}}^{\mathrm{miss}}$ significance $\mathcal{S}_{p_{\mathrm{T}}^{\mathrm{miss}}} = \frac{p_{\mathrm{T}}^{\mathrm{miss}}}{\sigma(p_{\mathrm{T}}^{\mathrm{miss}})}$, where $\sigma(p_{\mathrm{T}}^{\mathrm{miss}})$ denotes the $p_{\mathrm{T}}^{\mathrm{miss}}$ resolution, accounting for the resolution of the reconstructed physics objects entering the $p_{\mathrm{T}}^{\mathrm{miss}}$ computation [76, 77].

After the reconstruction of all physics objects, a sequential overlap removal procedure, as detailed in table 2, is applied to resolve ambiguities by keeping one single object in case of overlapping objects, based on ΔR matching, shared ID tracks or calorimeter energy clusters, according to a predefined priority.

6 Signature and backgrounds

The $H \to \gamma\gamma_{\mathrm{d}}$ signal is characterised by the presence of a single photon and $p_{\mathrm{T}}^{\mathrm{miss}}$. Although the z-component of the γ_{d} momentum cannot be reconstructed, the m_{T} distribution features a broad peak around the Higgs boson mass. In the ggF channel, the final state contains no leptons, while hadronic jets may originate from gluon radiation. The same final state also covers the VBF channel and VH production with hadronic decay of the vector bosons.

JHEP10(2026)270

Remove	Keep	Matching criteria
Muon	Electron	Muon with calorimeter deposits and shared ID track
Electron	Muon	Shared ID track
Jet	Electron	$\Delta R < 0.2$
Electron	Jet	$0.2 < \Delta R < 0.4$
Electron	Electron	Shared ID track, electron with lower p_{T} removed
Jet	Muon	Number of tracks < 3 and $\Delta R < 0.2$
Muon	Jet	$0.2 < \Delta R < 0.4$
τ-lepton	Electron	$\Delta R < 0.2$
τ-lepton	Muon	$\Delta R < 0.2$
Jet	τ-lepton	$\Delta R < 0.2$
Photon	Electron	Shared calorimeter energy clusters
Photon	Muon	$\Delta R < 0.4$
Jet	Photon	$\Delta R < 0.4$

Table 2. Overview of the sequential overlap removal procedure applied to reconstructed objects and the corresponding matching criteria based on the ΔR separation and shared ID tracks. If two objects overlap based on the matching criteria described in the third column, the object in the first column is removed while the one in the second column is retained. The table is ordered according to the object priority used in the overlap removal procedure.

Due to the trigger thresholds on $p_{\mathrm{T}}^{\mathrm{miss}}$ and photon p_{T}^{γ} (section 4), optimised as a compromise between signal acceptance and trigger rate, the selected signal events are mostly Higgs bosons recoiling against jets, resulting in a boosted topology.

The analysis is significantly affected by background from jets and electrons misidentified as photons, as well as by events reconstructed with large $p_{\mathrm{T}}^{\mathrm{miss}}$, due to mismeasurement or misreconstruction of physics objects (referred to as *fake* $p_{\mathrm{T}}^{\mathrm{miss}}$). In addition, in this signature both the photon and the $p_{\mathrm{T}}^{\mathrm{miss}}$ have no associated tracks, therefore the reconstruction of the PV is particularly challenging, since it relies exclusively on tracks originating from the underlying event and from additional jets. When the PV is misidentified, HS jets can be incorrectly classified as PU jets and consequently removed from $p_{\mathrm{T}}^{\mathrm{miss}}$ computation, thus enhancing the contribution from fake $p_{\mathrm{T}}^{\mathrm{miss}}$ background. The SM background events with similar signatures can be classified in the following categories.

- **Genuine photon**: $Z(\to \nu\nu)\gamma$ (irreducible background) or $W(\to \ell\nu)\gamma$ and $Z(\to \ell\ell)\gamma$ where the lepton(s) ℓ are not reconstructed. An additional contribution arises from γ+jets processes with a direct photon, γ(dir)+jets, with fake $p_{\mathrm{T}}^{\mathrm{miss}}$ originating primarily from lost or mismeasured jets.
- **Electrons misidentified as photons ($e \rightsquigarrow \gamma$)**: mostly $W(\to e\nu)$ + jets events.
- **Jets misidentified as photons ($j \rightsquigarrow \gamma$)**: dominantly multijets and γ+jets with a fragmentation photon (γ(frag)+jets) — in the latter, the photon is considered as $j \rightsquigarrow \gamma$,

JHEP10(2026)270

since it is embedded in a hadronic jet and therefore not isolated. Such events pass the analysis selections when associated with fake $p_{\mathrm{T}}^{\mathrm{miss}}$. A smaller contribution arises from $Z(\to \nu\nu)$+jets and $W(\to \ell\nu)$+jets processes.

7 Event selection

Events satisfying the trigger selections described in section 4 are further required to satisfy a set of offline requirements, designed to isolate the signal.

7.1 Baseline selection

Events are required to have exactly one selected photon with $p_{\mathrm{T}}^{\gamma} > 50$ GeV and no additional *baseline* photons, $p_{\mathrm{T}}^{\mathrm{miss}} > 100$ GeV, a transverse mass $m_{\mathrm{T}} > 80$ GeV, no *baseline* leptons nor b-tagged jets, and at most three central jets. Jet cleaning requirements [74] are applied to reject events with bad quality jets, which may arise from electronic noise or non-collision background. The veto on the b-tagged jets is applied to reduce the contribution from background processes with top quarks. The requirements on p_{T}^{γ} and m_{T} are aligned with the trigger thresholds, exploiting the fast trigger turn-on, while a more conservative requirement is applied to $p_{\mathrm{T}}^{\mathrm{miss}}$ as a compromise between signal acceptance and background rejection.

As discussed in section 6, low track activity can lead to an incorrect identification of the PV. This effect has a significant impact on $p_{\mathrm{T}}^{\mathrm{miss}}$-related observables, particularly when HS jets are misclassified as PU jets and consequently excluded from the $p_{\mathrm{T}}^{\mathrm{miss}}$ reconstruction. In such events, the reconstructed $p_{\mathrm{T}}^{\mathrm{miss}}$ distribution becomes artificially harder for γ+jets and multijets backgrounds and softer for the signal, enhancing background acceptance while reducing signal efficiency. Moreover, the PV misidentification distorts the transverse mass distribution, thereby degrading the signal-to-background discrimination, since the loss of HS jets results in a final state with one photon back-to-back with $p_{\mathrm{T}}^{\mathrm{miss}}$, for both signal and background events. This leads to values of m_{T} above 140 GeV, reflecting the p_{T}^{γ} and $p_{\mathrm{T}}^{\mathrm{miss}}$ thresholds of 50 GeV and 100 GeV, respectively. To mitigate this effect, a boosted decision tree (BDT) is trained on signal and background simulations using TMVA AdaBoost [78], to identify and reject events with a misidentified PV. This approach ensures a good control of the background modelling at the baseline selection level and, therefore, in all the analysis regions. The BDT uses information related to the reconstructed vertex properties, jet multiplicity, and the angular separation between the photon, jets, and $p_{\mathrm{T}}^{\mathrm{miss}}$, as summarised in table 3. The vertex BDT also further suppresses the contribution from non-collision background events with a photon. In particular, the position of the vertex inferred from the photon trajectory in the calorimeter (photon pointing) is used as one of the input variables, favouring events in which the photon originates from the PV. The distribution of the BDT score for events with correct and incorrect PV identification is shown in figure 3 for signal and background processes separately, confirming a good discriminating power. As highlighted in figure 4, a requirement on the misidentified vertex BDT score of $\mathrm{BDT}_{\mathrm{vertex}} > 0.1$ provides an almost complete suppression of events with a misidentified PV for both signal and background, especially when combined with the signal region (SR) selection described below. The efficiency of this selection for signal events, relative to the other baseline requirements, is approximately 55%, increasing to $\sim$ 95% in the SR. The

JHEP10(2026)270

Variable	Description
$\log\left(\sum p_{\mathrm{T}}^2(\text{tracks})\right)$	Logarithm of the sum of the squared transverse momenta of tracks associated with the vertex.
$\lvert\Delta\phi(\vec{p}_{\mathrm{vtx}}, \vec{p}_{\gamma})\rvert$	Azimuthal separation between the momentum of the tracks associated with the vertex and the photon direction.
$\lvert\Delta\phi(\vec{p}_{\mathrm{T}}^{\mathrm{miss}}, \vec{p}_{\mathrm{T}}^{j_1})\rvert$	Azimuthal separation between the missing transverse momentum and the leading jet.
$\lvert\Delta\phi(\mathrm{j}_1, \mathrm{j}_2)\rvert$	Azimuthal separation between the two leading jets.
$\Delta p_{\mathrm{T}}^{\mathrm{miss}}$	Difference between the missing transverse momentum computed without JVT requirements and the nominal reconstruction.
$\mathcal{S}_{p_{\mathrm{T}}^{\mathrm{miss}}}$	Significance of the missing transverse momentum.
$(z_{\mathrm{vtx}} - z_{\gamma})/\sigma(z_{\gamma})$	Distance along the longitudinal (z) axis between the reconstructed primary vertex and the vertex position inferred from the photon trajectory (photon pointing), normalised by the photon pointing resolution. The photon trajectory is reconstructed using its energy deposits in the first and second layer of the ECAL.
z_{skew}	Skewness of the z distribution of tracks associated with the vertex.
Number of central jets	Number of reconstructed jets in the central region ($\lvert\eta\rvert < 2.5$).
$(p_{\mathrm{T}}^{\mathrm{miss}} + p_{\mathrm{T}}^{\gamma})/\sum p_{\mathrm{T}}^{\mathrm{jet}}$	Transverse momentum balance between the photon+$p_{\mathrm{T}}^{\mathrm{miss}}$ system and the reconstructed jets.
z_{kurt}	Kurtosis of the z distribution of tracks associated with the vertex.

Table 3. Description of the input features of the misidentified vertex BDT, in order of importance.

$\mathrm{BDT}_{\mathrm{vertex}}$ distribution is validated in the main analysis regions defined below, as well as in a dedicated region with $m_{\mathrm{T}} > 200$ GeV and no leptons, enriched with $W\gamma$ and $Z\gamma$ processes with a topology similar to that of the signal. In all cases, good agreement between data and the background expectation is observed for $\mathrm{BDT}_{\mathrm{vertex}} > 0.1$, and the acceptance of this requirement is found to be consistent between data and the background prediction. Therefore, no systematic uncertainty is assigned to the $\mathrm{BDT}_{\mathrm{vertex}}$ selection.

JHEP10(2026)270

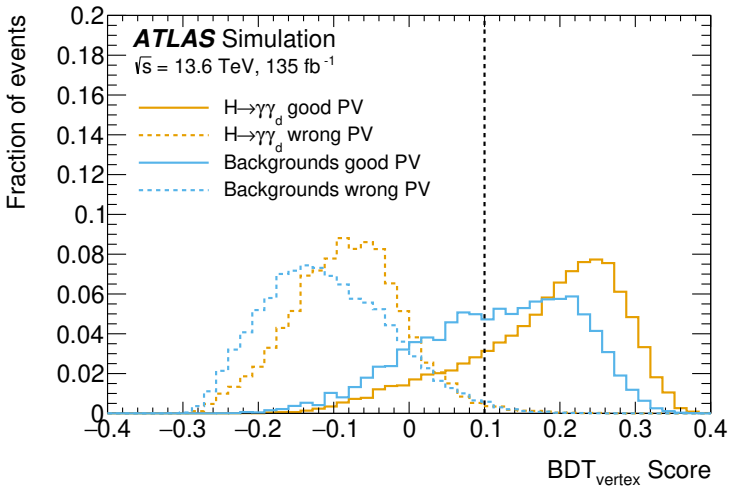


Figure 3. Normalised distributions of the $\mathrm{BDT}_{\mathrm{vertex}}$ score for events with correctly identified PV (solid line) and misidentified PV (dashed line). The distribution is shown for the sum of all signal channels and background processes. The vertical dashed line indicates the selection applied in the analysis.

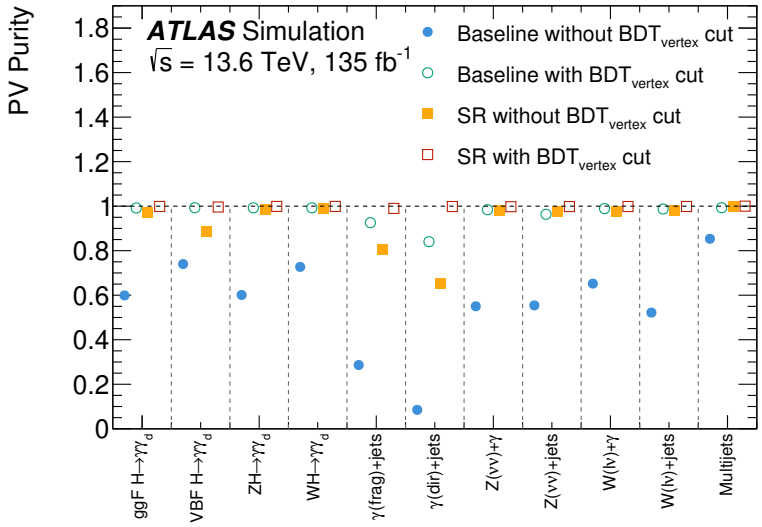


Figure 4. Fraction of events with the correct PV for the $H \to \gamma\gamma_{\mathrm{d}}$ signals and for different background processes, with different selections applied: the baseline selection and the SR, with and without the $\mathrm{BDT}_{\mathrm{vertex}}$ requirement.

7.2 Signal region

In addition to the *baseline* selection, the SR definition, summarised in table 4, includes requirements on the photon kinematics, angular separations between the photon, $p_{\mathrm{T}}^{\mathrm{miss}}$ and jets, as well as further $p_{\mathrm{T}}^{\mathrm{miss}}$-related variables. The latter include the $\mathcal{S}_{p_{\mathrm{T}}^{\mathrm{miss}}}$ and the difference $\Delta p_{\mathrm{T}}^{\mathrm{miss}} = p_{\mathrm{T,noJVT}}^{\mathrm{miss}} - p_{\mathrm{T}}^{\mathrm{miss}}$, where $p_{\mathrm{T,noJVT}}^{\mathrm{miss}}$ is defined in section 5. In particular, the requirement of $\mathcal{S}_{p_{\mathrm{T}}^{\mathrm{miss}}} > 6$ further suppresses events with *fake* $p_{\mathrm{T}}^{\mathrm{miss}}$, which typically exhibit lower significance values. Moreover, events are required to satisfy $\Delta p_{\mathrm{T}}^{\mathrm{miss}} > -10$ GeV to reduce

JHEP10(2026)270

Selection	SR	Low $\mathcal{S}_{p_{\mathrm{T}}^{\mathrm{miss}}}$ CR	1μ CR	2μ CR
Photon	1 (*selected*) with $p_{\mathrm{T}} > 50$ GeV			
$p_{\mathrm{T}}^{\mathrm{miss}}$	> 100 GeV			
m_{T}	> 80 GeV			
$\mathrm{BDT}_{\mathrm{vertex}}$	> 0.1			
$N_{e,\tau}$	0 (*baseline*)			
$N_{b\text{-jets}}$	0			
$N_{\mathrm{jet}}^{\mathrm{central}}$	≤ 3			—
N_{μ}	0 (*baseline*)		1 (*selected*)	2 (*selected*)
$\mathcal{S}_{p_{\mathrm{T}}^{\mathrm{miss}}}$	> 6	$[2, 6]$	> 6	—
$\lvert\Delta\phi(\vec{p}_{\mathrm{T}}^{\mathrm{miss}}, \vec{p}_{\mathrm{T}}^{\mathrm{miss},\gamma})\rvert$	> 1.25			
$\Delta p_{\mathrm{T}}^{\mathrm{miss}}$	> -10 GeV			—
$\lvert\Delta\phi(\vec{p}_{\mathrm{T}}^{\mathrm{miss}}, \vec{p}_{\mathrm{T}}^{\mathrm{miss,jet}})\rvert$	< 0.75			—
$\lvert\Delta\phi(j_1, j_2)\rvert$	< 2.5			—
$\lvert\eta^{\gamma}\rvert$	< 1.75			—
$m_{\mu\mu\gamma}$	—			> 100 GeV

Table 4. Summary of the selections applied in the signal (SR) and control (CR) regions. In the CRs with muons, the $p_{\mathrm{T}}^{\mathrm{miss}}$ is recomputed treating muons as invisible particles.

the contribution from incorrect PV identification. If a PU vertex is identified as the HS one, the standard $p_{\mathrm{T}}^{\mathrm{miss}}$ computation rejects the HS jets while retaining PU jets. In this scenario, the $p_{\mathrm{T,noJVT}}^{\mathrm{miss}}$ is expected to be closer to the true $p_{\mathrm{T}}^{\mathrm{miss}}$ than the standard reconstruction, resulting in negative $\Delta p_{\mathrm{T}}^{\mathrm{miss}}$ values for events with no expected true $p_{\mathrm{T}}^{\mathrm{miss}}$. Additionally, restricting the photon pseudorapidity to $|\eta_{\gamma}| < 1.75$ reduces background contributions from $W/Z + \gamma$ processes. Further requirements $|\Delta\phi(\vec{p}_{\mathrm{T}}^{\mathrm{miss}}, \vec{p}_{\mathrm{T}}^{\mathrm{miss},\gamma})| > 1.25$ and $|\Delta\phi(\vec{p}_{\mathrm{T}}^{\mathrm{miss}}, \vec{p}_{\mathrm{T}}^{\mathrm{miss,jet}})| < 0.75$ are imposed on the azimuthal separation between the $\vec{p}_{\mathrm{T}}^{\mathrm{miss}}$ and its photon or jet term, $\vec{p}_{\mathrm{T}}^{\mathrm{miss},\gamma}$ and $\vec{p}_{\mathrm{T}}^{\mathrm{miss,jet}}$ (i.e. the negative vector sum of the $\vec{p}_{\mathrm{T}}$ of all photons or jets in the event). The selection on $|\Delta\phi(\vec{p}_{\mathrm{T}}^{\mathrm{miss}}, \vec{p}_{\mathrm{T}}^{\mathrm{miss},\gamma})|$ is particularly effective in rejecting residual background from events with a misidentified PV while preserving the acceptance of the boosted Higgs boson signal. Finally the azimuthal separation between the two central jets with the highest p_{T} is required to be $|\Delta\phi(j_1, j_2)| < 2.5$.

The signal selection efficiency is 0.25% for the ggF channel, and 1.06%, 1.25% and 0.66% for the VBF, WH, and ZH channels, respectively. The largest efficiency loss is due to the trigger decision, followed by the $p_{\mathrm{T}}^{\mathrm{miss}}$ selection, which retains 15% of the events selected by the trigger. The dominant Higgs boson production mode is ggF (68% of the selected signal events), followed by VBF (23%), WH (6%) and ZH (3%).

8 Analysis strategy and background modelling

In addition to the SR, multiple orthogonal regions illustrated in figure 5, are used in the analysis. Three Control Regions (CRs), enriched in $W\gamma$, $Z\gamma$ and $j \rightsquigarrow \gamma$ contributions and defined in table 4, are used to constrain the corresponding backgrounds in a maximum-

JHEP10(2026)270

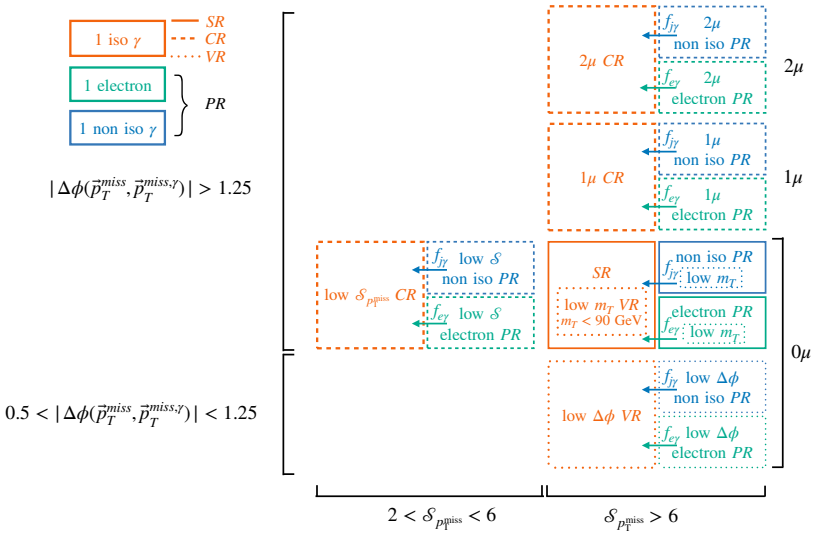


Figure 5. Schematic overview of the signal (SR), control (CR), validation (VR) and probe (PR) regions used in the analysis. Different colours correspond to different final states. Events with one isolated (iso) photon are selected in the SR (continuous lines), CRs (dashed lines) and VRs (dotted lines), while events with a single electron or non isolated photon are used for the corresponding PRs. Data in the PRs are scaled by the fake factors indicated by the arrows ($f_{e\gamma}$ and $f_{j\gamma}$) to estimate the $j \rightsquigarrow \gamma$ and $e \rightsquigarrow \gamma$ contribution in each analysis region.

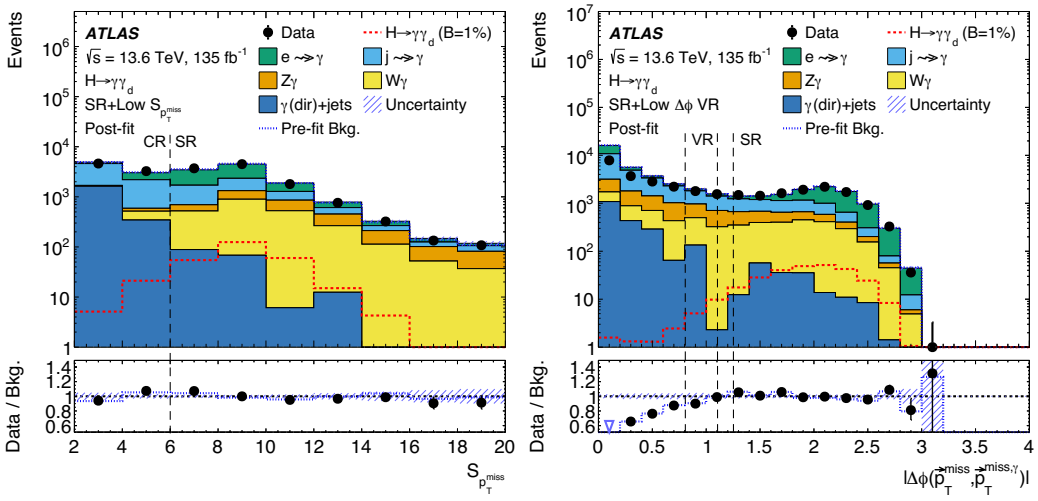
likelihood fit. Validation Regions (VRs), designed to be kinematically close to the SR, are used to validate the modelling of $j \rightsquigarrow \gamma$ and $e \rightsquigarrow \gamma$. In addition, dedicated regions, referred to as Probe Regions (PRs), are employed for the $j \rightsquigarrow \gamma$ and $e \rightsquigarrow \gamma$ data-driven estimates as detailed later.

The 1μ CR and the 2μ CR are employed to normalise the MC simulations of $W\gamma$ and $Z\gamma$ respectively to data. They are defined in a similar way to the SR, but requiring either one or two selected muons. To emulate the SR kinematics, muons are treated as invisible in the $p_{\mathrm{T}}^{\mathrm{miss}}$ reconstruction. In the 2μ CR, some of the SR requirements, as detailed in table 4 are removed to increase the available number of events. The contribution from the γ(dir)+jets background due to fake $p_{\mathrm{T}}^{\mathrm{miss}}$ is estimated purely from MC, as it accounts for about 2% of the total.

The background from $e \rightsquigarrow \gamma$ or $j \rightsquigarrow \gamma$ is estimated in all the analysis regions by rescaling data in PRs, by fake factors evaluated as described in sections 8.1 and 8.2. For the $e \rightsquigarrow \gamma$ background, electron PRs are defined for each analysis region, replacing the selected photon by a selected electron, and an electron trigger is also required, for consistency with the evaluation of the $e \rightsquigarrow \gamma$ fake factors, as explained in section 8.1. For the $j \rightsquigarrow \gamma$ background, PRs with a non-isolated photon, $\gamma^{\mathrm{non-isol}}$, are introduced by requiring $\Upsilon > 0.1$, in order to ensure a negligible contamination from genuine photons.

Due to the large systematic uncertainty affecting the $j \rightsquigarrow \gamma$ component, the low $\mathcal{S}_{p_{\mathrm{T}}^{\mathrm{miss}}}$ CR, defined by requiring $2 < \mathcal{S}_{p_{\mathrm{T}}^{\mathrm{miss}}} < 6$, is included in the fit to provide an additional constraint on this background. The post-fit $\mathcal{S}_{p_{\mathrm{T}}^{\mathrm{miss}}}$ distribution is shown in figure 6(a), with the dashed line

JHEP10(2026)270



(a) (b)

Figure 6. Post-fit distributions of (a) $\mathcal{S}_{p_{\mathrm{T}}^{\mathrm{miss}}}$ in the signal region (SR) and low-$\mathcal{S}_{p_{\mathrm{T}}^{\mathrm{miss}}}$ control region (CR), and of (b) $|\Delta\phi(\vec{p}_{\mathrm{T}}^{\,\mathrm{miss}}, \vec{p}_{\mathrm{T}}^{\,\mathrm{miss},\gamma})|$ in the SR and low-$\Delta\phi$ validation region (VR), for data and the expected SM background. The dashed vertical lines mark the boundaries of the SR and the CR/VR. The $H \to \gamma\gamma_{\mathrm{d}}$ signal, assuming $\mathcal{B}_{\gamma\gamma_{\mathrm{d}}} = 1\%$, is overlaid as a dotted line and includes the ggF, VBF, WH, and ZH production modes. The pre-fit prediction is overlaid as a dashed line. The uncertainties include both the statistical and the systematic components. The lower panels show the ratios of data to expected background yields post-fit (dots) and pre-fit (dotted line). The downward-pointing triangle marks a ratio point located below the bottom edge of the ratio plot.

highlighting the boundary between the low $\mathcal{S}_{p_{\mathrm{T}}^{\mathrm{miss}}}$ CR and the SR. The $e \rightsquigarrow \gamma$ contribution is further constrained in the low m_{T} region of the SR that is dominated by $W(e\nu)$+jets events with the electron being misidentified as a photon, yielding a m_{T} value close to the W-boson mass. In particular, the low m_{T} VR, with $80 < m_{\mathrm{T}} < 90$ GeV, has very little signal, and is also used to validate the $e \rightsquigarrow \gamma$ background before performing the fit. In addition, a low $\Delta\phi$ VR, with $0.8 < |\Delta\phi(\vec{p}_{\mathrm{T}}^{\,\mathrm{miss}}, \vec{p}_{\mathrm{T}}^{\,\mathrm{miss},\gamma})| < 1.1$, provides a sample orthogonal both to the SR and the low $\mathcal{S}_{p_{\mathrm{T}}^{\mathrm{miss}}}$ CR to also validate the modelling of the $j \rightsquigarrow \gamma$ background at high $\mathcal{S}_{p_{\mathrm{T}}^{\mathrm{miss}}}$ values. Figure 6(b) shows the post-fit $|\Delta\phi(\vec{p}_{\mathrm{T}}^{\,\mathrm{miss}}, \vec{p}_{\mathrm{T}}^{\,\mathrm{miss},\gamma})|$ distribution for events passing all the SR requirements except for the $|\Delta\phi(\vec{p}_{\mathrm{T}}^{\,\mathrm{miss}}, \vec{p}_{\mathrm{T}}^{\,\mathrm{miss},\gamma})|$ one, highlighting the SR and low $\Delta\phi$ VR boundaries with dashed vertical lines. This observable is particularly sensitive to PV misidentification at low values, which corresponds to events with low p_{T} or no jets, where the photon and the $p_{\mathrm{T}}^{\mathrm{miss}}$ are nearly back-to-back. A residual mismodelling in this region is therefore expected even after applying the $\mathrm{BDT}_{\mathrm{vertex}}$ requirement, primarily due to events with a correct PV being misclassified by the BDT as an incorrect PV. Despite this, the agreement is relatively good and it improves with increasing $|\Delta\phi(\vec{p}_{\mathrm{T}}^{\,\mathrm{miss}}, \vec{p}_{\mathrm{T}}^{\,\mathrm{miss},\gamma})|$ values, as expected.

8.1 Estimation of $e \rightsquigarrow \gamma$

The fake factor for $e \rightsquigarrow \gamma$ estimation is defined as:

$$f_{e\gamma} = \frac{N(e \rightsquigarrow \gamma)}{N(e \rightsquigarrow e)}, \tag{8.1}$$

JHEP10(2026)270

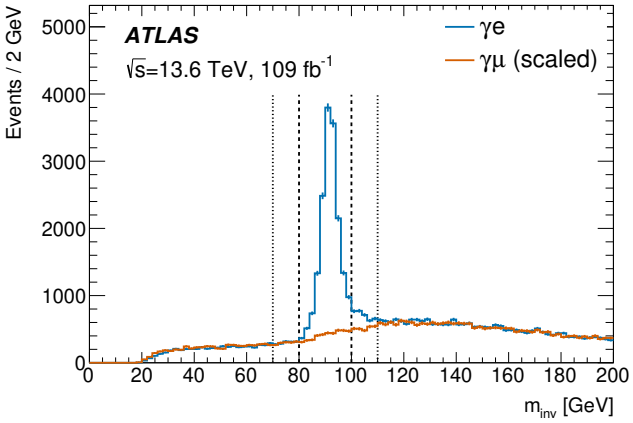


Figure 7. Invariant mass of reconstructed γe and $\gamma\mu$ pairs from data, the latter being rescaled so that its sidebands match those of the former. The vertical dashed lines show the window used to compute $f_{e\gamma}$, while the vertical dotted lines mark the sidebands used for the normalisation of the $\gamma\mu$ distribution. Plots are inclusive in p_{T}^{γ} and η^{γ}, and show only data taken in 2024. Similar plots are obtained from 2023 data.

where $N(e \rightsquigarrow \gamma)$ and $N(e \rightsquigarrow e)$ denote respectively the numbers of electrons reconstructed as photons or as electrons. The values of the $f_{e\gamma}$ are computed directly from data, exploiting the $Z \to e^+e^-$ process, where prompt isolated photons are absent. While $N(e \rightsquigarrow \gamma)$ is counted from reconstructed photons in γe events selected by a single electron trigger, $N(e \rightsquigarrow e)$ is counted from both e^+ and e^- in e^+e^- events selected by a dielectron trigger. Both numbers are calculated in an invariant mass window $m_{\mathrm{inv}} \in [80, 100]$ GeV around the Z peak, m_{inv} being the invariant mass of the γe or the e^+e^- pair.

While the e^+e^- events provide a rather pure sample of $Z \to e^+e^-$, the γe events contain a large number of genuine photons, mostly from the $W(\to e\nu)\gamma$ process, which must be subtracted. This is achieved by exploiting lepton universality, and selecting a sample of $\gamma\mu$ events. To account for the different reconstruction efficiency for e and μ, the invariant mass spectrum of the $\gamma\mu$ events is normalised to that of the γe in two sidebands $m_{\mathrm{inv}} < 70$ GeV and $m_{\mathrm{inv}} > 110$ GeV, as displayed in figure 7. The complete definition of the fake factor is therefore:

$$f_{e\gamma} = \frac{N_{\gamma e}^{\mathrm{peak}} - N_{\gamma\mu}^{\mathrm{peak}} \dfrac{N_{\gamma e}^{\mathrm{side}}}{N_{\gamma\mu}^{\mathrm{side}}}}{N_{ee}^{\mathrm{peak}}}. \tag{8.2}$$

The value of $f_{e\gamma}$ is computed separately for 2023 and 2024 datasets as a function of η^{γ}, since no significant dependence on p_{T}^{γ} is observed. The values of $f_{e\gamma}$ are weakly dependent on the choice of the peak width and on the sidebands. Each variation is treated as a systematic uncertainty, and are all combined in quadrature with the statistical uncertainty. The values of $f_{e\gamma}$ range between ~ 0.027 in the barrel and ~ 0.054 in the endcaps, with overall relative uncertainties between 3% and 8%.

The e-PR must satisfy both the analysis trigger, to guarantee the same event topology as the SR and CRs, and the electron trigger, for consistency with the $f_{e\gamma}$ evaluation. However,

JHEP10(2026)270

the $f_{e\gamma}$ evaluation does not consider the analysis trigger, therefore a further correction is necessary, to account for the efficiency of the analysis trigger on reconstructed γ and e:

$$f_{e\gamma}^{\text{corr}} = f_{e\gamma} \frac{\epsilon_{\gamma}^{\text{trig}}}{\epsilon_{e}^{\text{trig}}}, \tag{8.3}$$

where $\epsilon_{\gamma}^{\text{trig}}$ and $\epsilon_{e}^{\text{trig}}$ are the fraction of events that pass the analysis trigger, in events containing a genuine photon (SR-like) and a genuine electron (e-PR-like) respectively. The only trigger requirement affecting the evaluation of $f_{e\gamma}$ is that on the reconstructed photon, therefore the effects of the $p_{\text{T}}^{\text{miss}}$ and m_{T} selections need to be disentangled. This is achieved by applying offline cuts on $p_{\text{T}}^{\text{miss}}$ and m_{T} higher than the trigger-level cuts, to ensure being in the plateau of the trigger efficiency turn-on curves. To evaluate $\epsilon_{\gamma}^{\text{trig}}$, $\gamma\mu$ events were selected by a muon trigger. The muon is treated as invisible in the offline evaluation of $p_{\text{T}}^{\text{miss}}$, and $(p_{\text{T}}^{\text{miss}})^{\mu\text{-inv}} > 150$ GeV and $(m_{\text{T}})^{\mu\text{-inv}} > 100$ GeV are required. The trigger-level evaluation of $p_{\text{T}}^{\text{miss}}$ does not consider muons, therefore they are also treated as invisible by the analysis trigger. The fraction of events that satisfy the analysis trigger criteria provides the value of $\epsilon_{\gamma}^{\text{trig}}$. Similarly, $\epsilon_{e}^{\text{trig}}$ is evaluated on events with an electron, selected from data by an electron trigger, and fulfilling $p_{\text{T}}^{\text{miss}} > 200$ GeV and $m_{\text{T}} > 100$ GeV. The fraction of events that satisfy the analysis trigger criteria provides the value of $\epsilon_{e}^{\text{trig}}$. Both $\epsilon_{\gamma}^{\text{trig}}$ and $\epsilon_{e}^{\text{trig}}$ are computed as a function of p_{T}, to better track the trigger efficiency turn-on. While $\epsilon_{\gamma}^{\text{trig}}$ reaches full efficiency for $p_{\text{T}} > 60$ GeV, $\epsilon_{e}^{\text{trig}}$ saturates at about 90%, as the photon trigger is not fully optimal for electrons. The variations of $\epsilon_{\gamma}^{\text{trig}}$ and $\epsilon_{e}^{\text{trig}}$ when applying different cuts on $p_{\text{T}}^{\text{miss}}$ and m_{T} are treated as systematic uncertainties and combined in quadrature. The resulting trigger correction factor is between 1.06 and 1.26 with an overall relative uncertainty between 3% and 12%.

The validation of the $e \rightsquigarrow \gamma$ background in the low m_{T} VR is displayed in figure 8, showing good agreement before the fit.

8.2 Estimation of $j \rightsquigarrow \gamma$

The $j \rightsquigarrow \gamma$ fake factor is defined as

$$f_{j\gamma} = \frac{N(j \rightsquigarrow \gamma)}{N(j \rightsquigarrow \gamma^{\text{non-isol}})}, \tag{8.4}$$

where $N(j \rightsquigarrow \gamma)$ and $N(j \rightsquigarrow \gamma^{\text{non-isol}})$ denote the numbers of jets reconstructed as isolated or non-isolated photons, respectively. Isolated and non-isolated reconstructed photons are defined by requiring isolation $\Upsilon < 0.022$ and $\Upsilon > 0.1$, respectively. The evaluation of the fake factor relies on the distribution of the isolation for $j \rightsquigarrow \gamma$ satisfying the `Tight` identification, $\Phi^{\texttt{Tight}}(\Upsilon)$, and is calculated as:

$$f_{j\gamma} = \frac{\int_{-\infty}^{+0.022} \mathrm{d}\Upsilon \, \Phi^{\texttt{Tight}}(\Upsilon)}{\int_{+0.1}^{+\infty} \mathrm{d}\Upsilon \, \Phi^{\texttt{Tight}}(\Upsilon)}. \tag{8.5}$$

The $\Phi^{\texttt{Tight}}(\Upsilon)$ distribution cannot be directly extracted from data, as the `Tight` photon selection contains comparable contributions from $j \rightsquigarrow \gamma$ and genuine photons. Moreover, $\Phi^{\texttt{Tight}}(\Upsilon)$ is not well modelled by the MC, and depends on the MC generator used. Therefore

JHEP10(2026)270

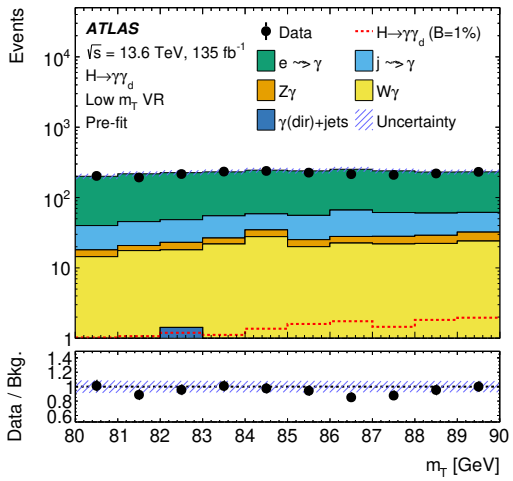


Figure 8. Pre-fit distribution of m_{T} for data and the expected SM background in the low-m_{T} VR. The $H \to \gamma\gamma_{\mathrm{d}}$ signal, assuming $\mathcal{B}_{\gamma\gamma_{\mathrm{d}}} = 1\%$, is overlaid as a dashed line and includes the ggF, VBF, WH, and ZH production modes. The uncertainties include both statistical and systematic components. The lower panel shows the ratio of data to expected background yields.

$\Phi^{\texttt{Tight}}(\Upsilon)$ has to be inferred, as explained in the following. Photons satisfying the $\texttt{Loose}'$ selection[2] (see section 5) are enriched in $j \rightsquigarrow \gamma$, therefore the isolation distribution $\Phi^{\texttt{Loose}'}(\Upsilon)$ of $j \rightsquigarrow \gamma$ in the $\texttt{Loose}'$ selection can be extracted from data. However, the photon selection affects the isolation, making $\Phi^{\texttt{Loose}'}$ broader than $\Phi^{\texttt{Tight}}$. To infer $\Phi^{\texttt{Tight}}$ from $\Phi^{\texttt{Loose}'}$, an affine transform is applied to the Υ of all $\texttt{Loose}'$ photons:

$$\Upsilon^{\texttt{Tight}} = m^{\texttt{Tight}} + \frac{w^{\texttt{Tight}}}{w^{\texttt{Loose}'}} \left(\Upsilon^{\texttt{Loose}'} - m^{\texttt{Loose}'} \right), \tag{8.6}$$

then all the obtained values of $\Upsilon^{\texttt{Tight}}$ are used to build $\Phi^{\texttt{Tight}}$. In eq. (8.6), m and w are the median and the 16%-to-84% half-width of the isolation distributions in the $\texttt{Loose}'$ and $\texttt{Tight}$ samples. While $m^{\texttt{Loose}'}$ and $w^{\texttt{Loose}'}$ can be computed from the observed $\Phi^{\texttt{Loose}'}$ in data, $m^{\texttt{Tight}}$ and $w^{\texttt{Tight}}$ are inferred, with the help of $j \rightsquigarrow \gamma$ from W+jets and Z+jets MC samples, assuming that

$$\left(\frac{m^{\texttt{Tight}} - m^{\texttt{Loose}'}}{w^{\texttt{Loose}'}} \right) = R_m \left(\frac{m^{\texttt{Tight}}_{\mathrm{MC}} - m^{\texttt{Loose}'}_{\mathrm{MC}}}{w^{\texttt{Loose}'}_{\mathrm{MC}}} \right), \qquad \left(\frac{w^{\texttt{Tight}}}{w^{\texttt{Loose}'}} \right) = R_w \left(\frac{w^{\texttt{Tight}}_{\mathrm{MC}}}{w^{\texttt{Loose}'}_{\mathrm{MC}}} \right), \tag{8.7}$$

where $m^{\texttt{Tight}}_{\mathrm{MC}}$, $m^{\texttt{Loose}'}_{\mathrm{MC}}$, $w^{\texttt{Tight}}_{\mathrm{MC}}$, $w^{\texttt{Loose}'}_{\mathrm{MC}}$ are extracted from the Z+jets and W+jets MC samples. The values of R_m and R_w are estimated by exploiting the various $\texttt{Loose}''$ photon selections (see section 5), which are closer to the $\texttt{Tight}$ selection. The $\texttt{Loose}''$ selections in data are still dominated by $j \rightsquigarrow \gamma$, therefore $m^{\texttt{Loose}''}$ and $w^{\texttt{Loose}''}$ (i.e. the median and half-width in the $\texttt{Loose}''$ selection) can be evaluated in data from the observed $\Phi^{\texttt{Loose}''}$, and eq. (8.7) can be used with each of the $\texttt{Loose}''$ instead of the $\texttt{Tight}$ selection, to derive R_m and

[2] $\texttt{Loose}'$ photons are selected in events satisfying the analysis trigger. This is possible, as the $\texttt{Tight}$ selection at trigger level is looser than at analysis level. The contamination of genuine photons in the $\texttt{Loose}'$ sample is estimated to be $\lesssim 5\%$, from simulations.

JHEP10(2026)270

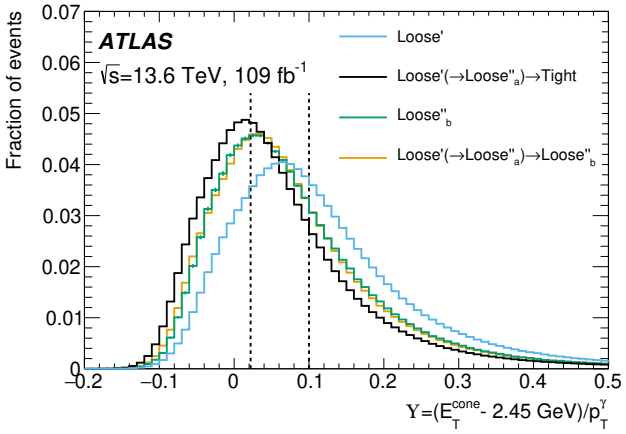


Figure 9. Distributions of the isolation $\Upsilon = (E_T^{\text{cone}} - 2.45\ \text{GeV})/p_T^{\gamma}$ for reconstructed photons, used for the $j \rightsquigarrow \gamma$ background estimate. The figure displays the distribution from the $\texttt{Loose}'$ photon sample (enriched in $j \rightsquigarrow \gamma$), and an example of extrapolated distribution for the $\texttt{Tight}$ sample ($\texttt{Loose}'(\rightarrow \texttt{Loose}''_{\text{a}}) \rightarrow \texttt{Tight}$), using a $\texttt{Loose}''_{\text{a}}$ sample to compute R_m and R_w. The two dashed vertical lines mark the 'isolated' ($\Upsilon < 0.022$) and the 'non-isolated' ($\Upsilon > 0.1$) regions. Plots are inclusive in p_{T}^{γ} and η^{γ}, and show only data taken in 2024. Similar plots are obtained from 2023 data. The figure also shows the observed and extrapolated distributions for a different $\texttt{Loose}''_{\text{b}}$ sample.

R_w. Different choices of $\texttt{Loose}''$ selections (labelled $\texttt{Loose}''_{\text{a}}$ in the following, where a flags the different definitions) provide different values of R_m and R_w, and therefore different $\Phi_{\text{a}}^{\texttt{Tight}}(\Upsilon)$. Since each of the $\texttt{Loose}''$ selections is obtained by applying at most one requirement on one of the strips shower shapes, this procedure allows the effect of one strips shower shape at a time to be probed in the $\texttt{Loose}' \rightarrow \texttt{Tight}$ extrapolation.

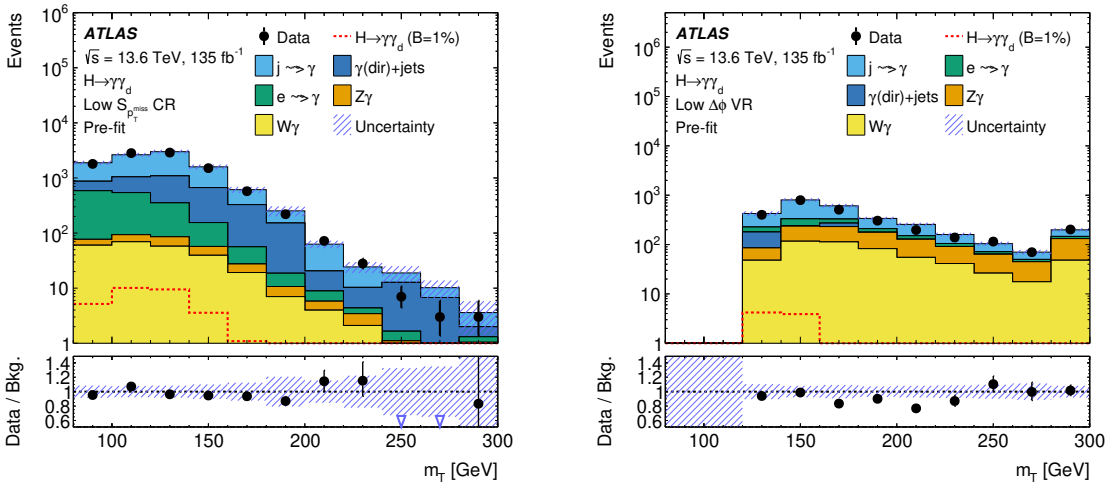
In summary, the affine transform of eq. (8.6) depends on the R_m and R_w parameters. These are evaluated to achieve a $\texttt{Loose}' \rightarrow \texttt{Loose}''_{\text{a}}$ extrapolation that reproduces at best the observed $\texttt{Loose}''_{\text{a}}$ sample, and are then applied to the $\texttt{Loose}' \rightarrow \texttt{Tight}$ extrapolation. This process is symbolised as $\texttt{Loose}'(\rightarrow \texttt{Loose}''_{\text{a}}) \rightarrow \texttt{Tight}$, and provides an extrapolated distribution $\Phi_{\text{a}}^{\texttt{Tight}}(\Upsilon)$. The observed isolation distribution for $\texttt{Loose}'$ photons and one of the extrapolated distributions for $\texttt{Tight}$ photons are displayed in figure 9. The reliability of the extrapolation is validated by comparing several extrapolated distributions $\texttt{Loose}'(\rightarrow \texttt{Loose}''_{\text{a}}) \rightarrow \texttt{Loose}''_{\text{b}}$ with the observed $\texttt{Loose}''_{\text{b}}$ ones. An example is shown in figure 9.

For each extrapolated distribution $\Phi_{\text{a}}^{\texttt{Tight}}(\Upsilon)$, a different fake factor $(f_{j\gamma})_{\text{a}}$ is computed. The final fake factor is computed as the arithmetic mean of all $(f_{j\gamma})_{\text{a}}$, and a conservative systematic uncertainty is set as half the envelope of all their values.

The fake factor is computed separately for 2023 and 2024 datasets as a function of η^{γ}. The limited number of MC events prohibits studying its dependence on p_{T}^{γ}. The values of $f_{j\gamma}$ range from ~ 1.5 in the ECAL barrel, up to ~ 2.5 in the endcaps, with relative uncertainties between 10% and 15%.

The obtained $j \rightsquigarrow \gamma$ prediction is validated, before the fit, in both the low $\mathcal{S}_{p_{\text{T}}^{\text{miss}}}$ CR and the low $\Delta\phi$ VR, as shown in figure 10.

JHEP10(2026)270



(a) (b)

Figure 10. Pre-fit distribution of m_{T} for data and the expected SM background in (a) the low $\mathcal{S}_{p_{\mathrm{T}}^{\mathrm{miss}}}$ CR and (b) the low $\Delta\phi$ VR, enriched in $j \rightsquigarrow \gamma$. The $H \to \gamma\gamma_{\mathrm{d}}$ signal, assuming $\mathcal{B}_{\gamma\gamma_{\mathrm{d}}} = 1\%$, is overlaid as a dashed line and includes the ggF, VBF, WH, and ZH production modes. The uncertainties include both statistical and systematic components. The lower panel shows the ratio of data to expected background yields. The downward-pointing triangles mark ratio points located below the bottom edge of the ratio plot.

9 Systematic uncertainties

Multiple sources of systematic uncertainty are considered in the analysis. The experimental and theoretical uncertainties are applied only to the MC simulations of the signal and $V\gamma$ background, while their impact on the γ(dir)+jets simulation is expected to be negligible compared to its statistical fluctuations. Additional systematic uncertainties arise from the data-driven background estimates. The impact of the different sources of uncertainty in the fitted value of $\mathcal{B}_{\gamma\gamma_{\mathrm{d}}}$ is summarised in table 5. The contributions are evaluated using the covariance matrix decomposition method [79] and include both statistical and systematic components. The dominant contribution to the total uncertainty arises from the statistical component (88%), including contributions from both the data and the background. The dominant systematic contribution arises from experimental uncertainties (42%), primarily driven by jet-related effects. This is followed by uncertainties associated with the $e \rightsquigarrow \gamma$ and $j \rightsquigarrow \gamma$ data-driven methods (17%), and by theoretical uncertainties (17%).

9.1 Experimental uncertainties

The uncertainty in the integrated luminosity is 1.9%, derived from the calibration of the LUCID-2 detector and complemented by information from the ID and the calorimeters [33]. This uncertainty is applied as a global normalisation uncertainty to all MC samples, including both signal and background processes. A systematic uncertainty is associated with the pileup reweighting procedure applied to simulated events to correct for mismodelling of PU interactions in simulation.

JHEP10(2026)270

Category	Contribution to uncertainty in the $\mathcal{B}_{\gamma\gamma_d}$
Statistical uncertainties	88%
Data	74%
Background	48%
Experimental systematic uncertainties	42%
Luminosity	4.6%
Pile-up reweighting	7%
Pile-up corrections in jets calibration	36%
Jets	18%
Photons	3.7%
Muons	2.1%
$p_{\mathrm{T}}^{\mathrm{miss}}$	<1%
Trigger	<1%
Systematic on data-driven methods uncertainties	17%
$j \rightsquigarrow \gamma$	11%
$e \rightsquigarrow \gamma$	13%
Theoretical systematic uncertainties	17%

Table 5. Post-fit relative impact of each source of uncertainty on the total uncertainty of the signal yields, as obtained through the covariance matrix decomposition method. The overall impacts of statistical, experimental, data-driven and theoretical systematic uncertainties are shown, followed by the individual contributions.

Further uncertainties are associated with the reconstruction and isolation efficiency and with the energy calibration and resolution of photons, muons and jets. Photon efficiency uncertainties are estimated by using Run 2 data and MC simulations [68], with an additional uncertainty included to account for differences between Run 2 and Run 3, as derived from simulation. The uncertainties related to photon energy calibration and resolution are evaluated following the methodology described in ref. [80], using the Run 3 data collected between 2022 and 2024. All contributions are summed in quadrature and considered fully correlated in photon η, resulting in one systematic uncertainty associated with the energy calibration, and one with the energy resolution.

Multiple sources of uncertainties are considered for muons. The uncertainties affecting the muon momentum scale and resolution are separated into charge-dependent and charge-independent components [65]. Additional uncertainties are associated with muon reconstruction and isolation efficiencies, as well as with the track-to-vertex association efficiency, each of which is split into statistical and systematic components [66].

Jet reconstruction is affected by uncertainties related to jet vertex tagging and to the jet energy scale (JES) and resolution (JER). The uncertainty in the NN-JVT and fJVT calibrations [71, 72] is derived from $Z \to \mu\mu$ and $Z \to ee$ events in 2022–2023 data and is dominated by PU modelling uncertainties, particularly at low p_{T}. The JES and JER uncertainties [59, 81, 82] include contributions from area subtraction, PU residual corrections, absolute energy scale, and global sequential calibration [83], and are evaluated using Run 3 MC simulations. The uncertainty in the in situ calibration is derived from Run 2 data, with

JHEP10(2026)270

an additional uncertainty included to cover differences between Run 2 and Run 3. Further uncertainties account for residual effects related to variations in the vertexing algorithm, calorimeter noise thresholds, and modelling differences in the forward calorimeter region. Among these systematic uncertainties, the dominant contribution arises from PU residual corrections, which is quoted separately in table 5. An additional jet-related source of systematic uncertainty arises from flavour tagging [84].

The $p_{\mathrm{T}}^{\mathrm{miss}}$ is affected by three sources of systematic uncertainty [76, 85], related to the modelling of its soft term and evaluated using Run 3 data collected in 2022–2023 and the corresponding MC simulations. One scale uncertainty is obtained by scaling up and down the parallel projection of the soft-term along the hard-term, while two resolution uncertainties are derived by smearing the parallel and perpendicular projections of the soft-term along the hard-term.

Finally, a systematic uncertainty is assigned to the trigger efficiency, as described in section 4, to account for the observed discrepancy between data and MC simulations in the trigger efficiency curves.

9.2 Uncertainties in data-driven methods

Three additional sources of systematic uncertainty are associated with the data-driven estimates of the $e \rightsquigarrow \gamma$ and $j \rightsquigarrow \gamma$ backgrounds. As described in section 8.1, for the $e \rightsquigarrow \gamma$ background, one systematic uncertainty accounts for the dependence of the $f_{e\gamma}$ fake factor on the peak width and the definition of the sidebands, while the second contribution is associated with the trigger correction factors. The third data-driven systematic uncertainty is associated with the extrapolation from $\Phi^{\texttt{Loose}'}$ to $\Phi^{\texttt{Tight}}$ in the $j \rightsquigarrow \gamma$ estimation, as described in section 8.2.

9.3 Theoretical uncertainties

Theoretical uncertainties related to the modelling of quantum chromodynamics (QCD) effects are considered for background and signal MC samples, arising from variations of the renormalisation and factorisation scales, the value of the strong coupling constant, and the PDF uncertainties. The latter are evaluated following the PDF4LHC21 prescription [44]. The uncertainty associated with missing higher-order corrections is evaluated by independently varying the renormalisation and factorisation scales by factors of 0.5 and 2.0 relative to their nominal values and taking the envelope of the resulting variations, while the uncertainty related to the strong coupling constant α_{s} is obtained by varying its value by ± 0.001.

10 Statistical treatment and results

To maximise the sensitivity to the Higgs boson mass peak, the transverse mass m_{T} is used as the discriminating variable in the binned maximum-likelihood fit in all regions, except for the 2μ CR, which is treated as a single inclusive bin due to limited statistical precision. The m_{T} binning is optimised such that the bulk of the expected signal is contained in the two central bins, defined as $110 < m_{\mathrm{T}} < 140$ GeV and $140 < m_{\mathrm{T}} < 200$ GeV, while the lower and upper bins provide additional constraints on the background normalisation. In particular, the first bin ($80 < m_{\mathrm{T}} < 110$ GeV) contains the low-m_{T} VR and is dominated by the $e \rightsquigarrow \gamma$

JHEP10(2026)270

	SR	low $\mathcal{S}_{E_{\mathrm{T}}^{\mathrm{miss}}}$ CR	1 μ CR	2 μ CR
Pre-fit ggF $H \to \gamma\gamma_{\mathrm{d}}$	166 ± 24	18.2 ± 4.9	–	–
Pre-fit VBF $H \to \gamma\gamma_{\mathrm{d}}$	56.9 ± 5.7	9.6 ± 1.6	–	–
Pre-fit WH $H \to \gamma\gamma_{\mathrm{d}}$	14.7 ± 1.4	1.41 ± 0.31	0.149 ± 0.018	–
Pre-fit ZH $H \to \gamma\gamma_{\mathrm{d}}$	8.19 ± 0.85	0.72 ± 0.19	0.0073 ± 0.0075	0.0249 ± 0.0097
$Z\gamma$	1332 ± 90	95 ± 21	120 ± 8.8	412 ± 25
$W\gamma$	2253 ± 68	224 ± 55	3635 ± 80	0.677 ± 0.058
$e \rightsquigarrow \gamma$	4810 ± 113	1302 ± 43	124.5 ± 3.5	11.46 ± 0.45
$j \rightsquigarrow \gamma$	2726 ± 105	5879 ± 149	941 ± 37	188 ± 10
γ(dir)+jets	175.7 ± 3.6	2437 ± 62	0.0469 ± 0.0010	–
Total	11298 ± 101	9936 ± 98	4821 ± 69	612 ± 23
Data	11327	9934	4802	596

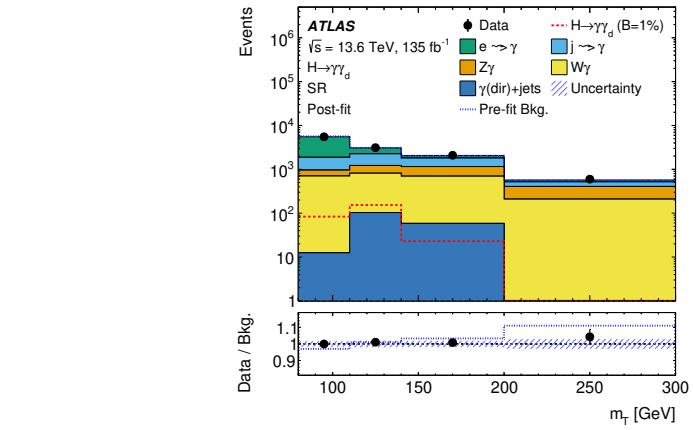
Table 6. Data and background yields in the SR and CRs, after the background-only fit. The pre-fit expected signal yields are also shown for each Higgs boson production channel, assuming $\mathcal{B}_{\gamma\gamma_{\mathrm{d}}} = 1\%$. Contributions below 10^{-5} are shown as "–". Uncertainties include statistical and systematic components. The individual background uncertainties can be correlated and therefore do not add in quadrature to the total background uncertainty.

background, allowing an effective constraint on this contribution. This choice optimises the sensitivity by balancing the shape information against the statistical precision in each bin.

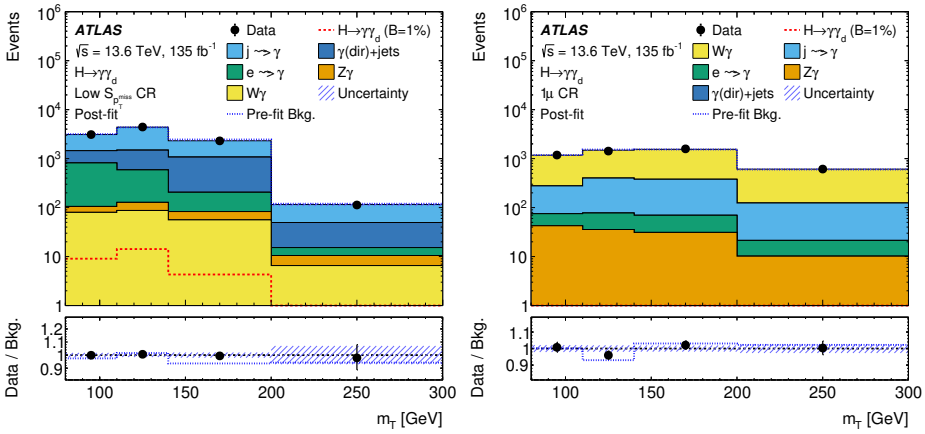
The likelihood function is constructed as the product of Poisson probability distribution functions describing the event counts in each m_{T} bin of the SR and CRs, as functions of the expected signal and background yields. The branching ratio $\mathcal{B}_{\gamma\gamma_{\mathrm{d}}}$ is included in the fit as the parameter of interest (POI). In addition, two normalisation factors, $k_{W\gamma}$ and $k_{Z\gamma}$, are applied to the $W\gamma$ and $Z\gamma$ background processes respectively, and included as free parameters in the fit, primarily constrained by the corresponding 1μ and 2μ CRs. Systematic uncertainties affecting the signal and background yields are incorporated into the likelihood model as independent nuisance parameters with a Gaussian constraint centred at zero with a width corresponding to the associated uncertainty. The experimental and data-driven systematic errors are treated as fully correlated across all regions, and experimental systematic errors are also correlated amongst all MC samples. Theoretical uncertainties are treated as uncorrelated across samples. All nuisance parameters are assumed to be mutually uncorrelated. The fit model is implemented in the TRExFitter [86] framework.

A background-only fit is first performed in the SR and CRs, with $\mathcal{B}_{\gamma\gamma_{\mathrm{d}}}$ set to zero, and the $k_{W\gamma}$ and $k_{Z\gamma}$ normalisation factors left free. The fitted values are $k_{W\gamma} = 0.93^{+0.08}_{-0.08}$ and $k_{Z\gamma} = 1.03^{+0.12}_{-0.11}$. The post-fit m_{T} distributions for data and the expected SM background are shown in figure 11, while the corresponding yields are reported in table 6. The yields and background composition in each analysis region, including the VRs, are also summarised in figure 12. Good agreement is observed between data and the SM background expectation in all the analysis regions, and the data are consistent with the background-only hypothesis with an observed p_0-value of 0.37.

JHEP10(2026)270



(a)



(b) (c)

Figure 11. Distribution of m_{T} for data and for the expected SM background after the background-only fit, in the (a) SR and (b, c) CRs. The $H \to \gamma\gamma_{\mathrm{d}}$ signal, assuming $\mathcal{B}_{\gamma\gamma_{\mathrm{d}}} = 1\%$, is shown as a dashed line and includes the ggF, VBF, WH and ZH production modes. The pre-fit prediction is overlaid as a dotted line. The uncertainties include both statistical and systematic components determined by the multiple-bin fit. The lower panels show the ratios of data to expected background yields post-fit (dots) and pre-fit (dotted line).

A second fit is then performed including the signal contribution and the branching ratio $\mathcal{B}_{\gamma\gamma_{\mathrm{d}}}$ as the POI. The results are consistent with the background-only hypothesis, with the best-fit value $\mathcal{B}_{\gamma\gamma_{\mathrm{d}}} = 0.002^{+0.006}_{-0.006}$. Since no significant excess over the SM prediction is observed, upper limits on the branching ratio of the exotic decay $H \to \gamma\gamma_{\mathrm{d}}$ are set using the profile likelihood ratio test statistic and the $\mathrm{CL_s}$ approach [87], in the asymptotic approximation [88]. An observed (expected) upper limit on $\mathcal{B}_{\gamma\gamma_{\mathrm{d}}}$ of 1.4% (1.2%) is obtained at 95% CL. This result can be compared with previous searches carried out on the VBF [17] and ZH [16] production channels in Run 2, as well as their combination [20], as summarised in figure 13. The present analysis provides constraints on the $H \to \gamma\gamma_{\mathrm{d}}$ decay comparable to the observed (expected) upper limits of 1.3% (1.5%) from the Run 2 combination, which are the most stringent limits from previous searches. A combination of this analysis with Run 2

JHEP10(2026)270

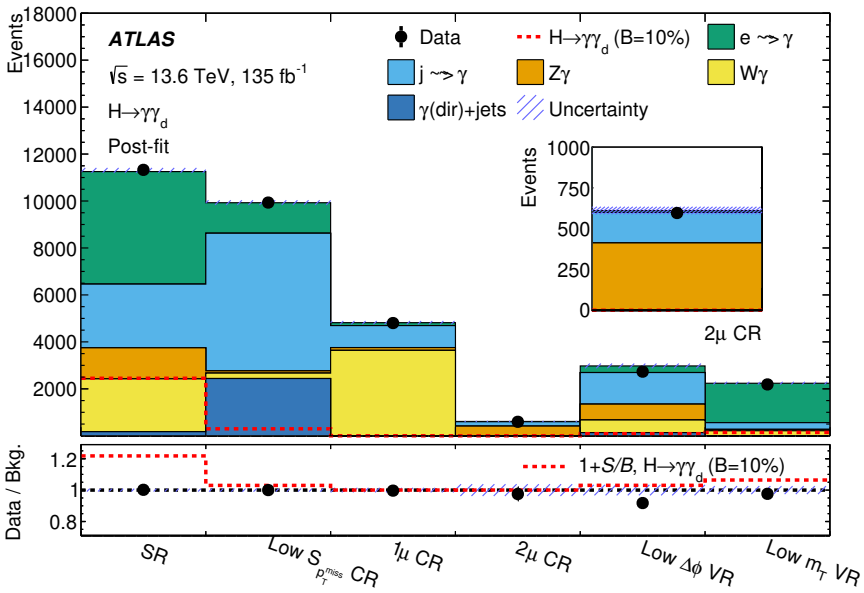


Figure 12. Observed data and post-fit background yields in the SR, CRs, and VRs after the background-only fit. The expected signal yields are overlaid, assuming $\mathcal{B}_{\gamma\gamma_d} = 10\%$ for visualisation purposes. The lower panel shows the ratio of the data to the background, together with the signal contribution defined as $1 + S/B$, where S and B denote the signal and background yields.

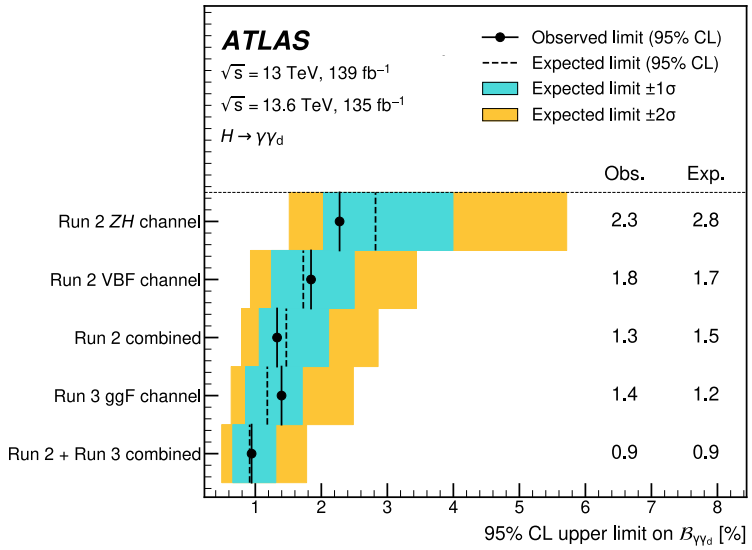


Figure 13. Summary of the 95% CL upper limits on $\mathcal{B}_{\gamma\gamma_d}$, achieved by the Run 2 searches (top three rows: ZH [16], VBF [17], and their combination [20]) and by this analysis (4th row). The overall Run 2 + Run 3 combination is displayed in the bottom row.

JHEP10(2026)270

results is performed, treating systematic uncertainties as uncorrelated between Run 2 and Run 3 searches, and adopting for the different Run 2 channels the same correlation scheme as in ref. [20]. As a conservative approach, the signal modelling is treated as uncorrelated between Run 2 and Run 3 searches, as the former were not sensitive to the ggF production mode, which is the dominant contribution in the present analysis, while the VBF and VH channels account for only $\sim 30\%$ of the signal yield. The combination yields an observed (expected) upper limit of 0.9% (0.9%) on $\mathcal{B}_{\gamma\gamma_\mathrm{d}}$.

11 Conclusion

A search for semi-visible decays of the SM Higgs boson into a photon and $p_\mathrm{T}^\mathrm{miss}$ is presented. The analysis exploits a dedicated topological trigger with reduced $p_\mathrm{T}^\mathrm{miss}$ and p_T^γ thresholds, allowing the gluon-gluon fusion production channel to be targeted for the first time in ATLAS and extending the sensitivity to a previously unexplored kinematic region. The analysis is performed using Run 3 pp collision data at $\sqrt{s} = 13.6$ TeV, collected by the ATLAS detector in 2023 and 2024, corresponding to an integrated luminosity of 135 fb^{-1}.

The impact of hard-scatter primary vertex misidentification due to low track activity is strongly mitigated using a dedicated BDT discriminant. Novel data driven techniques are employed to estimate the background arising from electrons and jets misidentified as photons, while the normalisation of the background processes with a genuine photon is obtained using MC simulations constrained by data in dedicated control regions.

No significant excess over the SM expectation is observed. The results are interpreted in terms of a $H \to \gamma\gamma_\mathrm{d}$ decay, yielding an observed (expected) 95% CL upper limit on the branching ratio of 1.4% (1.2%) at 95% CL, comparable to the best limit from previous searches, set by the ATLAS Run 2 combination. A combination with previous ATLAS Run 2 searches improves the observed (expected) limit to 0.9% (0.9%), representing the most stringent constraint to date on this decay mode.

Acknowledgments

We thank CERN for the very successful operation of the LHC and its injectors, as well as the support staff at CERN and at our institutions worldwide without whom ATLAS could not be operated efficiently.

The crucial computing support from all WLCG partners is acknowledged gratefully, in particular from CERN, the ATLAS Tier-1 facilities at TRIUMF/SFU (Canada), NDGF (Denmark, Norway, Sweden), CC-IN2P3 (France), KIT/GridKA (Germany), INFN-CNAF (Italy), NL-T1 (Netherlands), PIC (Spain), RAL (U.K.) and BNL (U.S.A.), the Tier-2 facilities worldwide and large non-WLCG resource providers. Major contributors of computing resources are listed in ref. [89].

We gratefully acknowledge the support of ANPCyT, Argentina; YerPhI, Armenia; ARC, Australia; BMWFW and FWF, Austria; ANAS, Azerbaijan; CNPq and FAPESP, Brazil; NSERC, NRC and CFI, Canada; CERN; ANID, Chile; CAS, MOST, NSFC and FRFCU, China; Minciencias, Colombia; MEYS CR, Czech Republic; DNRF and DNSRC, Denmark; IN2P3-CNRS and CEA-DRF/IRFU, France; SRNSFG, Georgia; BMFTR, HGF and MPG,

JHEP10(2026)270

Germany; GSRI, Greece; RGC and Hong Kong SAR, China; ICHEP and Academy of Sciences and Humanities, Israel; INFN, Italy; MEXT and JSPS, Japan; CNRST, Morocco; NWO, Netherlands; RCN, Norway; MNiSW, Poland; FCT, Portugal; MNE/IFA, Romania; MSTDI, Serbia; MSSR, Slovakia; ARIS and MVZI, Slovenia; DSI/NRF, South Africa; MICIU/AEI, Spain; SRC and Wallenberg Foundation, Sweden; SERI, SNSF and Cantons of Bern and Geneva, Switzerland; NSTC, Taipei; TENMAK, Türkiye; STFC/UKRI, United Kingdom; DOE and NSF, United States of America.

Individual groups and members have received support from BCKDF, CANARIE, CRC and DRAC, Canada; CERN-CZ, FORTE and PRIMUS, Czech Republic; COST, ERC, ERDF, Horizon 2020 and Marie Skłodowska-Curie Actions, European Union; Investissements d'Avenir Labex, Investissements d'Avenir Idex and ANR, France; DFG and AvH Foundation, Germany; Herakleitos, Thales and Aristeia programmes co-financed by EU-ESF and the Greek NSRF, Greece; BSF-NSF and MINERVA, Israel; NCN and NAWA, Poland; La Caixa Banking Foundation, CERCA and AGAUR programs from Generalitat de Catalunya and PROMETEO and GenT Programmes Generalitat Valenciana, Spain; Göran Gustafssons Stiftelse, Sweden; The Royal Society and Leverhulme Trust, United Kingdom; Eric and Wendy Schmidt Fund for Strategic Innovation, United States of America.

In addition, individual members wish to acknowledge support from Chile: Agencia Nacional de Investigación y Desarrollo (ANID FONDECYT reg. 1230987, FONDECYT 1230812, FONDECYT 1240864, Fondecyt 3240661, Fondecyt Regular 1240721); China: Fundamental Research Funds for the Central Universities (010-63263105), Chinese Ministry of Science and Technology (MOST-2023YFA1605700, MOST-2023YFA1609300), National Natural Science Foundation of China (NSFC 12275265, NSFC-W2543005); Czech Republic: Czech Science Foundation (GACR — 24-11373S), Ministry of Education Youth and Sports (ERC-CZ-LL2327, FORTE CZ.02.01.01/00/22_008/0004632); EU: H2020 European Research Council (ERC — 101002463); European Union: European Research Council (BARD No. 101116429, ERC — 101219398, ERC 101089007), European Regional Development Fund (HE COFUND GA No.101081355, ERDF), Marie Sklodowska-Curie Actions (GAP-101168829); France: Agence Nationale de la Recherche (ANR-21-CE31-0013, ANR-22-EDIR-0002, ANR-24-CE31-0504-01); Germany: Deutsche Forschungsgemeinschaft (DFG — 469666862); China: Research Grants Council (GRF); Italy: Istituto Nazionale di Fisica Nucleare (LHC-MIUR — 28003/2025), Ministero dell'Università e della Ricerca (NextGenEU I53D23000820006 M4C2.1.1, SOE2024_0000023); Japan: Japan Society for the Promotion of Science (JSPS KAKENHI JP25H0063, JSPS KAKENHI JP22H04944, JSPS KAKENHI JP24K23939, JSPS KAKENHI JP24KK0251, JSPS KAKENHI JP25H00650, JSPS KAKENHI JP25H01291, JSPS KAKENHI JP25K01011, JSPS KAKENHI JP25K01023, JSPS KAKENHI JP25KK0047); Poland: Polish National Science Centre (NCN OPUS 2023/51/B/ST2/02507, NCN OPUS nr 2022/47/B/ST2/03059, UMO-2019/34/E/ST2/00393, UMO-2021/42/E/ST2/00350, UMO-2022/47/O/ST2/00148, UMO-2023/49/B/ST2/04085, UMO-2023/51/B/ST2/00920, UMO-2024/53/N/ST2/00869); Spain: Agència de Gestió d'Ajuts Universitaris i de Recerca. (AGAUR — 2023 BP 00141), Ministry of Science and Innovation (RYC2019-028510-I, RYC2020-030254-I, RYC2021-031273-I, RYC2022-038164-I), Ministerio de Ciencia, Innovación y Universidades/Agencia Estatal de Investigación

(EU NextGenerationEU (PRTR-C17.I1), PID2022-142604OB-C22); Sweden: Carl Trygger Foundation (Carl Trygger Foundation CTS 22:2312), Swedish Research Council (Swedish Research Council 2023-04654, VR 2021-03651, VR 2022-03845, VR 2022-04683, VR 2023-03403, VR 2024-05451, VR 2025-05940), Knut and Alice Wallenberg Foundation (KAW 2023.0366); United Kingdom: The Binks Trust, Royal Society (NIF-R1-231091); United States of America: U.S. Department of Energy (ECA DE-AC02-76SF00515), John Templeton Foundation (John Templeton Foundation 63206), Neubauer Family Foundation.

Data Availability Statement. The public release of data supporting the findings of this article will follow the CERN Open Data Policy [90]. The values of relevant plots and tables associated with this article are stored in HEPData (https://www.hepdata.net/record/ins3168549 for this paper).

Code Availability Statement. The ATLAS collaboration's Athena software, including the configuration of the event generators, is open source (http://gitlab.cern.ch/atlas/athena).

Open Access. This article is distributed under the terms of the Creative Commons Attribution License (CC-BY4.0), which permits any use, distribution and reproduction in any medium, provided the original author(s) and source are credited.

References

[1] D. Curtin et al., *Exotic decays of the 125 GeV Higgs boson*, *Phys. Rev. D* **90** (2014) 075004 [arXiv:1312.4992] [INSPIRE].

[2] J.J. Fan, A. Katz, L. Randall and M. Reece, *Dark-disk universe*, *Phys. Rev. Lett.* **110** (2013) 211302 [arXiv:1303.3271] [INSPIRE].

[3] M. Heikinheimo, M. Raidal, C. Spethmann and H. Veermäe, *Dark matter self-interactions via collisionless shocks in cluster mergers*, *Phys. Lett. B* **749** (2015) 236 [arXiv:1504.04371] [INSPIRE].

[4] K.M. Zurek, *Asymmetric dark matter: theories, signatures, and constraints*, *Phys. Rept.* **537** (2014) 91 [arXiv:1308.0338] [INSPIRE].

[5] C. Petersson, A. Romagnoni and R. Torre, *Higgs decay with monophoton + MET signature from low scale supersymmetry breaking*, *JHEP* **10** (2012) 016 [arXiv:1203.4563] [INSPIRE].

[6] D. Suematsu, *Neutralino decay in the mu problem solvable extra U(1) models*, *Phys. Rev. D* **57** (1998) 1738 [hep-ph/9708413] [INSPIRE].

[7] M.L. Graesser, *Experimental constraints on Higgs boson decays to TeV-scale right-handed neutrinos*, arXiv:0705.2190 [INSPIRE].

[8] J. Beacham et al., *Physics beyond colliders at CERN: beyond the Standard Model working group report*, *J. Phys. G* **47** (2020) 010501 [arXiv:1901.09966] [INSPIRE].

[9] P. Harris, P. Schuster and J. Zupan, *Snowmass white paper: new flavors and rich structures in dark sectors*, in the proceedings of the *Snowmass 2021*, Seattle, U.S.A., 17–26 July 2022 [arXiv:2207.08990] [INSPIRE].

JHEP10(2026)270

[10] M. Deliyergiyev, *Recent progress in search for dark sector signatures*, *Open Phys.* **14** (2016) 281 [arXiv:1510.06927] [INSPIRE].

[11] M. Fabbrichesi, E. Gabrielli and G. Lanfranchi, *The physics of the dark photon: a primer*, Springer (2021) [DOI:10.1007/978-3-030-62519-1] [arXiv:2005.01515] [INSPIRE].

[12] E. Gabrielli, M. Heikinheimo, B. Mele and M. Raidal, *Dark photons and resonant monophoton signatures in Higgs boson decays at the LHC*, *Phys. Rev. D* **90** (2014) 055032 [arXiv:1405.5196] [INSPIRE].

[13] S. Biswas, E. Gabrielli, M. Heikinheimo and B. Mele, *Dark-photon searches via Higgs-boson production at the LHC*, *Phys. Rev. D* **93** (2016) 093011 [arXiv:1603.01377] [INSPIRE].

[14] H. Beauchesne and C.-W. Chiang, *Observability of the Higgs boson decay to a photon and a dark photon*, *Phys. Rev. D* **108** (2023) 015018 [arXiv:2304.04165] [INSPIRE].

[15] H. Beauchesne and C.-W. Chiang, *Is the decay of the Higgs boson to a photon and a dark photon currently observable at the LHC?*, *Phys. Rev. Lett.* **130** (2023) 141801 [arXiv:2205.10976] [INSPIRE].

[16] ATLAS collaboration, *Search for dark photons from Higgs boson decays via ZH production with a photon plus missing transverse momentum signature from pp collisions at $\sqrt{s} = 13$ TeV with the ATLAS detector*, *JHEP* **07** (2023) 133 [arXiv:2212.09649] [INSPIRE].

[17] ATLAS collaboration, *Observation of electroweak production of two jets in association with an isolated photon and missing transverse momentum, and search for a Higgs boson decaying into invisible particles at 13 TeV with the ATLAS detector*, *Eur. Phys. J. C* **82** (2022) 105 [arXiv:2109.00925] [INSPIRE].

[18] CMS collaboration, *Search for dark photons in decays of Higgs bosons produced in association with Z bosons in proton-proton collisions at $\sqrt{s} = 13$ TeV*, *JHEP* **10** (2019) 139 [arXiv:1908.02699] [INSPIRE].

[19] CMS collaboration, *Search for dark photons in Higgs boson production via vector boson fusion in proton-proton collisions at $\sqrt{s} = 13$ TeV*, *JHEP* **03** (2021) 011 [arXiv:2009.14009] [INSPIRE].

[20] ATLAS collaboration, *Combination of searches for Higgs boson decays into a photon and a massless dark photon using pp collisions at $\sqrt{s} = 13$ TeV with the ATLAS detector*, *JHEP* **08** (2024) 153 [arXiv:2406.01656] [INSPIRE].

[21] CMS collaboration, *Search for exotic decays of a Higgs boson into undetectable particles and one or more photons*, *Phys. Lett. B* **753** (2016) 363 [arXiv:1507.00359] [INSPIRE].

[22] ATLAS collaboration, *Search for dark matter in association with an energetic photon in pp collisions at $\sqrt{s} = 13$ TeV with the ATLAS detector*, *JHEP* **02** (2021) 226 [arXiv:2011.05259] [INSPIRE].

[23] ATLAS collaboration, *Search for high-mass resonances in photon plus missing transverse momentum signatures in pp collisions at $\sqrt{s} = 13$ TeV with the ATLAS detector*, ATL-PHYS-PUB-2023-003 (2023) [INSPIRE].

[24] ATLAS collaboration, *The ATLAS experiment at the CERN Large Hadron Collider*, 2008 *JINST* **3** S08003 [INSPIRE].

[25] ATLAS collaboration, *The ATLAS experiment at the CERN Large Hadron Collider: a description of the detector configuration for run 3*, 2024 *JINST* **19** P05063 [arXiv:2305.16623] [INSPIRE].

JHEP10(2026)270

[26] ATLAS collaboration, *ATLAS Insertable B-Layer technical design report*, CERN-LHCC-2010-013 (2010) [INSPIRE].

[27] ATLAS IBL collaboration, *Production and integration of the ATLAS Insertable B-Layer*, 2018 *JINST* **13** T05008 [arXiv:1803.00844] [INSPIRE].

[28] ATLAS collaboration, *ATLAS liquid argon calorimeter: technical design report*, CERN-LHCC-96-41 (1996) [INSPIRE].

[29] ATLAS collaboration, *Readiness of the ATLAS liquid argon calorimeter for LHC collisions*, *Eur. Phys. J. C* **70** (2010) 723 [arXiv:0912.2642] [INSPIRE].

[30] ATLAS collaboration, *The ATLAS trigger system for LHC run 3 and trigger performance in 2022*, 2024 *JINST* **19** P06029 [arXiv:2401.06630] [INSPIRE].

[31] ATLAS collaboration, *Software and computing for run 3 of the ATLAS experiment at the LHC*, *Eur. Phys. J. C* **85** (2025) 234 [*Erratum ibid.* **85** (2025) 907] [arXiv:2404.06335] [INSPIRE].

[32] ATLAS collaboration, *ATLAS data quality operations and performance for 2015–2018 data-taking*, 2020 *JINST* **15** P04003 [arXiv:1911.04632] [INSPIRE].

[33] ATLAS collaboration, *Preliminary luminosity calibration of the ATLAS 13.6 TeV data recorded in 2024 and combination with the 2022 and 2023 measurements*, ATL-DAPR-PUB-2025-001 (2025) [INSPIRE].

[34] ATLAS collaboration, *The ATLAS simulation infrastructure*, *Eur. Phys. J. C* **70** (2010) 823 [arXiv:1005.4568] [INSPIRE].

[35] GEANT4 collaboration, *GEANT4 — a simulation toolkit*, *Nucl. Instrum. Meth. A* **506** (2003) 250 [INSPIRE].

[36] ATLAS collaboration, *Emulating the impact of additional proton–proton interactions in the ATLAS simulation by presampling sets of inelastic Monte Carlo events*, *Comput. Softw. Big Sci.* **6** (2022) 3 [arXiv:2102.09495] [INSPIRE].

[37] K. Werner, F.-M. Liu and T. Pierog, *Parton ladder splitting and the rapidity dependence of transverse momentum spectra in deuteron-gold collisions at RHIC*, *Phys. Rev. C* **74** (2006) 044902 [hep-ph/0506232] [INSPIRE].

[38] C. Bierlich et al., *A comprehensive guide to the physics and usage of PYTHIA 8.3*, *SciPost Phys. Codeb.* **2022** (2022) 8 [arXiv:2203.11601] [INSPIRE].

[39] T. Pierog et al., *EPOS LHC: test of collective hadronization with data measured at the CERN Large Hadron Collider*, *Phys. Rev. C* **92** (2015) 034906 [arXiv:1306.0121] [INSPIRE].

[40] ATLAS collaboration, *The Pythia 8 A3 tune description of ATLAS minimum bias and inelastic measurements incorporating the Donnachie-Landshoff diffractive model*, ATL-PHYS-PUB-2016-017 (2016) [INSPIRE].

[41] R.D. Ball et al., *Parton distributions with LHC data*, *Nucl. Phys. B* **867** (2013) 244 [arXiv:1207.1303] [INSPIRE].

[42] S. Alioli, P. Nason, C. Oleari and E. Re, *A general framework for implementing NLO calculations in shower Monte Carlo programs: the POWHEG BOX*, *JHEP* **06** (2010) 043 [arXiv:1002.2581] [INSPIRE].

[43] S. Frixione, P. Nason and C. Oleari, *Matching NLO QCD computations with parton shower simulations: the POWHEG method*, *JHEP* **11** (2007) 070 [arXiv:0709.2092] [INSPIRE].

[44] PDF4LHC Working Group collaboration, *The PDF4LHC21 combination of global PDF fits for the LHC run III*, *J. Phys. G* **49** (2022) 080501 [arXiv:2203.05506] [INSPIRE].

JHEP10(2026)270

[45] K. Hamilton, P. Nason, E. Re and G. Zanderighi, *NNLOPS simulation of Higgs boson production*, *JHEP* **10** (2013) 222 [arXiv:1309.0017] [INSPIRE].

[46] LHC Higgs Cross Section Working Group collaboration, *Handbook of LHC Higgs cross sections: 4. Deciphering the nature of the Higgs sector*, arXiv:1610.07922 [DOI:10.23731/CYRM-2017-002] [INSPIRE].

[47] A. Karlberg et al., *Ad interim recommendations for the Higgs boson production cross sections at* $\sqrt{s} = 13.6$ *TeV*, arXiv:2402.09955 [INSPIRE].

[48] J. Pumplin et al., *New generation of parton distributions with uncertainties from global QCD analysis*, *JHEP* **07** (2002) 012 [hep-ph/0201195] [INSPIRE].

[49] L. Carloni and T. Sjostrand, *Visible effects of invisible hidden valley radiation*, *JHEP* **09** (2010) 105 [arXiv:1006.2911] [INSPIRE].

[50] Sherpa collaboration, *Event generation with Sherpa 2.2*, *SciPost Phys.* **7** (2019) 034 [arXiv:1905.09127] [INSPIRE].

[51] S. Schumann and F. Krauss, *A parton shower algorithm based on Catani-Seymour dipole factorisation*, *JHEP* **03** (2008) 038 [arXiv:0709.1027] [INSPIRE].

[52] S. Hoeche, F. Krauss, M. Schonherr and F. Siegert, *A critical appraisal of NLO+PS matching methods*, *JHEP* **09** (2012) 049 [arXiv:1111.1220] [INSPIRE].

[53] S. Catani, F. Krauss, R. Kuhn and B.R. Webber, *QCD matrix elements + parton showers*, *JHEP* **11** (2001) 063 [hep-ph/0109231] [INSPIRE].

[54] NNPDF collaboration, *Parton distributions for the LHC run II*, *JHEP* **04** (2015) 040 [arXiv:1410.8849] [INSPIRE].

[55] S. Mrenna and P. Skands, *Automated parton-shower variations in Pythia 8*, *Phys. Rev. D* **94** (2016) 074005 [arXiv:1605.08352] [INSPIRE].

[56] T. Sjostrand, S. Mrenna and P.Z. Skands, *A brief introduction to PYTHIA 8.1*, *Comput. Phys. Commun.* **178** (2008) 852 [arXiv:0710.3820] [INSPIRE].

[57] ATLAS collaboration, *ATLAS Pythia 8 tunes to 7 TeV data*, ATL-PHYS-PUB-2014-021 (2014) [INSPIRE].

[58] ATLAS collaboration, *Performance of the missing transverse momentum triggers for the ATLAS detector during Run-2 data taking*, *JHEP* **08** (2020) 080 [arXiv:2005.09554] [INSPIRE].

[59] ATLAS collaboration, *Jet reconstruction and performance using particle flow with the ATLAS detector*, *Eur. Phys. J. C* **77** (2017) 466 [arXiv:1703.10485] [INSPIRE].

[60] ATLAS collaboration, *Readiness of the ATLAS tile calorimeter for LHC collisions*, *Eur. Phys. J. C* **70** (2010) 1193 [arXiv:1007.5423] [INSPIRE].

[61] ATLAS collaboration, *Track and vertex reconstruction with the ATLAS inner detector*, arXiv:2605.07585 [INSPIRE].

[62] ATLAS collaboration, *Electron and photon energy calibration with the ATLAS detector using LHC run 2 data*, 2024 *JINST* **19** P02009 [arXiv:2309.05471] [INSPIRE].

[63] ATLAS collaboration, *Electron and photon efficiencies in LHC run 2 with the ATLAS experiment*, *JHEP* **05** (2024) 162 [arXiv:2308.13362] [INSPIRE].

[64] ATLAS collaboration, *Electron reconstruction and identification in the ATLAS experiment using the 2015 and 2016 LHC proton-proton collision data at* $\sqrt{s} = 13$ *TeV*, *Eur. Phys. J. C* **79** (2019) 639 [arXiv:1902.04655] [INSPIRE].

JHEP10(2026)270

[65] ATLAS collaboration, *Muon reconstruction and identification efficiency in ATLAS using the full Run 2 pp collision data set at* $\sqrt{s} = 13$ *TeV*, *Eur. Phys. J. C* **81** (2021) 578 [arXiv:2012.00578] [INSPIRE].

[66] ATLAS collaboration, *Muon reconstruction performance of the ATLAS detector in proton–proton collision data at* $\sqrt{s} = 13$ *TeV*, *Eur. Phys. J. C* **76** (2016) 292 [arXiv:1603.05598] [INSPIRE].

[67] ATLAS collaboration, *Measurement of the photon identification efficiencies with the ATLAS detector using LHC run 2 data collected in 2015 and 2016*, *Eur. Phys. J. C* **79** (2019) 205 [arXiv:1810.05087] [INSPIRE].

[68] ATLAS collaboration, *Electron and photon performance measurements with the ATLAS detector using the 2015–2017 LHC proton-proton collision data*, 2019 *JINST* **14** P12006 [arXiv:1908.00005] [INSPIRE].

[69] M. Cacciari, G.P. Salam and G. Soyez, *The anti-*k_t *jet clustering algorithm*, *JHEP* **04** (2008) 063 [arXiv:0802.1189] [INSPIRE].

[70] M. Cacciari, G.P. Salam and G. Soyez, *FastJet user manual*, *Eur. Phys. J. C* **72** (2012) 1896 [arXiv:1111.6097] [INSPIRE].

[71] ATLAS collaboration, *Performance of pile-up mitigation techniques for jets in pp collisions at* $\sqrt{s} = 8$ *TeV using the ATLAS detector*, *Eur. Phys. J. C* **76** (2016) 581 [arXiv:1510.03823] [INSPIRE].

[72] ATLAS collaboration, *Identification and rejection of pile-up jets at high pseudorapidity with the ATLAS detector*, *Eur. Phys. J. C* **77** (2017) 580 [*Erratum ibid.* **77** (2017) 712] [arXiv:1705.02211] [INSPIRE].

[73] ATLAS collaboration, *Transforming jet flavour tagging at ATLAS*, *Nature Commun.* **17** (2026) 541 [arXiv:2505.19689] [INSPIRE].

[74] ATLAS collaboration, *Selection of jets produced in 13 TeV proton-proton collisions with the ATLAS detector*, ATLAS-CONF-2015-029 (2015) [INSPIRE].

[75] ATLAS collaboration, *Identification of hadronic tau lepton decays using neural networks in the ATLAS experiment*, ATL-PHYS-PUB-2019-033 (2019) [INSPIRE].

[76] ATLAS collaboration, *The performance of missing transverse momentum reconstruction and its significance with the ATLAS detector using* $140\,fb^{-1}$ *of* $\sqrt{s} = 13$ *TeV pp collisions*, *Eur. Phys. J. C* **85** (2025) 606 [arXiv:2402.05858] [INSPIRE].

[77] ATLAS collaboration, *Object-based missing transverse momentum significance in the ATLAS detector*, ATLAS-CONF-2018-038 (2018) [INSPIRE].

[78] Y. Freund and R.E. Schapire, *A decision-theoretic generalization of on-line learning and an application to boosting*, *J. Comput. Syst. Sci.* **55** (1997) 119 [INSPIRE].

[79] A. Pinto et al., *Uncertainty components in profile likelihood fits*, *Eur. Phys. J. C* **84** (2024) 593 [arXiv:2307.04007] [INSPIRE].

[80] ATLAS collaboration, *Electron and photon energy calibration with the ATLAS detector using 2015–2016 LHC proton-proton collision data*, 2019 *JINST* **14** P03017 [arXiv:1812.03848] [INSPIRE].

[81] ATLAS collaboration, *Topological cell clustering in the ATLAS calorimeters and its performance in LHC Run 1*, *Eur. Phys. J. C* **77** (2017) 490 [arXiv:1603.02934] [INSPIRE].

JHEP10(2026)270

[82] ATLAS collaboration, *Jet energy scale and resolution measured in proton–proton collisions at $\sqrt{s} = 13$ TeV with the ATLAS detector*, *Eur. Phys. J. C* **81** (2021) 689 [arXiv:2007.02645] [INSPIRE].

[83] ATLAS collaboration, *New techniques for jet calibration with the ATLAS detector*, *Eur. Phys. J. C* **83** (2023) 761 [arXiv:2303.17312] [INSPIRE].

[84] ATLAS collaboration, *ATLAS b-jet identification performance and efficiency measurement with $t\bar{t}$ events in pp collisions at $\sqrt{s} = 13$ TeV*, *Eur. Phys. J. C* **79** (2019) 970 [arXiv:1907.05120] [INSPIRE].

[85] W. Balunas et al., *A flexible and efficient approach to missing transverse momentum reconstruction*, *Comput. Softw. Big Sci.* **8** (2024) 2 [arXiv:2308.15290] [INSPIRE].

[86] ATLAS collaboration, *TRExFitter* Zenodo (2026).

[87] A.L. Read, *Presentation of search results: the CL_s technique*, *J. Phys. G* **28** (2002) 2693 [INSPIRE].

[88] G. Cowan, K. Cranmer, E. Gross and O. Vitells, *Asymptotic formulae for likelihood-based tests of new physics*, *Eur. Phys. J. C* **71** (2011) 1554 [*Erratum ibid.* **73** (2013) 2501] [arXiv:1007.1727] [INSPIRE].

[89] ATLAS collaboration, *ATLAS computing acknowledgements*, ATL-SOFT-PUB-2026-001 (2026).

[90] *CERN Open Data Policy for the LHC experiments*, CERN-OPEN-2020-013 (2020) [DOI:10.17181/CERN.QXNK.8L2G].

[91] *Athena software*, http://gitlab.cern.ch/atlas/athena.

[92] *HEPData*, https://www.hepdata.net/record/ins3168549.

JHEP10(2026)270

The ATLAS collaboration

G. Aad[102], E. Aakvaag[17], B. Abbott[121], S. Abdelhameed[83b], K. Abeling[54], N.J. Abicht[48], S.H. Abidi[30], M. Aboelela[44], A. Aboulhorma[36e], H. Abramowicz[154], B.S. Acharya[68a,68b,a], A. Ackermann[62a], J. Ackerschott[55], C. Adam Bourdarios[4], L. Adamczyk[85a], S.V. Addepalli[146], M. J. Addison[101], J. Adelman[117], A. Adiguzel[22c], T. Adye[135], A.A. Affolder[137], Y. Afik[39], M.N. Agaras[13], A. Aggarwal[100], C. Agheorghiesei[28c], A. Ahmad[83a], F. Ahmadov[38,b], S. Ahuja[165], X. Ai[113c], G. Aielli[75a,75b], A. Aikot[165], M. Ait Tamlihat[36e], T.P.A. Åkesson[98], D. Akiyama[170], N.N. Akolkar[25], S. Aktas[168], G.L. Alberghi[24b], J. Albert[167], U. Alberti[20], P. Albicocco[52], S. Alderweireldt[51], Z.L. Alegria[122], M. Aleksa[37], I.N. Aleksandrov[38], C. Alexa[28b], T. Alexopoulos[10], F. Alfonsi[24b], M. Algren[55], M. Alhroob[169], B. Ali[133], H. M. J. Ali[91,c], S. Ali[32], S.W. Alibocus[92], M. Aliev[34c], G. Alimonti[70a], C. Allaire[65], B.M.M. Allbrooke[149], D. R. Allen[122], J. S. Allen[101], J.F. Allen[51], C.S. Alley[1], E.R. Almazan[137], A. Aloisio[71a,71b], F. Alonso[90], C. Alpigiani[140], A. Alvarez Fernandez[100], M. Alves Cardoso[55], M.G. Alviggi[71a,71b], Y. Amaral Coutinho[81b], C. Amelung[37], M. Amerl[101], T. Amezza[128], B. Amini[53], K. Amirie[158], A. Amirkhanov[38], D. Amperiadou[155], C. Anastopoulos[142], T. Andeen[11], J.K. Anders[92], A. C. Anderson[58], A. Andreazza[70a,70b], S. Angelidakis[9], A. Angerami[41], A.V. Anisenkov[38], A. Annovi[73a], C. Antel[37], E. Antipov[148], M. Antonelli[52], F. Anulli[74a], M. Aoki[82], T. Aoki[156], M.A. Aparo[13], L. Aperio Bella[47], M. Apicella[31], C. Appelt[154], A. Apyan[27], M. Arampatzi[10], S. J. Arbiol Val[86], C. Arcangeletti[52], A.T.H. Arce[50], M. Arcuri[43b,43a], J-F. Arguin[108], S. Argyropoulos[155], J.-H. Arling[47], O. Arnaez[4], A.P. Arnold[94], H. Arnold[148], G. Artoni[74a,74b], H. Asada[111], S. Asatryan[175], N.A. Asbah[37], R. A. Ashby Pickering[169], A. M. Aslam[95], J. Assahsah[36d], K. Assamagan[30], R. Astalos[29a], K. S. V. Astrand[98], S. Atashi[162], R.J. Atkin[34a], H. Atmani[36f], P.A. Atmasiddha[129], K. Augsten[133], A.D. Auriol[40], V.A. Austrup[101], A.S. Avad[94], G. Avolio[37], A. Azzam[13], D. Babal[29b], H. Bachacou[136], K. Bachas[155,d], A. Bachiu[35], E. Bachmann[49], M. J. Backes[62a], A. Badea[39], T.M. Baer[106], M. Bahmani[19], D. Bahner[53], K. Bai[124], L. Baines[94], O.K. Baker[174], D. Bakshi Gupta[8], L.E. Balabram Filho[81b], V. Balakrishnan[121], R. Balasubramanian[4], P. Balek[85a], E. Ballabene[24b,24a], F. Balli[136], L.M. Baltes[62a], W.K. Balunas[127], I. Bamwidhi[83c], E. Banas[86], M. Bandieramonte[130], S. Bansal[25], L. Barak[154], M. Barakat[47], E.L. Barberio[105], D. Barberis[18b], M. Barbero[102], M. Z. Barel[116], T. Barillari[110], M-S. Barisits[37], T. Barklow[146], P. Baron[134], D.A. Baron Moreno[101], A. Baroncelli[61], A.J. Barr[127,e], J.D. Barr[96], F. Barreiro[99], J. Barreiro Guimarães da Costa[14], M.G. Barros Teixeira[131a], F. Bartels[37], R. Bartoldus[146], A.E. Barton[91], P. Bartos[29a], M. Baselga[48], S. Bashiri[86], A. Bassalat[65,f], M.J. Basso[159a], S. Bataju[44], R. Bate[166], R.L. Bates[58], M. Battaglia[137], D. Battulga[19], M. Bauce[74a,74b], L. Bauckhage[47], P. Bauer[25], L. T. Bayer[47], L.T. Bazzano Hurrell[31], T. Beau[128], J.Y. Beaucamp[90], S. Beauceron[128], P.H. Beauchemin[161], P. Bechtle[25], H.P. Beck[20,g], K. Becker[169], A.J. Beddall[80], V.A. Bednyakov[38], C.P. Bee[148], L.J. Beemster[16], M. Begalli[81d], M. Begel[30], J.K. Behr[47], J.F. Beirer[37], F. Beisiegel[25], I.B. Belean[28d], M. Belfkir[83c], G. Bella[154], L. Bellagamba[24b], A. Bellerive[35], C.D. Bellgraph[67], P. Bellos[21], I. Benaoumeur[21], D. Benchekroun[36a], F. Bendebba[36a], Y. Benhammou[154],

JHEP10(2026)270

K.C. Benkendorfer[167], L. Beresford[47], M. Beretta[52], E. Bergeaas Kuutmann[163], N. Berger[4], B. Bergmann[133], J. Beringer[18a], M. Berkat[136], G. Bernardi[5], C. Bernius[146], F.U. Bernlochner[25], A. Berrocal Guardia[13], T. Berry[95], P. Berta[134], A. Berti[131a], R. Bertrand[102], S. Bethke[110], A. Betti[74a,74b], T.F. Beumker[173], A.J. Bevan[94], L. Bezio[55], N.K. Bhalla[53], S. Bharthuar[110], S. Bhatta[148], P. Bhattarai[146], Z.M. Bhatti[118], K. D. Bhide[164], V.S. Bhopatkar[122], R.M. Bianchi[130], G. Bianco[24b,24a], O. Biebel[109], M. Biglietti[76a], P. Bijl[53], C. S. Billingsley[44], Y. Bimgdi[36f], M. Bindi[54], A. Bingham[173], A. Bingul[22b], C. Bini[74a,74b], M. Biros[134], S. Biryukov[149], T. Bisanz[48], E. Bisceglie[24b,24a], J.P. Biswal[135], D. Biswas[144], M. Biyabi[14], I. Bloch[47], A. Blue[58], U. Blumenschein[94], V.S. Bobrovnikov[38], L. Boccardo[56b,56a], M. Boehler[53], D. Bogavac[13], L. S. Boggia[128], V. Boisvert[95], P. Bokan[163], T. Bold[85a], M. Bomben[5], M. Bona[94], M. Boonekamp[136], A.G. Borbély[58], G. Borissov[91], A. Borkar[168], D. Bortoletto[127], M. Borysova[171], D. Boscherini[24b], M. Bosman[13], K. Bouaouda[36a], L. Boudet[136], J. Boudreau[130], E.V. Bouhova-Thacker[91], D. Boumediene[40], R. Bouquet[56b,56a], A. Boveia[120], D. Boye[30], I.R. Boyko[38], L. Bozianu[55], J. Bracinik[21], N. Brahimi[4], G. Brandt[173], O. Brandt[33], B. Brau[103], R. Brener[171], L. Brenner[116], R. Brenner[163], S. Bressler[171], M. Brettell[96], G. Brianti[116], D. Britton[58], D. Britzger[110], I. Brock[25], R. Brock[107], H. Bronson[129], G. Brooijmans[41], A.J. Brooks[67], E. M. Brooks[159b], E. Brost[30], L.M. Brown[167,159a], L.E. Bruce[60], T.L. Bruckler[127], P.A. Bruckman de Renstrom[86], B. Brüers[47], A. Bruni[24b], G. Bruni[24b], D. Brunner[46a,46b], M. Bruschi[24b], N. Bruscino[74a,74b], T. Buanes[17], Q. Buat[140], D. Buchin[110], A.G. Buckley[58], J. Bucko[134], M. Buhring[49], O. Bulekov[80], B.A. Bullard[146], T. O. Buratovich[90], S. Burdin[92], C.D. Burgard[48], A.M. Burger[89], B. Burghgrave[8], O. Burlayenko[53], J. Burleson[164], J.C. Burzynski[121], V. Büscher[100], P.J. Bussey[58], O. But[25], J.M. Butler[26], C.M. Buttar[58], J.M. Butterworth[96], P. Butti[37], W. Buttinger[135], C.J. Buxo Vazquez[107], A.R. Buzykaev[38], S. Cabrera Urbán[165], L. Cadamuro[65], H. Cai[37], Y. Cai[24b,112c,24a], Y. Cai[112a], M.A. Cairo[129], V.M.M. Cairo[37], O. Cakir[3a], N. Calace[37], P. Calafiura[18a], G. Calderini[128], P. Calfayan[35], L. Calic[98], G. Callea[58], L.P. Caloba[81b], D. Calvet[40], S. Calvet[40], R. Camacho Toro[128], S. Camarda[37], D. Camarero Munoz[27], P. Camarri[75a,75b], G. Camia[47], C. Camincher[37], M. Campanelli[96], A. Camplani[42], V. Canale[71a,71b], A.C. Canbay[3a], E. Canonero[95], J. Cantero[165], F. Capocasa[27], P. Cappelli[27], M. Capua[43b,43a], A. Carbone[70a,70b], R. Cardarelli[75a], J.C.J. Cardenas[8], M. P. Cardiff[27], G. Carducci[43b,43a], T. Carli[37], G. Carlino[71a], J.I. Carlotto[13], B.T. Carlson[130,h], E.M. Carlson[167], L. Carminati[70a,70b], A. Carnelli[4], M. Carnesale[37], S. Caron[115], E. Carquin[138g], I.B. Carr[105], S. Carrà[72a,72b], G. Carratta[24b,24a], C. Carrion Martinez[165], A.M. Carroll[124], N. Cartalade[40], M.P. Casado[13,i], P. Casolaro[71a,71b], M. Caspar[47], F. Cassinese[90], F. Castiglioni[73a,73b], W.R. Castiglioni[39], F.L. Castillo[4], V. Castillo Gimenez[165], N.F. Castro[131a,131e], A. Catinaccio[37], J.R. Catmore[126], T. Cavaliere[4], V. Cavaliere[30], E. Celebi[80], S. Cella[30], V. Cepaitis[55], K. Cerny[123], A.S. Cerqueira[81a], A. Cerri[73a,j], L. Cerrito[75a,75b], F. Cerutti[18a], B. Cervato[70a,70b], A. Cervelli[24b], G. Cesarini[52], S.A. Cetin[80], V. C. Chabalala[34j], P.M. Chabrillat[128], R. Chakkappai[65], S. Chakraborty[169], A. Chambers[60], J. Chan[18a], J.D. Chapman[33], E. Chapon[136], D.G. Charlton[21], C. Chauhan[132], Y. Che[112a], S. Chekanov[6], G.A. Chelkov[38,k], H. Chen[30], J. Chen[141a],

JHEP10(2026)270

J. Chen[145], M. Chen[59], S. Chen[87], S.J. Chen[112a], X. Chen[141a], X. Chen[15,l], Z. Chen[61], C.L. Cheng[146], H.C. Cheng[63a], S. Cheong[146], A. Cheplakov[38], E. Cherepanova[116], E. Cheu[7], K. Cheung[64], L. Chevalier[136], G. Chiarelli[73a], G. Chiodini[69a], A.S. Chisholm[21], J. L. Chisholm[166], A. Chitan[28b], M. Chitishvili[165], M.V. Chizhov[38,m], K. Chmiel[76a,76b], K. Choi[11], Y. Chou[140], E.Y.S. Chow[115], G. Christou[51], K.L. Chu[171], M.C. Chu[63a], Z. Chubinidze[52], J. Chudoba[132], J.J. Chwastowski[86], D. Cieri[110], K.M. Ciesla[85a], V. Cindro[93], A. Ciocio[18a], F. Cirotto[71a,71b], Z.H. Citron[171], M. Citterio[70a], D.A. Ciubotaru[28b], A. Clark[55], P.J. Clark[51], N. Clarke Hall[37], C. Clarry[158], S.E. Clawson[37], C. Clement[46a,46b], L. Clissa[24b,24a], Y. Coadou[102], M. Cobal[68a,68c], A. Coccaro[56b], M. G. Cochran Branson[140], R.F. Coelho Barrue[131a], R. Coelho Lopes De Sa[103], S. Coelli[70a], M.M. Cohen[129], L. S. Colangeli[158], B. Cole[41], P. Collado Soto[99], J. Collot[59], M.R. Coluccia[69a], I. Combes[65], P. Conde Muiño[131a,131g], L.H.J. Condren[162], M.P. Connell[34c], S.H. Connell[34c], E.I. Conroy[161], M. Contreras Cossio[11], F. Conventi[71a,n], A.M. Cooper-Sarkar[127], L. Corazzina[74a,74b], F. A. Corchia[24b,24a], A. Cordeiro Oudot Choi[140], L.D. Corpe[40], M. Corradi[74a,74b], F. Corriveau[104,o], A. Cortes-Gonzalez[156], M.J. Costa[165], F. Costanza[4], D. Costanzo[142], J. Couthures[4], G. Cowan[95], K. Cranmer[172], L. Cremer[48], D. Cremonini[24b,24a], S. Crépé-Renaudin[59], F. Crescioli[128], T. Cresta[72a,72b], M. Cristinziani[144], M. Cristoforetti[77a,77b], T. M. Critchley[55], E. Critelli[96], A. Cueto[99], H. Cui[96], Z. Cui[7], B.M. Cunnett[149], W.R. Cunningham[58], E. Cuppini[110], F. Curcio[165], J. R. Curran[51], G. D'amen[30], V. D'Amico[109], M. D'Andrea[56b,56a], G. D'anniballe[73a,73b], S. D'Auria[70a,70b], A. D'Avanzo[71a,71b], L. D'Eramo[40], A. D'Onofrio[71a,71b], M. D'Onofrio[92], M. D'uffizi[101], M.J. Da Cunha Sargedas De Sousa[56b,56a], J.V. Da Fonseca Pinto[81b], C. Da Via[101], W. Dabrowski[85a], T. Dado[37], S. Dahbi[151], T. Dai[106], D. Dal Santo[20], C. Dallapiccola[103], M. Dam[42], J.R. Dandoy[35], D. Dannheim[37], M. Danninger[145], V. Dao[148], G. Darbo[56b], F. Dattola[47], T. Davidek[134], J. Davidson[169], I. Dawson[94], K. De[8], C. De Almeida Rossi[158], N. De Biase[47], S. De Castro[24b,24a], N. De Groot[115], P. de Jong[116], H. De la Torre[117], A. De Maria[112a], S. De Miranda Rimes[81d], A. De Salvo[74a], U. De Sanctis[75a,75b], F. De Santis[69a,69b], A. De Santo[149], J.B. De Vivie De Regie[59], K.G. De Vries[116], J. Debevc[93], D.V. Dedovich[38], J. Degens[92], A.M. Deiana[44], J. Del Peso[99], L. Delagrange[27], F. Deliot[136], C.M. Delitzsch[48], A. Dell'Acqua[37], L. Dell'Asta[70a,70b], M. Della Pietra[71a,71b], D. Della Volpe[55], M. Delmastro[4], C.C. Delogu[56b,56a], P.A. Delsart[59], S. Demers[174], M. Demichev[38], H. Denizli[22a,p], M.G. Depala[92], D. Derendarz[86], L. Derin[56b,56a], F. Derue[128], P. Dervan[92,†], A. M. Desai[1], K. Desch[25], F.A. Di Bello[73a,73b], A. Di Ciaccio[75a,75b], L. Di Ciaccio[4], D. Di Croce[37], C. Di Donato[71a,71b], A. Di Girolamo[37], G. Di Gregorio[65], A. Di Luca[77a,77b], B. Di Micco[76a,76b], R. Di Nardo[76a,76b], K.F. Di Petrillo[39], M. Diamantopoulou[154], F.A. Dias[116], M.A. Diaz[138a,138b], A. R. Didenko[38], M. Didenko[165], S.D. Diefenbacher[18a], E.B. Diehl[106], S. Díez Cornell[47], C. Diez Pardos[144], C. Dimitriadi[147], A. Dimitrievska[21], A. Dimri[148], Y. Ding[61], J. Dingfelder[25], T. Dingley[127], I-M. Dinu[28b], S.J. Dittmeier[62b], F. Dittus[37], M. Divisek[134], B. Dixit[92], F. Djama[102], T. Djobava[152b], C. Doglioni[101,98], A. Dohnalova[29a], Z. Dolezal[134], K.M. Dona[39], M. Donadelli[81d], B. Dong[107], J. Donini[40], J. Dopke[135], A. Doria[71a], N. Dos Santos Fernandes[131a],

JHEP10(2026)270

I.A. Dos Santos Luz[81e], P. Dougan[44], M.T. Dova[90], A.T. Doyle[58], M.P. Drescher[54], E. Dreyer[171], I. Drivas-koulouris[10], M. Drnevich[118], D. Du[61], T. Du[39], T.A. du Pree[116], Z. Duan[112a], M. Dubau[4], F. Dubinin[38], M. Dubovsky[29a], E. Duchovni[171], G. Duckeck[109], P. K. Duckett[96], O.A. Ducu[28b], D. Duda[51], A. Dudarev[37], M.M. Dudek[86], E. R. Duden[27], L. Duflot[65], M. Dührssen[37], I. Duminica[28g], A.E. Dumitriu[28b], M. Dunford[62a], T. Duong[4], A. Duperrin[102], A.F. Duque Bran[40], H. Duran Yildiz[3a], A. Durglishvili[152b], G.I. Dyckes[18a], M. Dyndal[85a], B.S. Dziedzic[37], G.H. Eberwein[127], B. Eckerova[29a], J.C. Egan[96], S. Eggebrecht[54], E. Egidio Purcino De Souza[81e], G. Eigen[17], K. Einsweiler[18a], T. Ekelof[163], P.A. Ekman[98], S. El Farkh[36b], Y. El Ghazali[61], H. El Jarrari[104], A. El Moussaouy[36a], I. Elbaz[154], D. Elitez[37], M. Ellert[163], F. Ellinghaus[173], T.A. Elliot[95], J. Elmsheuser[30], M. Elsawy[83b], M. Elsing[37], D. Emeliyanov[135], Y. Enari[82], S. Epari[108], D. Ernani Martins Neto[86], F. Ernst[37], M. Escalier[65], C. Escobar[165], R. Estevam De Paula[81c], E. Etzion[154], G. Evans[131a,131b], H. Evans[67], L.S. Evans[47], S. Ezzarqtouni[36a], F. Fabbri[24b,24a], L. Fabbri[24b,24a], G. Facini[96], V. Fadeyev[137], D. Fakoudis[100], S. Falciano[74a], L.F. Falda Ulhoa Coelho[27], F. Fallavollita[110], G. Falsetti[43b,43a], J. Faltova[134], C. Fan[164], K. Y. Fan[63b], Y. Fan[14], Y. Fang[14,112c], M. Fanti[70a,70b], M. Faraj[68a,68c], Z. Farazpay[97], A. Farbin[8], A. Farilla[76a], K. Farman[151], J. N. Farr[174], M. S. Farrington[60], S.M. Farrington[135,51], F. Fassi[36e], D. Fassouliotis[9], L. Fayard[65], G. Fazzino[62b], P. Federic[134], P. Federicova[132], M. Feickert[172], L. Feligioni[102], D.E. Fellers[18a], C. Feng[113b], Y. Feng[14], Z. Feng[65], B. Fernandez Barbadillo[91], P. Fernandez Martinez[66], C. Fernandez Ruiz[33], J. Ferrando[91], A. Ferrari[163], P. Ferrari[116,115], R. Ferrari[72a], D. Ferrere[55], C. Ferretti[106], M. P. Fewell[1], D. Fiacco[74a,74b], F. Fiedler[100], P. Fiedler[133], S. Filimonov[38], M.S. Filip[28b,q], A. Filipčič[93], M. Filipig[68a,68c], E.K. Filmer[159a], F. Filthaut[115], M.C.N. Fiolhais[131a,131c,r], L. Fiorini[165], W.C. Fisher[107], T. Fitschen[101], I. Fleck[144], P. Fleischmann[106], T. Flick[173], M. Flores[34d,s], L.R. Flores Castillo[63a], M. Foll[126], F.M. Follega[77a,77b], N. Fomin[33], A. Formica[136], M. Fornasiero[149], A.C. Forti[101], N. Forti[24b,24a], E. Fortin[102], A.W. Fortman[18a], L. Foster[18a], L. Fountas[9], H. Fox[91], P. Francavilla[73a,73b], S. Francescato[60], S. Franchellucci[20], M. Franchini[24b,24a], S. Franchino[62a], D. Francis[37], L. Franco[47], L. Franconi[47], M. Franklin[60], G. Frattari[37], Y.Y. Frid[154], N. Fritzsche[37], A. Froch[55], D. Froidevaux[37], J.A. Frost[135], Y. Fu[107], S. Fuenzalida Garrido[138g], Y.C. Fujikake[137], M. Fujimoto[148], K. Y. Fung[63a], E. Furtado De Simas Filho[81e], M. Furukawa[156], M. Fuste Costa[47], P. Fuste Martin[13], J. Fuster[165], A. Gaa[54], A. Gabrielli[24b,24a], A. Gabrielli[158], G. Gagliardi[56b,56a], L.G. Gagnon[146], S. Galantzan[154], J. Gallagher[1], E.J. Gallas[127], A.L. Gallen[163], B.J. Gallop[135], K.K. Gan[120], Y. Gao[51], Z. Gao[112a], A. Garabaglu[140], F.M. Garay Walls[138a,138b], C. García[165], A. Garcia Alonso[116], A.G. Garcia Caffaro[174], J.E. García Navarro[165], M. A. Garcia Ruiz[23b], M. Garcia-Sciveres[18a], G.L. Gardner[129], R.W. Gardner[39], N. Garelli[161], R.B. Garg[146], J.M. Gargan[33], C.A. Garner[158], C.M. Garvey[34a], V. K. Gassmann[161], G. Gaudio[72a], A.J. Gavin[94], J. Gavranovic[93], I.L. Gavrilenko[131a], C. Gay[166], G. Gaycken[124], A. Gekow[120], C. Gemme[56b], M.H. Genest[59], A. D. Gentry[114], S. George[95], T. Geralis[45], A. A. Gerwin[121], P. Gessinger-Befurt[37], M. Ghani[169], K. Ghorbanian[94], A. Ghosal[144], A. Ghosh[162], A. Ghosh[7], B. Giacobbe[24b], S. Giagu[74a,74b], A. Giannini[61], S.M. Gibson[95],

JHEP10(2026)270

D.T. Gil[85b], B.J. Gilbert[41], D. Gillberg[35], G. Gilles[116], D.M. Gingrich[2,t], M.P. Giordani[68a,68c], P.F. Giraud[136], G. Giugliarelli[68a,68c], D. Giugni[70a], F. Giuli[75a,75b,u], I. Gkialas[9,v], B.C. Gladwyn[127], C. Glasman[99], M. Glazewska[20], R. M. Gleason[162], G. Glemža[47], I. Gnesi[24b,24a,w], Y. Go[30], M. Goblirsch-Kolb[37], B. Gocke[48], D. Godin[108], B. Gokturk[22a], S. Goldfarb[105], T. Golling[55], M.G.D. Gololo[34c], A. Golub[140], J.P. Gombas[107], A. Gomes[131a,131b], G. Gomes Da Silva[144], A.J. Gomez Delegido[37], R. Gonçalo[131a], A. Gongadze[152c], F. Gonnella[21], J.L. Gonski[146], R.Y. González Andana[51], S. González de la Hoz[165], M. V. Gonzalez Rodrigues[47], R. Gonzalez Suarez[163], S. Gonzalez-Sevilla[55], L. Goossens[37], B. Gorini[37], E. Gorini[69a,69b], A. Gorišek[93], T.C. Gosart[129], A.T. Goshaw[50], M.I. Gostkin[38], S. Goswami[122], C.A. Gottardo[37], S. A. Gotz[109], M. Gouighri[36b], A.G. Goussiou[140], N. Govender[34c], R. P. Grabarczyk[127], I. Grabowska-Bold[85a], K. Graham[35], E. Gramstad[126], S. Grancagnolo[69a,69b], C.M. Grant[1], P.M. Gravila[28f], F.G. Gravili[69a,69b], H.M. Gray[18a], M. Greco[110], M. J. Green[1], C. Grefe[25], A. S. Grefsrud[37], I.M. Gregor[47], K.T. Greif[162], P. Grenier[146], S.G. Grewe[110], K. Grimm[32], S. Grinstein[13,x], E. Gross[171], J. Grosse-Knetter[54], L.H. Grossman[18b], L. Guan[106], W. Guérin[89], G. Guerrieri[37], R. Guevara[126], R. Gugel[100], J.A.M. Guhit[106], A. Guida[19], E. Guilloton[169], S. Guindon[37], F. Guo[14,112c], J. Guo[141a], L. Guo[47], L. Guo[112b,y], Y. Guo[106], Y. Guo[41], A. Gupta[48], R. Gupta[130], S. Gupta[27], S. Gurbuz[25], S.S. Gurdasani[47], G. Gustavino[74a,74b], P. Gutierrez[121], L.F. Gutierrez Zagazeta[129], M. Gutsche[49], C. Gutschow[96], C. Gwenlan[127], C.B. Gwilliam[92], E.S. Haaland[126], A. Haas[118], M. Habedank[58], C. Haber[18a], R.J. Haberle[171], H.K. Hadavand[8], A. Haddad[40], A. Hadef[49], A.I. Hagan[91], J. J. Hahn[144], M. Haleem[168], J. Haley[122], G.D. Hallewell[102], J.A. Hallford[47], H. Hamdaoui[163], M. Hamer[25], S. E. D. Hammoud[65], E.J. Hampshire[95], L. Han[112a], L. Han[61], S. Han[14], K. Hanagaki[82], M. Hance[137], D.A. Hangal[41], H. Hanif[145], M.D. Hank[129], J.B. Hansen[42], P.H. Hansen[42], T. Harenberg[173], S. Harkusha[175], M.L. Harris[103], Y.T. Harris[25], J. Harrison[13], P.F. Harrison[169], M. L. E. Hart[96], N.M. Hartman[110], N.M. Hartmann[109], R. Z. Hasan[95,135], Y. Hasegawa[143], D. Hashimoto[111], F. Haslbeck[37], S. Hassan[126], R. Hauser[107], M. Haviernik[134], C.M. Hawkes[21], R.J. Hawkings[37], Y. Hayashi[156], D. Hayden[107], R.L. Hayes[116], C.P. Hays[127], J.M. Hays[94], H.S. Hayward[92], M. He[14,112c], Y. He[47], Y. He[96], V. Hedberg[98], J. Heilman[35], S. Heim[47], T. Heim[18a], J.J. Heinrich[124], L. Heinrich[110], J. Hejbal[132], M. Helbig[49], A. Held[172], S. Hellesund[17], C.M. Helling[166], F.N.E. Henry[58], H. Herde[98], Y. Hernández Jiménez[148], G. Herten[53], R. Hertenberger[109], L. Hervas[37], M.E. Hesping[100], N.P. Hessey[159a], J. Hessler[110], R. Hicks[129], M. Hidaoui[36b], N. Hidic[134], E. Hill[158], T. S. Hillersoy[17], S.J. Hillier[21], J.R. Hinds[107], F. Hinterkeuser[25], M. Hirose[125], S. Hirose[170], D. Hirschbuehl[173], B. Hiti[93], J. Hobbs[148], R. Hobincu[28e], N. Hod[171], A.M. Hodges[164], M.C. Hodgkinson[142], B.H. Hodkinson[127], A. Hoecker[37], D. D. Hofer[106], J. Hofer[165], J. Hofner[100], M. Holzbock[37], L.B.A.H. Hommels[33], V. Homsak[127], J. J. Hong[67], T.M. Hong[130], R. Honscheid[127], B.H. Hooberman[164], W.H. Hopkins[6], M. C. Hoppesch[164], Y. Horii[111], M. E. Horstmann[110], M.M. Horzela[54], S. Hou[151], M. R. Housenga[164], J. Howarth[58], J. Hoya[6], M. Hrabovsky[123], T. Hryn'ova[4], P.J. Hsu[64], S.-C. Hsu[140], T. Hsu[65], M. Hu[18a], P. Hu[63b], Q. Hu[61], S. Huang[33], X. Huang[14,112c], Y. Huang[134],

JHEP10(2026)270

Y. Huang[112b], Y. Huang[14], Z. Huang[65], Z. Hubacek[133], F. Huegging[25], T.B. Huffman[127], M. Hufnagel Maranha De Faria[81a], C. A. Hugli[47], M. Huhtinen[37], S.K. Huiberts[17], R. Hulsken[104], C. E. Hultquist[18a], D.L. Humphreys[103], N. Huseynov[12], J. Huston[107], B. Huth[37], J. Huth[60], L. Huth[47], R. Hyneman[7], G. Iacobucci[55], G. Iakovidis[30], L. Iconomidou-Fayard[65], J. P. Iddon[37], P. Iengo[71a,71b], Y. Iiyama[156], T. Iizawa[156], Y. Ikegami[82], D. Iliadis[155], N. Ilic[158], H. Imam[36a], G. Inacio Goncalves[81d], S. A. Infante Cabanas[138c], T. Ingebretsen Carlson[46a,46b], J. M. Inglis[94], G. Introzzi[72a,72b], M. Iodice[76a], V. Ippolito[74a,74b], R. K. Irwin[92], M. Ishino[156], W. Islam[172], C. Issever[19], O. N. Istaitia[65,f], S. Istin[22a,z], K. Itabashi[125], H. Ito[170], R. Iuppa[77a,77b], A. Ivina[171], F. Ivone[37], S. Izumiyama[111], V. Izzo[71a], P. Jacka[133], P. Jackson[1], P. R. Jacobson[50], P. Jain[47], K. Jakobs[53], J. Jamieson[58], W. Jang[156], S. Jankovych[116], B. K. Jashal[135], M. Javurkova[103], P. Jawahar[101], L. Jeanty[124], J. Jejelava[152a,aa], P. Jenni[53,ab], L. Jerala[93], C.E. Jessiman[35], H. Jia[166], J. Jia[148], K. Jia[146], X. Jia[110,112c], C. Jiang[51], Q. Jiang[63b], S. Jiggins[47], M. Jimenez Ortega[165], J. Jimenez Pena[13], S. Jin[112a], A. Jinaru[28b], O. Jinnouchi[139], P. Johansson[142], K.A. Johns[7], J.W. Johnson[137], F. A. Jolly[47], D.M. Jones[149], E. Jones[47], P. Jones[33], R.W.L. Jones[91], T.J. Jones[92], H.L. Joos[37], R. Joshi[120], J. Jovicevic[16], X. Ju[18a], J.J. Junggeburth[37], T. Junkermann[62a], A. Juste Rozas[13,x], M.K. Juzek[86], S. Kabana[138f], A. Kaczmarska[86], S. A. Kadir[146], M. Kado[110], H. Kagan[120], M. Kagan[146], A. Kahn[129], C. Kahra[100], T. Kaji[156], E. Kajomovitz[153], N. Kakati[171], N. Kakoty[13], S. Kandel[8], E. Kanellaki[45], N. Kanellos[10], S. Kang[50], D. Kar[34j,†], E. Karentzos[25], K. Karki[8], O. Karkout[116], S.N. Karpov[38], Z.M. Karpova[38], V. Kartvelishvili[91,152b], E. Kasimi[155], J. Katzy[47], S. Kaur[35], R. Kavak[37], K. Kawade[143], M.P. Kawale[121], C. Kawamoto[87], E.F. Kay[37], S. Kazakos[107], K. Kazakova[102], J.M. Keaveney[34a], R. Keeler[167], G.V. Kehris[60], J.S. Keller[35], J. M. Kelly[167], J.I. Kelsey[164], J.J. Kempster[149], O. Kepka[132], J. Kerr[159b], B.P. Kerridge[135], B.P. Kerševan[93], L. Keszeghova[29a], R. A. Khan[130], A. Khanov[122], M. Kholodenko[131a], T.J. Khoo[19], G. Khoriauli[168], Y. Khoulaki[36a], Y.A.R. Khwaira[128], D. Kim[6], D.W. Kim[18b], Y.K. Kim[39], N. Kimura[96], M.K. Kingston[54], F. Kirfel[25], J. Kirk[135], A.E. Kiryunin[110], S. Kita[156], O. Kivernyk[25], M. Klassen[37], C. Klein[35], L. Klein[168], M.H. Klein[44], U. Klein[92], A. Klimentov[30], P. Kluit[116], S. Kluth[110], E. Kneringer[78], T.M. Knight[158], A. Knue[48], M. Kobel[49], D. Kobylianskii[171], S.F. Koch[37], M. Kocian[146], P. Kodyš[134], D.M. Koeck[124], T. Koffas[35], K. Kojima[82], O. Kolay[49], I. Koletsou[4], T. Komarek[86], S. Kondo[156], K. Köneke[54], A.X.Y. Kong[1], T. Kono[119], N. Konstantinidis[96], P. Kontaxakis[55], B. Konya[98], R. Kopeliansky[41], S. Koperny[85a], R. Koppenhofer[53], I. Kopsalis[10], K. Korcyl[86], K. Kordas[155,ac], A. Korn[96], S. Korn[54], I. Korolkov[13], O. Kortner[110], S. Kortner[110], W.H. Kostecka[117], M. Kostov[29a], V.V. Kostyukhin[144], A. Kotsokechagia[37], A. Kotwal[50], A. Koulouris[37], A. Kourkoumeli-Charalampidi[72a,72b], O. Kovanda[124], R. Kowalewski[167], W. Kozanecki[124], G. Kramberger[93], P. Kramer[25], A. Krasznahorkay[103], A. C. Kraus[117], J.W. Kraus[173], J.A. Kremer[47], N. B. Krengel[144], T. Kresse[158], L. Kretschmann[173], J. Kretzschmar[92], P. Krieger[158], K. Krizka[21], K. Kroeninger[48], H. Kroha[110], J. Kroll[132], J. Kroll[129], K.S. Krowpman[107], U. Kruchonak[38], H. Krüger[25], N. Krumnack[79], J. Krupa[146], M.C. Kruse[50], O. Kuchinskaia[38], S. Kuday[3a], S. Kuehn[37], R. Kuesters[53], T. Kuhl[47],

JHEP10(2026)270

V. Kukhtin[38], Y. Kulchitsky[38], S. Kuleshov[138d,138b], J. Kull[1], E. V. Kumar[109], M. Kumar[34j], N. Kumari[47], P. Kumari[159b], A. Kupco[132], O. Kuprash[53], H. Kurashige[84], L.L. Kurchaninov[159a], O. Kurdysh[4], M. Kuze[139], A.K. Kvam[103], J. Kvita[123], N.G. Kyriacou[140], M. Laassiri[30], C. Lacasta[165], H. Lacker[19], D. Lacour[128], E. Ladygin[38], A. Lafarge[40], B. Laforge[128], T. Lagouri[174], F.Z. Lahbabi[36a], J. Lai[124], S. Lai[54], W. S. Lai[96], I.K. Lakomiec[54], J.E. Lambert[167], S. Lammers[67], W. Lampl[7], C. Lampoudis[155], G. Lamprinoudis[168], A.N. Lancaster[117], U. Landgraf[53], M.P.J. Landon[94], V.S. Lang[53], A.J. Lankford[162], F. Lanni[37], C. S. Lantz[164], K. Lantzsch[25], A. Lanza[72a], M. Lanzac Berrocal[165], T. Lari[70a], D. Larsen[17], L. Larson[11], F. Lasagni Manghi[24b], M. Lassnig[37], H.C. Lau[167], S.D. Lawlor[142], R. Lazaridou[162], M. Lazzaroni[70a,70b], E. T. T. Le[162], H. D. M. Le[107], E.M. Le Boulicaut[174], D.O. Le Guennec[136], L.T. Le Pottier[18a], B. Leban[24b,24a], F. Ledroit-Guillon[59], T.F. Lee[159b], L.L. Leeuw[34h], M. Lefebvre[167], C. Leggett[18a], L.M. Lehmann[116], W.A. Leight[103], W. Leinonen[115], A. Leisos[155,ad], M.A.L. Leite[81c], C.E. Leitgeb[19], R. Leitner[134], E. Lelak[134], K.J.C. Leney[44], T. Lenz[25], S. Leone[73a], C. Leonidopoulos[51], A. Leopold[147], J. LePage-Bourbonnais[35], R. Les[65], C.G. Lester[33], J. Levêque[4], L.J. Levinson[171], G. Levrini[24b,24a], M.P. Lewicki[86], C. Lewis[140], D.J. Lewis[4], L. Lewitt[142], A. Li[30], B. Li[113b], C-Q. Li[110], C. Li[106], H. Li[113b], H. Li[101], H. Li[15], H. Li[61], H. Li[113b], J. Li[141a], L. Li[141a], R. Li[174], S. Li[141b,141a], Y. Li[14], Z. Li[14,112c], Z. Li[61], S. Liang[14,112c], Z. Liang[14], M. Liberatore[136], B. Liberti[75a], G. B. Libotte[81d], M. Licchelli[70b], K. Lie[63c], J. Lieber Marin[81e], H. Lien[67], H. Lin[106], S. F. Lin[148], L. Linden[109], R.E. Lindley[7], J.H. Lindon[37], J. Ling[60], E. Lipeles[129], A. Lipniacka[17], A. Lister[166], J.D. Little[67], B. Liu[113a], B.X. Liu[112b], D. Liu[153], D. Liu[137], E. H. L. Liu[21], H. Liu[112b], J.K.K. Liu[118], K. Liu[141b], K. Liu[141b], M. Liu[61], M.Y. Liu[61], P. Liu[113b], Q. Liu[146], S. Liu[148], X. Liu[113b], Y. Liu[112b,112c], Y. Liu[164], Y.L. Liu[113b], Y.W. Liu[61], Z. Liu[65,ae], S.L. Lloyd[94], E.M. Lobodzinska[47], P. Loch[7], E. Lodhi[158], K. Lohwasser[142], E. Loiacono[122], J. D. Lomas[21], I. Longarini[162], R. Longo[24b,24a,w], A. Lopez Solis[13], N.A. Lopez-canelas[7], N. Lorenzo Martinez[4], A.M. Lory[109], M. Losada[83b], G. Löschcke Centeno[4], X. Lou[14,112c], P.A. Love[91], H. Lu[14], M. Lu[65], S. Lu[129], Y.J. Lu[151], H.J. Lubatti[140], C. Luci[74a,74b], F.L. Lucio Alves[112a], J.A. Lue[124], F. Luehring[67], B. S. Lunday[129], O. Lundberg[147], J. Lunde[37], N.A. Luongo[6], M.S. Lutz[158], A.B. Lux[26], D. Lynn[30], R. Lysak[132], V. Lysenko[133], E. Lytken[98], V. Lyubushkin[38], T. Lyubushkina[38], M.M. Lyukova[148], H. Ma[30], K. Ma[61], L.L. Ma[113b], W. Ma[61], Y. Ma[113b], B. Maček[93], P.C. Machado De Abreu Farias[81e], D. Macina[37], R. Madar[40], T. Madula[96], J. Maeda[84], T. Maeno[30], P.T. Mafa[34f], G. Magni[65], H. Maguire[142], M. Maheshwari[33], V. Maiboroda[65], G. Maineri[70a,70b], A. Maio[131a,131b,131d], K. Maj[85a], O. Majersky[47], S. Majewski[124], A. Makita[156], N. Makovec[65], V. Maksimovic[16], B. Malaescu[128], J. Malamant[126], Pa. Malecki[86], F. Malek[59,af], M. Mali[93], D. Malito[95], A. Maloizel[5], A. Malvezzi Lopes[81d], S. Malyukov[38], J. Mamuzic[93], G. Mancini[52], M. N. Mancini[27], G. Manco[72a,72b], S.S. Mandarry[149], I. Mandić[93], L. Manhaes de Andrade Filho[81a], I.M. Maniatis[171], J. Manjarres Ramos[89], D.C. Mankad[171], A. Mann[109], T. Manoussos[100], M.N. Mantinan[39], S. Manzoni[37], L. Mao[141a], X. Mapekula[34c], A. Marantis[155], R.R. Marcelo Gregorio[1], G. Marchiori[5], C. Marcon[70a],

JHEP10(2026)270

E. Maricic[16], M. Marinescu[47], S. Marium[47], M. Marjanovic[121], A. Markhoos[53], M. Markovitch[65], M. K. Maroun[103], M. C. Marr[145], T. L. Marsault[136], G. T. Marsden[101], Z. Marshall[18a], S. Marti-Garcia[165], J. Martin[96], T.A. Martin[135], V.J. Martin[51], B. Martin dit Latour[17], S. Martin-Haugh[135], F. Martina[69a,69b], L. Martinelli[74a,74b], V.I. Martinez Outschoorn[103], P. Martinez Suarez[37], G. Martinovicova[134], V.S. Martoiu[28b], A. Martone[89], A.C. Martyniuk[96], A. Marzin[37], D. Mascione[77a,77b], L. Masetti[100], J. Masik[101], A.L. Maslennikov[38], S.L. Mason[41], P. Massarotti[71a,71b], P. Mastrandrea[73a,73b], A. Mastroberardino[43b,43a], R. Mastrofrancesco[72a,72b], T. Masubuchi[125], T.T. Mathew[124], J. Matousek[134], D.M. Mattern[48], K. Mauer[47], J. Maurer[28b], T. Maurin[58], C. Mavungu Tsava[102], A. E. May[101], E. Mayer[40], R. Mazini[34j], S.M. Mazza[137], E. Mazzeo[37], J.P. Mc Gowan[167], S.P. Mc Kee[106], C.C. McCracken[166], E.F. McDonald[105], L. F. Mcelhinney[91], J.A. Mcfayden[149], R.P. McGovern[167], R.P. Mckenzie[34j], D.J. Mclaughlin[96], S.J. McMahon[135], C.M. Mcpartland[92], R.A. McPherson[167,o], S. Mehlhase[109], A. Mehta[92], D. Melini[165], B.R. Mellado Garcia[14,ag], A.H. Melo[54], F. Meloni[47], A.M. Mendes Jacques Da Costa[101], L. Meng[91], S. Menke[110], M. Mentink[37], E. Meoni[43b,43a], G. Mercado[117], S. Merianos[155], C. Merlassino[68a,68c], C. Meroni[70a,70b], J. Metcalfe[6], A.S. Mete[6], E. Meuser[100], C. Meyer[67], J-P. Meyer[136], O. Mezhenska[29b], Y. Miao[112a], R.P. Middleton[135], M. Mihovilovic[65], L. Mijović[51], G. Mikenberg[171], M. Mikestikova[132], M. Mikuž[93], H. Mildner[100], A. Milic[37], D.W. Miller[39], E. H. Miller[146], A. Milov[171], D.A. Milstead[46a,46b], T. Min[112a], I.A. Minashvili[152b], A.I. Mincer[118], B. Mindur[85a], M. Mineev[38], L.M. Mir[13], M. Miralles Lopez[58], M. Mironova[18a], M. Missio[40], A. Mitra[169], V.A. Mitsou[165], P.S. Miyagawa[94], R. Mizuhiki[84], T. Mkrtchyan[37], M. Mlinarevic[96], T. Mlinarevic[96], M. Mlynarikova[134], L. Mlynarska[85a], C. Mo[141a], H. Möbius[47], S. Mobius[20], M. H. Mohamed Farook[114], S. Mohapatra[41], M.F. Mohd Soberi[51], S. Mohiuddin[122], G. Mokgatitswane[34j], R. Mole[21], L. Moleri[171], U. Molinatti[127], M. E. Mollerach[31], L.G. Mollier[20], L. Monaco[37,58], B. Mondal[132], S. Mondal[134], K. Mönig[47], E. Monnier[102], L. Monsonis Romero[165], A. Montella[46a,46b], M. Montella[120], F. Montereali[76a,76b], F. Monticelli[90], S. Monzani[68a,68c], M.E.E. Moors[25], A. Morancho Tarda[42], N. Morange[65], M. Moreno Llácer[165], C. Moreno Martinez[55], J.M. Moreno Perez[23b], P. Morettini[56b], S. Morgenstern[62a], M. Morii[60], M. Morinaga[156], F. Morodei[74a,74b], P. Moschovakos[37], B. Moser[53], M. Mosidze[152b], T. Moskalets[44], P. Moskvitina[115], C.J. Mosomane[34b], J. Moss[32], T. Motta Quirino[81d], A. Moussa[36d], Y. Moyal[171,ah], H. Moyano Gomez[13], E.J.W. Moyse[103], T.G. Mroz[86], S. Muanza[102], M. Mucha[25], J. Mueller[130], D. Muller[144], G.A. Mullier[163], A.J. Mullin[33], J.J. Mullin[50], A.C. Mullins[44], A.E. Mulski[60], D.P. Mungo[158], D. Munoz Perez[122], F.J. Munoz Sanchez[101], W.J. Murray[169,135], E. Musajan[61], M. Muškinja[93], C. Mwewa[47], A.J. Myers[8], G. Myers[106], M. Myska[133], B.P. Nachman[146], I.A. Nadas[28d], K. Nagai[127], K. Nagano[82], R. Nagasaka[156], J.L. Nagle[30,ai], E. Nagy[102], A.M. Nairz[37], T. Nakagawa[87], Y. Nakahama[82], K. Nakamura[82], A. Nandi[62b], H. Nanjo[125], E.A. Narayanan[44], Y. Narukawa[156], L. Nasella[70a,70b], S. Nasri[83c], C. Nass[25], G. Navarro[23a], A. Nayaz[19], S. Nechaeva[24b,24a], F. Nechansky[132], L. Nedic[127], A. Negri[72a,72b], M. Negrini[24b], C. Nellist[116], C. Nelson[104], K. Nelson[106], S. Nemecek[132], M. Nessi[37,e], M.S. Neubauer[164], J. Newell[92], P.R. Newman[21], Y.W.Y. Ng[164],

JHEP10(2026)270

B. Ngair[83b], H.D.N. Nguyen[108], J.D. Nichols[121], R. Nicolaidou[136], J. Nielsen[137], M. Niemeyer[54], J. Niermann[37], N. Nikiforou[37], I. Nikolic-Audit[128], P. Nilsson[30], G. Ninio[154], A. Nisati[74a], D. Nishimura[156], R. Nisius[110], N. Nitika[171], E.K. Nkadimeng[34b], T. Nobe[156], D. Noll[146], T. Nommensen[150], M.B. Norfolk[142], B.J. Norman[35], L.C. Nosler[18a], M. Noury[36a], J. Novak[93], T. Novak[93], P. Novotny[171], R. Novotny[133], L. Nozka[123], K. Ntekas[37], D. Ntounis[146], N.M.J. Nunes De Moura Junior[81b], A.P. O'Neill[20], J. Ocariz[128], I. Ochoa[131a], A. Odella Rodriguez[13], S. Oerdek[47], J.T. Offermann[39], K. Ograbek[85a], A. Ogrodnik[86], A. Oh[101], C.C. Ohm[147], H. Oide[82], M.L. Ojeda[37], Y. Okumura[156], L.F. Oleiro Seabra[131a], I. Oleksiyuk[55], G. Oliveira Correa[13], D. Oliveira Damazio[30], J.L. Oliver[1], R. Omar[67], Y. Onoda[139], A. Onofre[131a,131e,aj], P.U.E. Onyisi[11], M.J. Oreglia[39], D. Orestano[76a,76b], R. Orlandini[76a,76b], R.S. Orr[158], L.M. Osojnak[41], Y. Osumi[111], G. Otero y Garzón[31], H. Otono[88], M. Ouchrif[36d], F. Ould-Saada[126], T. Ovsiannikova[140], M. Owen[58], R.E. Owen[135], S.A. Oyeniran[114], V.E. Ozcan[22a], F. Ozturk[86], N. Ozturk[8], S. Ozturk[80], H.A. Pacey[127], K. Pachal[159a], A. Pacheco Pages[13], C. Padilla Aranda[13], G. Padovano[74a,74b], S. Pagan Griso[18a], L. Pagani[75a,75b], J. Pampel[25], D.K. Panchal[11], C.E. Pandini[59], J.G. Panduro Vazquez[135], H.D. Pandya[1], H. Pang[136], P. Pani[47], G. Panizzo[68a,68c], L. Panwar[128,ak], L. Paolozzi[21], S. Parajuli[164], A. Paramonov[6], C. Paraskevopoulos[52], D. Paredes Hernandez[63b], S.R. Paredes Saenz[51], A. Pareti[72a,72b], K.R. Park[41], T.H. Park[110], F. Parodi[56b,56a], J.A. Parsons[41], J.A. Partridge[137], U. Parzefall[53], B.A. Paschen[18a], B. Pascual Dias[40], L. Pascual Dominguez[99], E. Pasqualucci[74a], S. Passaggio[56b], F. Pastore[95], P. Patel[86], U.M. Patel[50], J.R. Pater[101], T. Pauly[37], A. Paunovic[16], F. Pauwels[134], C.I. Pazos[161], M. Pedersen[126], R. Pedro[131a], O. Penc[132], C.C. Penelaud[128], S. Peng[15], G. D. Penn[174], B.S. Peralva[81d], A.P. Pereira Peixoto[140], L. Pereira Sanchez[146], D.V. Perepelitsa[30,ai], G. Perera[103], E. Perez Codina[37], M. Perganti[10], H. Pernegger[37], S. Perrella[74a,74b], K. Peters[47], R.F.Y. Peters[101], B.A. Petersen[37], T.C. Petersen[42], E. Petit[102], V. Petousis[133], A. R. Petri[70a,70b], V.A. Petrovic[96], T. Petru[134], M. Pettee[18a], A. Petukhov[80], K. Petukhova[37], R. Pezoa[138g], L. Pezzotti[24b,24a], G. Pezzullo[174], L. Pfaffenbichler[37], A. J. Pfleger[78], T. Pham[105], T.M. Pham[172], P.W. Phillips[135], G. Piacquadio[148], E. Pianori[18a], F. Piazza[124], R. Piegaia[31], D. Pietreanu[28b], A.D. Pilkington[101], T. Pilusa[34j], M. Pinamonti[68a,68c], J.L. Pinfold[2], G. Pinheiro Matos[41], B.C. Pinheiro Pereira[131a], J. Pinol Bel[13], A. E. Pinto Pinoargote[128], L. Pintucci[68a,68c], K. M. Piper[149], A. Pirttikoski[55], D.A. Pizzi[35], L. Pizzimento[63b], A. Plebani[33], M.-A. Pleier[30], V. Pleskot[134], E. Plotnikova[38], G. Poddar[94], R. Poettgen[98], L. Poggioli[128], S. Polacek[134], G. Polesello[72a], A. Poley[145], A. Polini[24b], C.S. Pollard[169], Z.B. Pollock[120], E. Pompa Pacchi[121], N. I. Pond[96], D. Ponomarenko[67], L. Pontecorvo[37], S. Popa[28a], G.A. Popeneciu[28d], A. Poreba[37], A. Portentoso[70b], D.M. Portillo Quintero[159a], S. Pospisil[133], M. A. Postill[142], P. Postolache[28c], K. Potamianos[169], P.A. Potepa[85a], I.N. Potrap[38], C.J. Potter[33], H. Potti[150], J. Poveda[165], M.E. Pozo Astigarraga[37], R. Pozzi[37], A. Prades Ibanez[75a,75b], S.R. Pradhan[142], J. Preston[95], J. Pretel[167], D. Price[101], M. Primavera[69a], L. Primomo[68a,68c], M.A. Principe Martin[99], R. Privara[123], T. Procter[85b], M.L. Proffitt[140], N. Proklova[129], K. Prokofiev[63c], G. Proto[110], J. Proudfoot[6],

JHEP10(2026)270

M. Przybycien[85a], W.W. Przygoda[85b], A. Psallidas[45], D. Pudzha[52], P. Puhl[57], H. I. Purnell[1], D. Pyatiizbyantseva[115], J. Qian[106], R. Qian[107], D. Qichen[127], Y. Qin[13], T. Qiu[51], A. Quadt[54], M. Queitsch-Maitland[101], G. Quetant[55], R.P. Quinn[166], D. Rafanoharana[110], J.L. Rainbolt[39], S. Rajagopalan[30], E. Ramakoti[38], L. Rambelli[56b,56a], I.A. Ramirez-Berend[35], K. Ran[106,112c], S. D. Randles[92], D. S. Rankin[129], N.P. Rapheeha[34j], H. Rasheed[28b], A. Rastogi[18a], S. Rave[100], S. Ravera[56b,56a], B. Ravina[37], I. Ravinovich[171], M. Raymond[37], A.L. Read[126], N.P. Readioff[142], D.M. Rebuzzi[72a,72b], A. S. Reed[58], K. Reeves[27], D. Reikher[37], T. Reisch[55], A. Rej[48], H. Ren[61], M. Renda[28b], F. Renner[47], A.G. Rennie[58], M. Repik[55], A.L. Rescia[43b,43a], S. Resconi[70a], M. Ressegotti[56b], S. Rettie[116], W.F. Rettie[35], M. M. Revering[33], O.L. Rezanova[38], P. Reznicek[134], H. Riani[36d], N. Ribaric[37], B. Ricci[68a,68c], E. Ricci[77a,77b], R. Richter[110], E. Richter-Was[85b], M. Ridel[128], S. Ridouani[36d], P. Riedler[37], E.M. Riefel[46a,46b], J. O. Rieger[116], M. Rimoldi[34c], L. Rinaldi[24b,24a], P. Rincke[163,54], G. Ripellino[163], I. Riu[13], J.C. Rivera Vergara[167], F. Rizatdinova[122], E. Rizvi[94], B.R. Roberts[39], S.S. Roberts[137], D. Robinson[33], A. Robson[58], A. Rocchi[75a,75b], C. Roda[73a,73b], F.A. Rodriguez[117], S. Rodriguez Bosca[37], Y. Rodriguez Garcia[23a], A.M. Rodríguez Vera[117], S. Roe[37], J.T. Roemer[37], O. Røhne[126], R.A. Rojas[37], Z. Rokavec[93], C.P.A. Roland[128], A. Romaniouk[78], E. Romano[72a,72b], M. Romano[24b], N. Rompotis[92], L. Roos[128], S. Rosati[74a], L. Roscher[47], B.J. Rosser[39], E. Rossi[127], E. Rossi[71a,71b], L.P. Rossi[60], L. Rossini[53], R. Rosten[138b], M. Rotaru[28b], R. Roth[37], F. A. Rothen[55], D. Rousseau[65], D. Rousso[47], S. Roy-Garand[55], A. Rozanov[102], Z. M. A. Rozario[58], Y. Rozen[153], A. Rubio Jimenez[165], V.H. Ruelas Rivera[19], T.A. Ruggeri[1], A. Ruggiero[127], A. Ruiz-Martinez[165], A. Rummler[37], G.B. Rupnik Boero[37], N.A. Rusakovich[38], S. Ruscelli[48], H.L. Russell[167], G. Russo[137], J.P. Rutherfoord[7], S. Rutherford Colmenares[118], M. Rybar[134], P. Rybczynski[85a], A. Ryzhov[44], M. A. E. Saadawy[44], F. Safai Tehrani[74a], S. Saha[1], B. Sahoo[171], B. T. Saifuddin[121], M. Saimpert[136], I. Sainz Saenz Diez[62a], G.T. Saito[81c], M. Saito[156], T. Saito[156], A. Sala[70a,70b], O. T. Salin[65], A. Salnikov[146], J. Salt[165], A. Salvador Salas[154], F. Salvatore[149], A. Salzburger[37], D. Sammel[53], E. Sampson[91], D. Sampsonidis[155,ac], D. Sampsonidou[124], M.A.A. Samy[58], J. Sánchez[165], H. Sandaker[126], C.O. Sander[47], J.A. Sandesara[172], M. Sandhoff[173], C. Sandoval[23b], L. Sanfilippo[62a], D.P.C. Sankey[135], T. Sano[87], A. Sansar[22c], A. Sansoni[52], M. Santana Queiroz[18b], L. Santi[37], C. Santoni[40], G. Santoro[43b,43a], H. Santos[131a,131b], L. Santos Pereira Trigo[47], E. Sanzani[24b,24a], K.A. Saoucha[83d], J.G. Saraiva[131a,131d], J. Sardain[7], S. Sarkar[50], O. Sasaki[82], K. Sato[160], C. Sauer[37], E. Sauvan[4], P. Savard[158,t], M. Savic[164], R. Sawada[156], C. Sawyer[135], L. Sawyer[97], A. M. Sayed[27], C. Sbarra[24b], A. Sbrizzi[24b,24a], R. Scaglioni[72a,72b], T. Scanlon[96], J. Schaarschmidt[140], U. Schäfer[100], A.C. Schaffer[65,44], D. Schaile[109], R.D. Schamberger[148], C. Scharf[19], M.M. Schefer[20], D. Scheirich[134], M. Schernau[138f], C. Scheulen[55], C. Schiavi[56b,56a], M. Schioppa[43b,43a], S. Schlenker[37], T. Schlomer[54], J. Schmeing[173], C. R. Schmidt[49], E. Schmidt[110], M. A. Schmidt[173], K. Schmieden[25], C. Schmitt[100], N. Schmitt[100], S. Schmitt[47], N.A. Schneider[109], L. Schoeffel[136], A. Schoening[62b], P.G. Scholer[35], E. Schopf[144], M. Schott[25], S. Schramm[55], T. Schroer[55], H-C. Schultz-Coulon[62a], M. Schumacher[53], B.A. Schumm[137], Ph. Schune[136],

JHEP10(2026)270

H.R. Schwartz[7], A. Schwartzman[146], T.A. Schwarz[106], Ph. Schwemling[136], R. Schwienhorst[107], F.G. Sciacca[20], A. Sciandra[30], G. Sciolla[27], S. A. Scoville[130], F. Scuri[73a], C.D. Sebastiani[37], K. Sedlaczek[117], S. Seguini[70b], A. Sehrawat[138b], S.C. Seidel[114], B.D. Seidlitz[41], C. Seitz[47], J.M. Seixas[81b,†], G. Sekhniaidze[71a], L. Selem[128], N. Semprini-Cesari[24b,24a], A. Semushin[175], V. Senthilkumar[116], L. Serin[65], M. Sessa[71a,71b], H. Severini[121], F. Sforza[56b,56a], A. Sfyrla[55], Q. Sha[14], H. Shaddix[117], A.H. Shah[33], R. Shaheen[147], J.D. Shahinian[129], M. Shamim[37], L.Y. Shan[14], M. Shapiro[18a], A. Sharma[37], A.S. Sharma[166], P. Sharma[30], K. Shaw[149], S.M. Shaw[101], D. Shemyakin[171], Q. Shen[14], D.J. Sheppard[145], P. Sherwood[96], L. Shi[112b], X. Shi[14], E.B. Shields[171], S. Shimizu[82], S. Shirabe[88], M. Shiyakova[38,al], M.J. Shochet[39], D.R. Shope[126], S. Shrestha[120,am], I. Shreyber[38], M.J. Shroff[104], P. Sicho[132], A.M. Sickles[164], E. Sideras Haddad[34j], A. C. Sidley[116], A. Sidoti[24b], F. Siegert[49], Dj. Sijacki[16], F. Sili[61], J.M. Silva[51], I. Silva Ferreira[81b], M.V. Silva Oliveira[30], S.B. Silverstein[46a], S. Simion[65], R. Simoniello[37], E.L. Simpson[101], H. Simpson[149], L.R. Simpson[6], S. Simsek[80], S. Singh[30], S. N. Singh[27], S. Sinha[47], S. Sinha[101], M. Sioli[24b,24a], K. Sioulas[9], E. Sitnikova[47], J. Sjölin[46a,46b], A. Skaf[54], E. Skorda[21], P. Skubic[121], M. Slawinska[86], I. Slazyk[17], I. Sliusar[126], V. Smakhtin[171], B.H. Smart[135], S.Yu. Smirnov[138b], Y. Smirnov[34c], O. Smirnova[98], J.L. Smith[101], M. B. Smith[35], R. Smith[146], H. Smitmanns[100], M. Smizanska[91], K. Smolek[133], P. Smolyanskiy[133], A.A. Snesarev[38], H.L. Snoek[116], R. M. Snyder[50], S. Snyder[30], R. Sobie[167,o], A. Soffer[154], C.A. Solans Sanchez[37], E.Yu. Soldatov[38], U. Soldevila[165], A.A. Solodkov[34j], S. Solomon[27], A. Soloshenko[38], O.V. Solovyanov[40], P. Sommer[49], A. Sopczak[133], A.L. Sopio[51], F. Sopkova[29b], J. D. Sorenson[114], I.R. Sotarriva Alvarez[139], V. Sothilingam[62a], O. J. Soto Sandoval[138c,138b], S. Sottocornola[67], R. Soualah[83a], D. South[47], N. Soybelman[171], S. Spagnolo[69a,69b], A.S. Spellman[124], D. Sperlich[53], B. Spisso[71a,71b], L. Splendori[102], M. Spousta[134], E.J. Staats[35], R. Stamen[62a], E. Stanecka[86], W. Stanek-Maslouska[47], M.V. Stange[49], B. Stanislaus[18a], M.M. Stanitzki[47], G.H. Stark[137], J. Stark[89], P. Staroba[132], P. Starovoitov[83d], R. Staszewski[86], C. Stauch[109], G. Stavropoulos[45], A. Stefl[37], A. Stein[100], P. Steinberg[30], B. Stelzer[145,159a], H.J. Stelzer[130], O. Stelzer[159a], H. Stenzel[57], T.J. Stevenson[149], G.A. Stewart[47], G. Stoicea[28b], M. Stolarski[131a], S. Stonjek[110], A. Straessner[49], J. Strandberg[147], S. Strandberg[46a,46b], M. Stratmann[173], M. Strauss[121], T. Strebler[102], P. Strizenec[29b], R. Ströhmer[168], D.M. Strom[124], R. Stroynowski[44], A. Strubig[46a,46b], S.A. Stucci[30], B. Stugu[17], J. Stupak[121], N.A. Styles[47], D. Su[146], S. Su[61], X. Su[61], D. Suchy[29a], A. D. Sudhakar Ponnu[54], L. Sudit[171], Y. Sue[82], K. Sugizaki[129], D.M.S. Sultan[127], L. Sultanaliyeva[25], S. Sultansoy[3b], S. Sun[172], W. Sun[14], S. Sundar Raman[166], N. Sur[98], J.P. Surdutovich[120], N. Suri Jr[174], M.R. Sutton[149], M. Svatos[132], P. N. Swallow[33], S.N. Swatman[37], M. Swiatlowski[159a], A. Swoboda[37], I. Sykora[29a], M. Sykora[134], T. Sykora[134], D. Ta[100], K. Tackmann[47,an], A. Taffard[162], R. Tafirout[159a], Y. Takubo[82], M. Talby[102], N.M. Tamir[154], A. Tanaka[156], J. Tanaka[156], R. Tanaka[65], M. Tanasini[148], Z. Tao[166], S. Tapia Araya[138g], S. Tapprogge[100], A. Tarek Abouelfadl Mohamed[37], S. Tarem[153], K. Tariq[14], G. Tarna[37], G.F. Tartarelli[70a], M. J. Tartarin[141b], P. Tas[134], M. Tasevsky[132], E. Tassi[43b,43a], A.C. Tate[164], Y. Tayalati[36e,ao], G.N. Taylor[105],

JHEP10(2026)270

W. Taylor[159b], R.J. Taylor Vara[165], A.S. Tegetmeier[89], P. Teixeira-Dias[95], J.J. Teoh[158], K. Terashi[156], J. Terron[99], S. Terzo[13], M. Testa[52], R.J. Teuscher[158,o], A. Thaler[78], T. Theveneaux-Pelzer[102], J.P. Thomas[21], E.A. Thompson[18a], P.D. Thompson[21], E. Thomson[129], R. E. Thornberry[30], T.M. Thory-Rao[21], C.N. Thotamuna Wijewardhana[148], C. Tian[61], Y. Tian[55], V. Tikhomirov[80], Yu.A. Tikhonov[38], D. Timoshyn[134], E.X.L. Ting[1], P. Tipton[174], A. Tishelman-Charny[30], K. Todome[139], S. Todorova-Nova[134], L. Toffolin[68a,68c], M. Togawa[82], J. Tojo[88], S. Tokár[29a], O. Toldaiev[67], A. J. Toler[103], G. Tolkachev[102], M. Tomoto[82], L. Tompkins[146], E. Torrence[124], H. Torres[89], D. I. Torres Arza[138g], E. Torres Reoyo[165], E. Torró Pastor[165], M. Toscani[31], C. Tosciri[39], M. Tost[11], D.R. Tovey[142], T. Trefzger[168], P.M. Tricarico[13], A. Tricoli[30], I.M. Trigger[159a], S. Trincaz-Duvoid[128], D.A. Trischuk[167], A. Tropina[38], D. Truncali[75a,75b], L. Truong[34c], M. Trzebinski[86], A. Trzupek[86], F. Tsai[148], A. Tsiamis[155], P.V. Tsiareshka[38], S. Tsigaridas[159a], A. Tsirigotis[155,ad], V. Tsiskaridze[152a], E.G. Tskhadadze[152a], H. F. Tsoi[129], Y. Tsujikawa[87], V. Tsulaia[18a], K. Tsuri[119], D. Tsybychev[148], Y. Tu[63b], A. Tudorache[28b], V. Tudorache[28b], S. B. Tuncay[127], S. Turchikhin[56b,56a], I. Turk Cakir[3a], R. Turra[70a], T. Turtuvshin[38,ap], P.M. Tuts[41], M. Uboldi[149], Y. Uematsu[82], F. Ukegawa[160], P.A. Ulloa Poblete[138c,138b], G. Unal[37], A. Undrus[30], J. Urban[29b], P. Urrejola[138e], G. Usai[8], R. Ushioda[157], M. Usman[108], F. Ustuner[51], Z. Uysal[80], V. Vacek[133], B. Vachon[104], A. Vaitkus[96], C. Valderanis[109], E. Valdes Santurio[46a,46b], M. Valente[37], S. Valentinetti[24b,24a], A. Valero[165], E. Valiente Moreno[165], S. Valjee[94], A. Vallier[89], J.A. Valls Ferrer[165], D. R. Van Arneman[116], R. Van Den Broucke[128], A. Van Der Graaf[48], H. Z. Van Der Schyf[34j], P. Van Gemmeren[6], M. Van Rijnbach[37], S. Van Stroud[96], I. Van Vulpen[116], P. Vana[134], M. Vanadia[75a,75b], U. M. Vande Voorde[147], W. Vandelli[37], E.R. Vandewall[146], D. Vannicola[154], R. Vari[74a], M. Varma[174], E.W. Varnes[7], C. Varni[85a], D. Varouchas[65], L. Varriale[165], K.E. Varvell[150], M.E. Vasile[28b], A. Vasileiadou[9], L. Vaslin[82], M. D. Vassilev[146], A. Vasyukov[38], L. M. Vaughan[122], R. Vavricka[134], T. Vazquez Schroeder[13], J. Veatch[32], V. Vecchio[101], M.J. Veen[103], I. Veliscek[30], I. Velkovska[93], L.M. Veloce[158], F. Veloso[131a,131c], A.G. Veltman[51], S.H. Venetianer[161], S. Veneziano[74a], A. Ventura[69a,69b], A. Verbytskyi[110], M. Verducci[73a,73b], C. Vergis[94], M. Verissimo De Araujo[81b], W. Verkerke[116], J.C. Vermeulen[116], C. Vernieri[146], M. Vessella[162], M.C. Vetterli[145,t], A. Vgenopoulos[100], N. Viaux Maira[138g,aq], L. Vicenik[133], T. Vickey[142], O.E. Vickey Boeriu[142], G.H.A. Viehhauser[127], L. Vigani[62b], M. Vigl[110], M. Villa[24b,24a], M. Villaplana Perez[165], E.M. Villhauer[39], E. Vilucchi[52], M. Vincent[165], M.G. Vincter[35], A. Visibile[116], A. Visive[116], C. Vittori[24b,24a], I. Vivarelli[24b,24a], M.I. Vivas Albornoz[47], E. Voevodina[110], F. Vogel[109], J.C. Voigt[49], P. Vokac[133], Yu. Volkotrub[85b], L. Vomberg[25], E. Von Toerne[25], B. Vormwald[37], K. Vorobev[50], M. Vos[165], K. Voss[144], M. Vozak[37], L. Vozdecky[121], N. Vranjes[16], M. Vranjes Milosavljevic[16], M. Vreeswijk[116], N.K. Vu[112a], R. Vuillermet[37], I. Vukotic[39], I. K. Vyas[35], J.F. Wack[33], A. Wada[111], S. Wada[160], C. Wagner[146], J.M. Wagner[18a], W. Wagner[173], S. Wahdan[173], H. Wahlberg[90], C. H. Waits[121], J. Walder[135], R. Walker[109], K. Walkingshaw Pass[58], W. Walkowiak[144], A. Wall[129], E.J. Wallin[98], T. Wamorkar[146], K. Wandall-Christensen[165], A. Wang[61], A.Z. Wang[137], C. Wang[47], C. Wang[11], H. Wang[18a], J. Wang[63c], P. Wang[101],

JHEP10(2026)270

P. Wang[96], R. Wang[60], R. Wang[106], R. Wang[6], S. Wang[14,ar], S.M. Wang[151], T. Wang[115], T. Wang[61], W. Wang[113c], W.T. Wang[127], X. Wang[164], X. Wang[141a], X. Wang[47], Y. Wang[148], Y. Wang[114], Z. Wang[14], Z. Wang[63b], C. Wanotayaroj[82], A. Warburton[104], A.L. Warnerbring[144], S. Waterhouse[96], A.T. Watson[21], H. Watson[51], M.F. Watson[21], E. Watton[37], G. Watts[140], B.M. Waugh[96], J. M. Webb[53], C. Weber[30], M.S. Weber[20], C. Wei[61], Y. Wei[53], A.R. Weidberg[127], E.J. Weik[118], J. Weingarten[48], C. Weiser[53], C.J. Wells[47], P.S. Wells[37], T. Wenaus[30], T. Wengler[37], N.S. Wenke[110], N. Wermes[25], D. Werner[47], M. Wessels[62a], A.M. Wharton[91], A. White[8], A.S. White[37], M.J. White[1], D. Whiteson[162], W. Wiedenmann[172], M. Wielers[135], R. Wierda[147], C. Wiglesworth[42], H.G. Wilkens[37], J. J. H. Wilkinson[33], S. Williams[33], S. Willocq[103], D.J. Wilson[101], P.J. Windischhofer[39], F.I. Winkel[31], F. Winklmeier[124], B.T. Winter[53], M. Wittgen[146], M. Wobisch[97], T. Wojtkowski[59], Z. Wolffs[116], J. Wollrath[37], M.W. Wolter[86], H. Wolters[131a,131c], M.C. Wong[137], E.L. Woodward[41], S.D. Worm[47], B.K. Wosiek[86], K. A. Wozniak[55], K.W. Woźniak[86], S. Wozniewski[54], K. Wraight[58], C. Wu[158], J. Wu[156], M. Wu[112b], M. Wu[115], S. Wu[14,ar], S.L. Wu[172], X. Wu[61], Y. Wu[61], Y.Q. Wu[158], Z. Wu[102], Z. Wu[112a], J. Wuerzinger[110], T.R. Wyatt[101], B.M. Wynne[51], S. Xella[42], L. Xia[112a], M. Xie[61], A. Xiong[124], I. Xiotidis[37], D. Xu[14], H. Xu[61], L. Xu[61], R. Xu[129], T. Xu[106], W. Xu[112a], Y. Xu[140], Z. Xu[51], R. Xue[130], B. Yabsley[150], S. Yacoob[11], Y. Yamaguchi[82], E. Yamashita[156], H. Yamauchi[160], T. Yamazaki[18a], Y. Yamazaki[84], F. Yan[2], S. Yan[58], Z. Yan[103], Z. Yan[141b], C. Yang[18a], H.J. Yang[141a], H.T. Yang[61], S. Yang[61], X. Yang[37], X. Yang[14], Y. Yang[156], Y. Yang[61], W-M. Yao[18a], C. L. Yardley[149], J. Ye[14], S. Ye[30], X. Ye[106], I. Yeletskikh[38], B. Yeo[18b], M.R. Yexley[96], T. P. Yildirim[127], K. Yorita[156], C. Young[146], C.J.S. Young[37], I.N.L. Young[58], N.D. Young[124], D. Yu[141b,5], Y. Yu[61], J. Yuan[14,112c,ar], M. Yuan[106], R. Yuan[141b], L. Yue[96], M. Zaazoua[61], B. Zabinski[86], I. Zahir[36a], Q.U.A. Zahoor[51], A. Zaio[56b,56a], Z.K. Zak[86], T. Zakareishvili[165], S. Zambito[55], J. Zang[156], R. Zanzottera[70a,70b], O. Zaplatilek[133], I. Zatocilova[53], E. Zaya[147], C. Zeitnitz[173], H. Zeng[14], D.T. Zenger Jr[27], T. Ženiš[29a], S. Zenz[94], W. Zhan[61], B. Zhang[169], D.F. Zhang[142], G. Zhang[14,ar], J. Zhang[113b], J. Zhang[6], L. Zhang[61], L. Zhang[112a], P. Zhang[14,112c], R. Zhang[112a], S. Zhang[14], Y. Zhang[140], Y. Zhang[96], Y. Zhang[61], Y. Zhang[112a], Z. Zhang[149], Z. Zhang[101], Z. Zhang[18a], Z. Zhang[113b], Z. Zhang[65], H. Zhao[140], T. Zhao[113b], Y. Zhao[35], Z. Zhao[61], Z. Zhao[61], A. Zhemchugov[38], J. Zheng[112a], K. Zheng[164], L. Zheng[113b], X. Zheng[61], Z. Zheng[146], D. Zhong[164], B. Zhou[106], B. Zhou[141b,141a], N. Zhou[141a], Y. Zhou[15], Y. Zhou[112a], Y. Zhou[7], Z. Zhou[61], J. Zhu[106], X. Zhu[141b], Y. Zhu[141a], X. Zhuang[14], K. Zhukov[67], P. Ziakas[4], N.I. Zimine[38], J. Zinsser[62b], M. Ziolkowski[144], L. Živković[16], A. Zoccoli[24b,24a], K. Zoch[37], A. Zografos[37], T.G. Zorbas[142], L. Zwalinski[37]

[1] *Department of Physics, University of Adelaide, Adelaide, Australia*
[2] *Department of Physics, University of Alberta, Edmonton AB, Canada*
[3a] *Department of Physics, Ankara University, Ankara, Türkiye*
[3b] *Division of Physics, TOBB University of Economics and Technology, Ankara, Türkiye*
[4] *LAPP, Université Savoie Mont Blanc, CNRS/IN2P3, Annecy, France*
[5] *APC, Université Paris Cité, CNRS/IN2P3, Paris, France*
[6] *High Energy Physics Division, Argonne National Laboratory, Argonne IL, U.S.A.*

JHEP10(2026)270

[7] Department of Physics, University of Arizona, Tucson AZ, U.S.A.
[8] Department of Physics, University of Texas at Arlington, Arlington TX, U.S.A.
[9] Physics Department, National and Kapodistrian University of Athens, Athens, Greece
[10] Physics Department, National Technical University of Athens, Zografou, Greece
[11] Department of Physics, University of Texas at Austin, Austin TX, U.S.A.
[12] Institute of Physics, Azerbaijan Academy of Sciences, Baku, Azerbaijan
[13] Institut de Física d'Altes Energies (IFAE), Barcelona Institute of Science and Technology, Barcelona, Spain
[14] Institute of High Energy Physics, Chinese Academy of Sciences, Beijing, China
[15] Physics Department, Tsinghua University, Beijing, China
[16] Institute of Physics, University of Belgrade, Belgrade, Serbia
[17] Department for Physics and Technology, University of Bergen, Bergen, Norway
[18a] Physics Division, Lawrence Berkeley National Laboratory, Berkeley CA, U.S.A.
[18b] University of California, Berkeley CA, U.S.A.
[19] Institut für Physik, Humboldt Universität zu Berlin, Berlin, Germany
[20] Albert Einstein Center for Fundamental Physics and Laboratory for High Energy Physics, University of Bern, Bern, Switzerland
[21] School of Physics and Astronomy, University of Birmingham, Birmingham, U.K.
[22a] Department of Physics, Bogazici University, Istanbul, Türkiye
[22b] Department of Physics Engineering, Gaziantep University, Gaziantep, Türkiye
[22c] Department of Physics, Istanbul University, Istanbul, Türkiye
[23a] Facultad de Ciencias y Centro de Investigaciónes, Universidad Antonio Nariño, Bogotá, Colombia
[23b] Departamento de Física, Universidad Nacional de Colombia, Bogotá, Colombia
[24a] Dipartimento di Fisica e Astronomia A. Righi, Università di Bologna, Bologna, Italy
[24b] INFN Sezione di Bologna, Italy
[25] Physikalisches Institut, Universität Bonn, Bonn, Germany
[26] Department of Physics, Boston University, Boston MA, U.S.A.
[27] Department of Physics, Brandeis University, Waltham MA, U.S.A.
[28a] Transilvania University of Brasov, Brasov, Romania
[28b] Horia Hulubei National Institute of Physics and Nuclear Engineering, Bucharest, Romania
[28c] Department of Physics, Alexandru Ioan Cuza University of Iasi, Iasi, Romania
[28d] National Institute for Research and Development of Isotopic and Molecular Technologies, Physics Department, Cluj-Napoca, Romania
[28e] National University of Science and Technology Politechnica, Bucharest, Romania
[28f] West University in Timisoara, Timisoara, Romania
[28g] Faculty of Physics, University of Bucharest, Bucharest, Romania
[29a] Faculty of Mathematics, Physics and Informatics, Comenius University, Bratislava, Slovak Republic
[29b] Department of Subnuclear Physics, Institute of Experimental Physics of the Slovak Academy of Sciences, Kosice, Slovak Republic
[30] Physics Department, Brookhaven National Laboratory, Upton NY, U.S.A.
[31] Universidad de Buenos Aires, Facultad de Ciencias Exactas y Naturales, Departamento de Física, y CONICET, Instituto de Física de Buenos Aires (IFIBA), Buenos Aires, Argentina
[32] California State University, CA, U.S.A.
[33] Cavendish Laboratory, University of Cambridge, Cambridge, U.K.
[34a] Department of Physics, University of Cape Town, Cape Town, South Africa
[34b] iThemba Labs, Western Cape, South Africa
[34c] Department of Mechanical Engineering Science, University of Johannesburg, Johannesburg, South Africa
[34d] National Institute of Physics, University of the Philippines Diliman (Philippines), Philippines
[34e] Department of Physics, Stellenbosch University, Matieland, South Africa
[34f] University of KwaZulu-Natal, School of Agriculture and Science, Mathematics, Westville, South Africa
[34g] University of South Africa, Department of Physics, Pretoria, South Africa
[34h] University of Pretoria, Department of Mechanical and Aeronautical Engineering, Pretoria, South Africa
[34i] University of Zululand, KwaDlangezwa, South Africa

JHEP10(2026)270

[34j] School of Physics, University of the Witwatersrand, Johannesburg, South Africa
[35] Department of Physics, Carleton University, Ottawa ON, Canada
[36a] Faculté des Sciences Ain Chock, Université Hassan II de Casablanca, Morocco
[36b] Faculté des Sciences, Université Ibn-Tofail, Kénitra, Morocco
[36c] Faculté des Sciences Semlalia, Université Cadi Ayyad, LPHEA-Marrakech, Morocco
[36d] LPMR, Faculté des Sciences, Université Mohamed Premier, Oujda, Morocco
[36e] Faculté des sciences, Université Mohammed V, Rabat, Morocco
[36f] Institute of Applied Physics, Mohammed VI Polytechnic University, Ben Guerir, Morocco
[37] CERN, Geneva, Switzerland
[38] Affiliated with an international laboratory covered by a cooperation agreement with CERN
[39] Enrico Fermi Institute, University of Chicago, Chicago IL, U.S.A.
[40] LPC, Université Clermont Auvergne, CNRS/IN2P3, Clermont-Ferrand, France
[41] Nevis Laboratory, Columbia University, Irvington NY, U.S.A.
[42] Niels Bohr Institute, University of Copenhagen, Copenhagen, Denmark
[43a] Dipartimento di Fisica, Università della Calabria, Rende, Italy
[43b] INFN Gruppo Collegato di Cosenza, Laboratori Nazionali di Frascati, Italy
[44] Physics Department, Southern Methodist University, Dallas TX, U.S.A.
[45] National Centre for Scientific Research "Demokritos", Agia Paraskevi, Greece
[46a] Department of Physics, Stockholm University, Sweden
[46b] Oskar Klein Centre, Stockholm, Sweden
[47] Deutsches Elektronen-Synchrotron DESY, Hamburg and Zeuthen, Germany
[48] Fakultät Physik, Technische Universität Dortmund, Dortmund, Germany
[49] Institut für Kern- und Teilchenphysik, Technische Universität Dresden, Dresden, Germany
[50] Department of Physics, Duke University, Durham NC, U.S.A.
[51] SUPA — School of Physics and Astronomy, University of Edinburgh, Edinburgh, U.K.
[52] INFN e Laboratori Nazionali di Frascati, Frascati, Italy
[53] Physikalisches Institut, Albert-Ludwigs-Universität Freiburg, Freiburg, Germany
[54] II. Physikalisches Institut, Georg-August-Universität Göttingen, Göttingen, Germany
[55] Département de Physique Nucléaire et Corpusculaire, Université de Genève, Genève, Switzerland
[56a] Dipartimento di Fisica, Università di Genova, Genova, Italy
[56b] INFN Sezione di Genova, Italy
[57] II. Physikalisches Institut, Justus-Liebig-Universität Giessen, Giessen, Germany
[58] SUPA — School of Physics and Astronomy, University of Glasgow, Glasgow, U.K.
[59] LPSC, Université Grenoble Alpes, CNRS/IN2P3, Grenoble INP, Grenoble, France
[60] Laboratory for Particle Physics and Cosmology, Harvard University, Cambridge MA, U.S.A.
[61] Department of Modern Physics and State Key Laboratory of Particle Detection and Electronics, University of Science and Technology of China, Hefei, China
[62a] Kirchhoff-Institut für Physik, Ruprecht-Karls-Universität Heidelberg, Heidelberg, Germany
[62b] Physikalisches Institut, Ruprecht-Karls-Universität Heidelberg, Heidelberg, Germany
[63a] Department of Physics, Chinese University of Hong Kong, Shatin, N.T., Hong Kong, China
[63b] Department of Physics, University of Hong Kong, Hong Kong, China
[63c] Department of Physics and Institute for Advanced Study, Hong Kong University of Science and Technology, Clear Water Bay, Kowloon, Hong Kong, China
[64] Department of Physics, National Tsing Hua University, Hsinchu, Taiwan
[65] IJCLab, Université Paris-Saclay, CNRS/IN2P3, 91405, Orsay, France
[66] Centro Nacional de Microelectrónica (IMB-CNM-CSIC), Barcelona, Spain
[67] Department of Physics, Indiana University, Bloomington IN, U.S.A.
[68a] INFN Gruppo Collegato di Udine, Sezione di Trieste, Udine, Italy
[68b] ICTP, Trieste, Italy
[68c] Dipartimento Politecnico di Ingegneria e Architettura, Università di Udine, Udine, Italy
[69a] INFN Sezione di Lecce, Italy
[69b] Dipartimento di Matematica e Fisica, Università del Salento, Lecce, Italy
[70a] INFN Sezione di Milano, Italy

JHEP10(2026)270

[70b] Dipartimento di Fisica, Università di Milano, Milano, Italy
[71a] INFN Sezione di Napoli, Italy
[71b] Dipartimento di Fisica, Università di Napoli, Napoli, Italy
[72a] INFN Sezione di Pavia, Italy
[72b] Dipartimento di Fisica, Università di Pavia, Pavia, Italy
[73a] INFN Sezione di Pisa, Italy
[73b] Dipartimento di Fisica E. Fermi, Università di Pisa, Pisa, Italy
[74a] INFN Sezione di Roma, Italy
[74b] Dipartimento di Fisica, Sapienza Università di Roma, Roma, Italy
[75a] INFN Sezione di Roma Tor Vergata, Italy
[75b] Dipartimento di Fisica, Università di Roma Tor Vergata, Roma, Italy
[76a] INFN Sezione di Roma Tre, Italy
[76b] Dipartimento di Matematica e Fisica, Università Roma Tre, Roma, Italy
[77a] INFN-TIFPA, Italy
[77b] Università degli Studi di Trento, Trento, Italy
[78] Universität Innsbruck, Department of Astro and Particle Physics, Innsbruck, Austria
[79] Department of Physics and Astronomy, Iowa State University, Ames IA, U.S.A.
[80] Istinye University, Sariyer, Istanbul, Türkiye
[81a] Departamento de Engenharia Elétrica, Universidade Federal de Juiz de Fora (UFJF), Juiz de Fora, Brazil
[81b] Universidade Federal do Rio De Janeiro COPPE/EE/IF, Rio de Janeiro, Brazil
[81c] Instituto de Física, Universidade de São Paulo, São Paulo, Brazil
[81d] Rio de Janeiro State University, Rio de Janeiro, Brazil
[81e] Federal University of Bahia, Bahia, Brazil
[82] KEK, High Energy Accelerator Research Organization, Tsukuba, Japan
[83a] Khalifa University of Science and Technology, Abu Dhabi, United Arab Emirates
[83b] New York University Abu Dhabi, Abu Dhabi, United Arab Emirates
[83c] United Arab Emirates University, Al Ain, United Arab Emirates
[83d] University of Sharjah, Sharjah, United Arab Emirates
[84] Graduate School of Science, Kobe University, Kobe, Japan
[85a] AGH University of Krakow, Faculty of Physics and Applied Computer Science, Krakow, Poland
[85b] Marian Smoluchowski Institute of Physics, Jagiellonian University, Krakow, Poland
[86] Institute of Nuclear Physics Polish Academy of Sciences, Krakow, Poland
[87] Faculty of Science, Kyoto University, Kyoto, Japan
[88] Research Center for Advanced Particle Physics and Department of Physics, Kyushu University, Fukuoka, Japan
[89] L2IT, Université de Toulouse, CNRS/IN2P3, UPS, Toulouse, France
[90] Instituto de Física La Plata, Universidad Nacional de La Plata and CONICET, La Plata, Argentina
[91] Physics Department, Lancaster University, Lancaster, U.K.
[92] Oliver Lodge Laboratory, University of Liverpool, Liverpool, U.K.
[93] Department of Experimental Particle Physics, Jožef Stefan Institute and Department of Physics, University of Ljubljana, Ljubljana, Slovenia
[94] Department of Physics and Astronomy, Queen Mary University of London, London, U.K.
[95] Department of Physics, Royal Holloway University of London, Egham, U.K.
[96] Department of Physics and Astronomy, University College London, London, U.K.
[97] Louisiana Tech University, Ruston LA, U.S.A.
[98] Fysiska institutionen, Lunds universitet, Lund, Sweden
[99] Departamento de Física Teorica C-15 and CIAFF, Universidad Autónoma de Madrid, Madrid, Spain
[100] Institut für Physik, Universität Mainz, Mainz, Germany
[101] School of Physics and Astronomy, University of Manchester, Manchester, U.K.
[102] CPPM, Aix-Marseille Université, CNRS/IN2P3, Marseille, France
[103] Department of Physics, University of Massachusetts, Amherst MA, U.S.A.
[104] Department of Physics, McGill University, Montreal QC, Canada
[105] School of Physics, University of Melbourne, Victoria, Australia

JHEP10(2026)270

[106] Department of Physics, University of Michigan, Ann Arbor MI, U.S.A.
[107] Department of Physics and Astronomy, Michigan State University, East Lansing MI, U.S.A.
[108] Group of Particle Physics, University of Montreal, Montreal QC, Canada
[109] Fakultät für Physik, Ludwig-Maximilians-Universität München, München, Germany
[110] Max-Planck-Institut für Physik (Werner-Heisenberg-Institut), Garching, Germany
[111] Graduate School of Science and Kobayashi-Maskawa Institute, Nagoya University, Nagoya, Japan
[112a] Department of Physics, Nanjing University, Nanjing, China
[112b] School of Science, Shenzhen Campus of Sun Yat-sen University, China
[112c] University of Chinese Academy of Science (UCAS), Beijing, China
[113a] School of Physics, Nankai University, Tianjin, China
[113b] Institute of Frontier and Interdisciplinary Science and Key Laboratory of Particle Physics and Particle Irradiation (MOE), Shandong University, Qingdao, China
[113c] School of Physics, Zhengzhou University, China
[114] Department of Physics and Astronomy, University of New Mexico, Albuquerque NM, U.S.A.
[115] Institute for Mathematics, Astrophysics and Particle Physics, Radboud University/Nikhef, Nijmegen, Netherlands
[116] Nikhef National Institute for Subatomic Physics and University of Amsterdam, Amsterdam, Netherlands
[117] Department of Physics, Northern Illinois University, DeKalb IL, U.S.A.
[118] Department of Physics, New York University, New York NY, U.S.A.
[119] Ochanomizu University, Otsuka, Bunkyo-ku, Tokyo, Japan
[120] Ohio State University, Columbus OH, U.S.A.
[121] Homer L. Dodge Department of Physics and Astronomy, University of Oklahoma, Norman OK, U.S.A.
[122] Department of Physics, Oklahoma State University, Stillwater OK, U.S.A.
[123] Palacký University, Joint Laboratory of Optics, Olomouc, Czech Republic
[124] Institute for Fundamental Science, University of Oregon, Eugene, OR, U.S.A.
[125] Graduate School of Science, University of Osaka, Osaka, Japan
[126] Department of Physics, University of Oslo, Oslo, Norway
[127] Department of Physics, Oxford University, Oxford, U.K.
[128] LPNHE, Sorbonne Université, Université Paris Cité, CNRS/IN2P3, Paris, France
[129] Department of Physics, University of Pennsylvania, Philadelphia PA, U.S.A.
[130] Department of Physics and Astronomy, University of Pittsburgh, Pittsburgh PA, U.S.A.
[131a] Laboratório de Instrumentação e Física Experimental de Partículas — LIP, Lisboa, Portugal
[131b] Departamento de Física, Faculdade de Ciências, Universidade de Lisboa, Lisboa, Portugal
[131c] Departamento de Física, Universidade de Coimbra, Coimbra, Portugal
[131d] Centro de Física Nuclear da Universidade de Lisboa, Lisboa, Portugal
[131e] Departamento de Física, Escola de Ciências, Universidade do Minho, Braga, Portugal
[131f] Departamento de Física Teórica y del Cosmos, Universidad de Granada, Granada (Spain), Spain
[131g] Departamento de Física, Instituto Superior Técnico, Universidade de Lisboa, Lisboa, Portugal
[132] Institute of Physics of the Czech Academy of Sciences, Prague, Czech Republic
[133] Czech Technical University in Prague, Prague, Czech Republic
[134] Charles University, Faculty of Mathematics and Physics, Prague, Czech Republic
[135] Particle Physics Department, Rutherford Appleton Laboratory, Didcot, U.K.
[136] IRFU, CEA, Université Paris-Saclay, Gif-sur-Yvette, France
[137] Santa Cruz Institute for Particle Physics, University of California Santa Cruz, Santa Cruz CA, U.S.A.
[138a] Departamento de Física, Pontificia Universidad Católica de Chile, Santiago, Chile
[138b] Millennium Institute for Subatomic physics at high energy frontier (SAPHIR), Santiago, Chile
[138c] Instituto de Investigación Multidisciplinario en Ciencia y Tecnología, y Departamento de Física, Universidad de La Serena, Chile
[138d] Universidad Andres Bello, Department of Physics, Santiago, Chile
[138e] Universidad San Sebastian, Recoleta, Chile
[138f] Instituto de Alta Investigación, Universidad de Tarapacá, Arica, Chile
[138g] Departamento de Física, Universidad Técnica Federico Santa María, Valparaíso, Chile
[139] Department of Physics, Institute of Science, Tokyo, Japan

JHEP10(2026)270

[140] Department of Physics, University of Washington, Seattle WA, U.S.A.
[141a] State Key Laboratory of Dark Matter Physics, School of Physics and Astronomy, Shanghai Jiao Tong University, Key Laboratory for Particle Astrophysics and Cosmology (MOE), SKLPPC, Shanghai, China
[141b] State Key Laboratory of Dark Matter Physics, Tsung-Dao Lee Institute, Shanghai Jiao Tong University, Shanghai, China
[142] Department of Physics and Astronomy, University of Sheffield, Sheffield, U.K.
[143] Department of Physics, Shinshu University, Nagano, Japan
[144] Department Physik, Universität Siegen, Siegen, Germany
[145] Department of Physics, Simon Fraser University, Burnaby BC, Canada
[146] SLAC National Accelerator Laboratory, Stanford CA, U.S.A.
[147] Department of Physics, Royal Institute of Technology, Stockholm, Sweden
[148] Departments of Physics and Astronomy, Stony Brook University, Stony Brook NY, U.S.A.
[149] Department of Physics and Astronomy, University of Sussex, Brighton, U.K.
[150] School of Physics, University of Sydney, Sydney, Australia
[151] Institute of Physics, Academia Sinica, Taipei, Taiwan
[152a] E. Andronikashvili Institute of Physics, Iv. Javakhishvili Tbilisi State University, Tbilisi, Georgia
[152b] High Energy Physics Institute, Tbilisi State University, Tbilisi, Georgia
[152c] University of Georgia, Tbilisi, Georgia
[153] Department of Physics, Technion, Israel Institute of Technology, Haifa, Israel
[154] Raymond and Beverly Sackler School of Physics and Astronomy, Tel Aviv University, Tel Aviv, Israel
[155] Department of Physics, Aristotle University of Thessaloniki, Thessaloniki, Greece
[156] International Center for Elementary Particle Physics and Department of Physics, University of Tokyo, Tokyo, Japan
[157] Graduate School of Science and Technology, Tokyo Metropolitan University, Tokyo, Japan
[158] Department of Physics, University of Toronto, Toronto ON, Canada
[159a] TRIUMF, Vancouver BC, Canada
[159b] Department of Physics and Astronomy, York University, Toronto ON, Canada
[160] Division of Physics and Tomonaga Center for the History of the Universe, Faculty of Pure and Applied Sciences, University of Tsukuba, Tsukuba, Japan
[161] Department of Physics and Astronomy, Tufts University, Medford MA, U.S.A.
[162] Department of Physics and Astronomy, University of California Irvine, Irvine CA, U.S.A.
[163] Department of Physics and Astronomy, University of Uppsala, Uppsala, Sweden
[164] Department of Physics, University of Illinois, Urbana IL, U.S.A.
[165] Instituto de Física Corpuscular (IFIC), Centro Mixto Universidad de Valencia — CSIC, Valencia, Spain
[166] Department of Physics, University of British Columbia, Vancouver BC, Canada
[167] Department of Physics and Astronomy, University of Victoria, Victoria BC, Canada
[168] Fakultät für Physik und Astronomie, Julius-Maximilians-Universität Würzburg, Würzburg, Germany
[169] Department of Physics, University of Warwick, Coventry, U.K.
[170] Waseda University, Tokyo, Japan
[171] Department of Particle Physics and Astrophysics, Weizmann Institute of Science, Rehovot, Israel
[172] Department of Physics, University of Wisconsin, Madison WI, U.S.A.
[173] Fakultät für Mathematik und Naturwissenschaften, Fachgruppe Physik, Bergische Universität Wuppertal, Wuppertal, Germany
[174] Department of Physics, Yale University, New Haven CT, U.S.A.
[175] Yerevan Physics Institute, Yerevan, Armenia

[a] Also at Department of Physics, King's College London, London, U.K.
[b] Also at Institute of Physics, Azerbaijan Academy of Sciences, Baku, Azerbaijan
[c] Also at Imam Mohammad Ibn Saud Islamic University, Saudi Arabia
[d] Also at Department of Physics, University of Thessaly, Greece
[e] Also at Département de Physique Nucléaire et Corpusculaire, Université de Genève, Genève, Switzerland
[f] Also at An-Najah National University, Nablus, Palestine
[g] Also at Department of Physics, University of Fribourg, Fribourg, Switzerland

JHEP10(2026)270

[h] Also at Department of Physics, Westmont College, Santa Barbara, U.S.A.
[i] Also at Departament de Fisica de la Universitat Autonoma de Barcelona, Barcelona, Spain
[j] Also at University of Siena, Italy
[k] Also at Affiliated with an institute formerly covered by a cooperation agreement with CERN
[l] Also at The Collaborative Innovation Center of Quantum Matter (CICQM), Beijing, China
[m] Also at Faculty of Physics, Sofia University, 'St. Kliment Ohridski', Sofia, Bulgaria
[n] Also at Università di Napoli Parthenope, Napoli, Italy
[o] Also at Institute of Particle Physics (IPP), Canada
[p] Also at Department of Physics, Bolu Abant Izzet Baysal University, Bolu, Türkiye
[q] Also at Faculty of Physics, University of Bucharest, Romania
[r] Also at Borough of Manhattan Community College, City University of New York, New York NY, U.S.A.
[s] Also at National Institute of Physics, University of the Philippines Diliman (Philippines), Philippines
[t] Also at TRIUMF, Vancouver BC, Canada
[u] Also at Universita degli Studi Link, Italy
[v] Also at Department of Financial and Management Engineering, University of the Aegean, Chios, Greece
[w] Also at University and INFN Torino, Torino, Italy
[x] Also at Institucio Catalana de Recerca i Estudis Avancats, ICREA, Barcelona, Spain
[y] Also at Henan University, China
[z] Also at Yeditepe University, Physics Department, Istanbul, Türkiye
[aa] Also at Institute of Theoretical Physics, Ilia State University, Tbilisi, Georgia
[ab] Also at CERN, Geneva, Switzerland
[ac] Also at Center for Interdisciplinary Research and Innovation (CIRI-AUTH), Thessaloniki, Greece
[ad] Also at Hellenic Open University, Patras, Greece
[ae] Also at Department of Modern Physics and State Key Laboratory of Particle Detection and Electronics, University of Science and Technology of China, Hefei, China
[af] Also at Department of Physics, Stellenbosch University, South Africa
[ag] Also at School of Physics, University of the Witwatersrand, Johannesburg, South Africa
[ah] Also at Department of Physics, Ben Gurion University of the Negev, Beer Sheva, Israel
[ai] Also at University of Colorado Boulder, Department of Physics, Colorado, U.S.A.
[aj] Also at Centre of Physics of the Universities of Minho and Porto (CF-UM-UP), Portugal
[ak] Also at Indian Institute of Technology (IIT), Jodhpur, India
[al] Also at Institute for Nuclear Research and Nuclear Energy (INRNE) of the Bulgarian Academy of Sciences, Sofia, Bulgaria
[am] Also at Washington College, Chestertown, MD, U.S.A.
[an] Also at Institut für Experimentalphysik, Universität Hamburg, Hamburg, Germany
[ao] Also at Institute of Applied Physics, Mohammed VI Polytechnic University, Ben Guerir, Morocco
[ap] Also at Institute of Physics and Technology, Mongolian Academy of Sciences, Ulaanbaatar, Mongolia
[aq] Also at Millennium Institute for Subatomic physics at high energy frontier (SAPHIR), Santiago, Chile
[ar] Also at University of Chinese Academy of Sciences (UCAS), Beijing, China
[†] Deceased

JHEP10(2026)270